UNIVERSITEIT VAN PRETORIA
UNIVERSITY OF PRETORIA
YUNIBESITHI YA PRETORIA

Synthesis and application of rhodium(I) Fischer carbene complexes

by

Granny Kabelo Ramollo

Submitted in partial fulfillment of the requirements for the degree

Magister Scientiae

In the Faculty of Natural and Agricultural Sciences

University of Pretoria

Supervisor: Dr DI Bezuidenhout

April 2016

Acknowledgements

I would like to thank my supervisor, Dr. D. I. Bezuidenhout for her guidance, support and understanding.

I want to thank my family, especially my aunt Meslinah Ramollo, and my friends for their support and interest.

I hereby gratefully acknowledge Sasol Technology R&D Pty. Ltd. South Africa for Financial support in the form of a bursary.

The financial assistance of the National Research Foundation (NRF) towards this research is hereby acknowledged. Opinions expressed and conclusions arrived at, are those of the author and are not necessarily to be attributed to the NRF.

Declaration

I, Granny Kabelo Ramollo, declare that the dissertation, which I hereby submit for the degree MSc. Chemistry at the University of Pretoria, is my own work and has not been previously submitted by me for a degree at this or any other tertiary institution.

The hydroformylation catalysis was completed by me in the laboratories of Dr. Gregory S. Smith at the University of Cape Town.

Crystal structure determination was done by Mr. David C. Liles (UP) and Dr. Hong Su (UCT)

Results obtained from this study have also been published in:

G. K. Ramollo, M. J. López-Gómez, D. C. Liles, L. C. Matsinha, G. S. Smith and D. I. Bezuidenhout, *Organometallics*, 2015, **34**, 5745–5753.

Signature:……

Date:……

Summary

Synthesis and application of rhodium(I) Fischer carbene complexes

by

Granny Kabelo Ramollo

Supervisor: Dr DI Bezuidenhout

Submitted in partial fulfillment of the requirements for the degree Magister Scientiae, Department of Chemistry, University of Pretoria

In this study, novel rhodium(I) carbene complexes were synthesized and fully characterized *via* a carbene ligand transfer methodology from Group 6 Fischer carbene complex precursors and subsequent ligand modification. The classic Fischer route was followed towards the isolation of mono- and biscarbene complexes of the form $[M(CO)_5\{C(OR)R'\}]$ [M = Cr, W; R = Me, Et; R' = 2-furyl, 2-thienyl, ferrocenyl] (complexes **1 – 6**, **9** and **10**), and $[M(CO)_5\mu\{C(OR)\text{-}R''\text{-}C(OR)\}M(CO)_5]$ [M = Cr; R = Me, Et; R'' = 2,2'-bithien-5,5'-diyl, 2,5-furadiyl, 1,1'-ferrocendiyl] (complexes **7**, **8** and **11**), respectively. Analogous aminocarbene complexes $[M(CO)_5\{C(NH_2)R'\}]$ [M = Cr, W; R' = 2-thienyl, ferrocenyl) (complexes **12** and **13**) were prepared by simple aminolyses of the alkoxycarbene complex precursors and all isolated products were characterized using NMR and FT-IR spectroscopic methods, the results of which were comparable with literature values.

Transmetallation techniques were employed in an attempt to transfer the carbene ligands to a rhodium(I) metal center of the dimeric $[Rh(cod)Cl]_2$ precursor to result in novel 2-furyl, 2-thienyl and ferrocenyl Fischer carbene complexes of rhodium(I). Only the ferrocenylcarbene complex **15** [Rh(cod)Cl{C(OEt)Fc) were found to be stable enough to isolate, as the heteroaryl (thienyl, furyl) substituted carbene ligands dissociated in solution, with resultant decomposition dimerization to form the corresponding alkene and starting $[Rh(cod)Cl]_2$ complex, as indicated by NMR spectroscopy.

The ferrocenylcarbene complex **15** was then employed as a precursor for the syntheses of all other rhodium(I) carbene complexes *via* cod ligand substitution and aminolysis reactions to isolate mono- and dicarbonylcarbene complexes **16** – **23**, [Rh(LL)Cl{C(X)Fc}] [LL = cod, $(CO)_2$, (CO, PPh_3), (CO, PCy_3), (CO, $P(OPh_3)$), (CO, $AsPh_3$); X = OEt,NH^nPr], with variable π-acceptor properties. Full characterization of the novel complexes were achieved by single crystal XRD and spectroscopic methods. From the FT-IR data

collected, the donor ability of the electronic environment around the rhodium(I) center was found to correlate with the known electron-donor ability of the coligands in the order PCy_3>PPh_3,$AsPh_3$>$P(OPh)_3$. This trend was corroborated by cyclic voltammetric methods through which the electron-withdrawing effects of the coligands were studied, and it was confirmed that the cod ligand is the most electron-donating whilst the dicarbonyls were found to be the least donating in the series. In addition, the increased electron donation of the aminocarbene ligands compared to the ethoxycarbene ligands was found to significantly influence the redox potentials of the metal centre in the studied complexes.

The isolated rhodium(I) Fischer carbene complexes **15** - **22** were screened as catalyst precursors for the hydroformylation of 1-octene. Good to excellent catalytic activities, with selectivity toward the formation of the linear nonanal, was observed. These results were found to be comparable to results reported for rhodium(I) *N*-heterocyclic carbene complexes. A mercury-drop test was done to exclude a heterogeneous catalytic mode of action. Finally, the stability of the catalyst precursor **15** (and **17**) was probed by an NMR experiment carried out under hydroformylation conditions. The Rh-$C_{carbene}$ bond is retained, although the presumed catalytically active species, the rhodium carbene carbonyl hydride complex could not be identified.

Table of Content

List of Figures

List of Schemes

List of Complexes

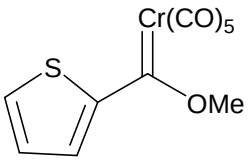

1

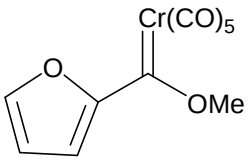

2

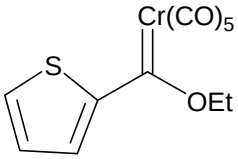

3

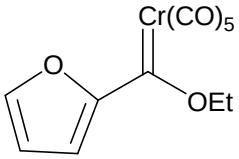

4

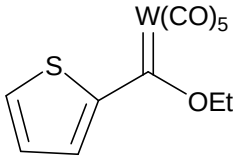

5

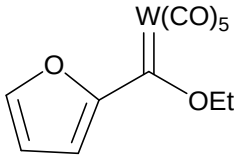

6

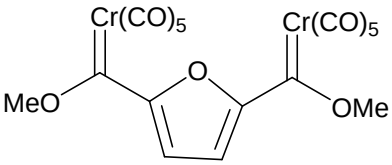

7

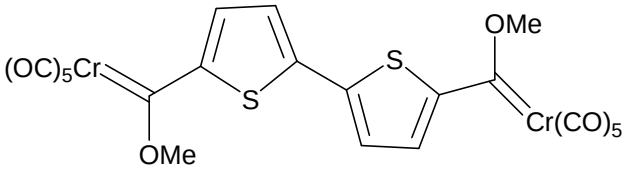

8

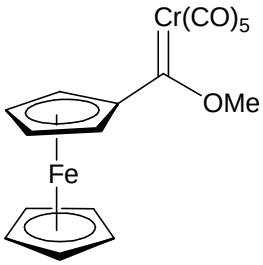

9

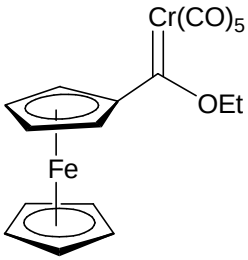

10

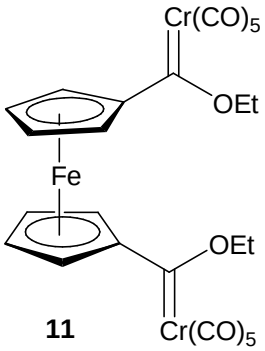

11

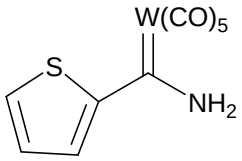

12

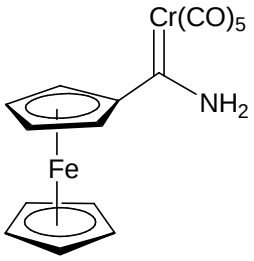

13

List of Novel Complexes

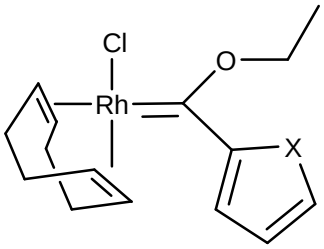

14A

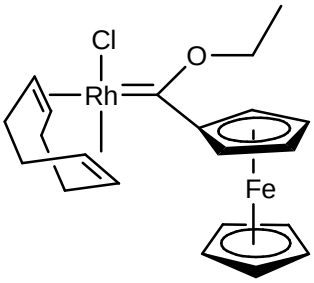

15

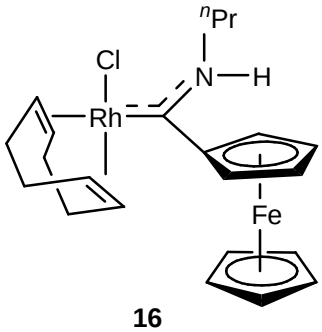

16

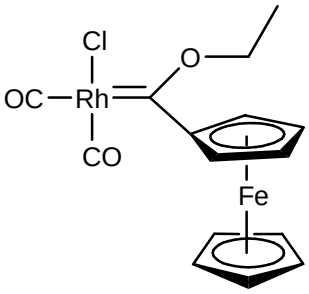

17

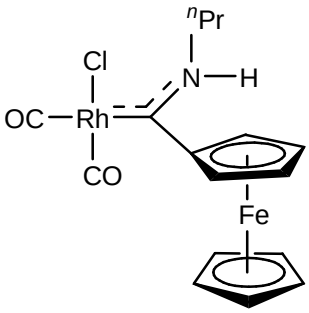

18

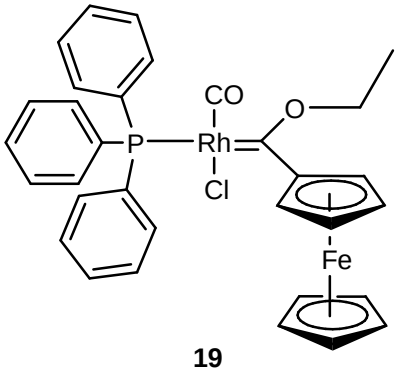

19

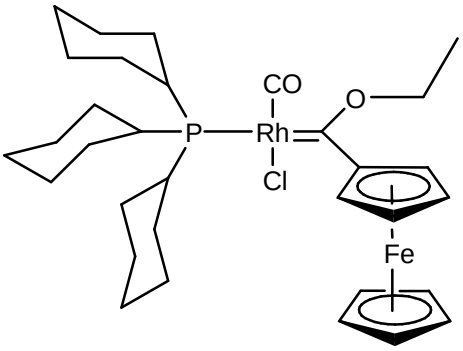

20

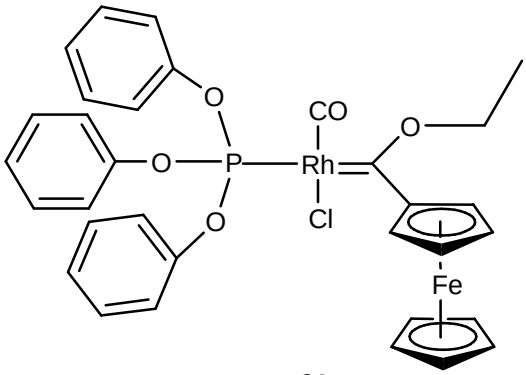

21

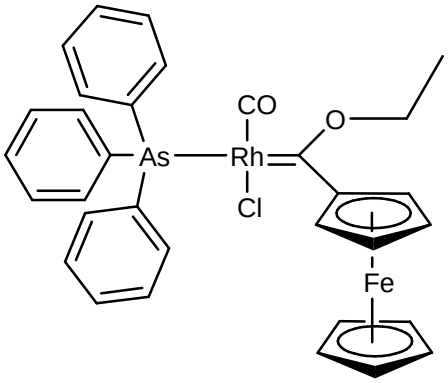

22

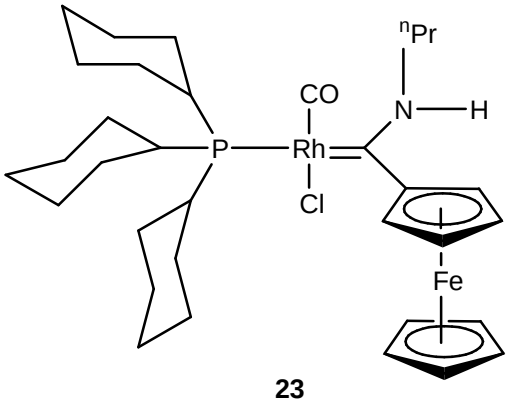

23

List of Abbreviations

Bu	butyl
cod	1, 5-cyclooctadiene
Cp	cyclopentadienyl
Cy	cyclohexyl
DCM	dichloromethane
dd	doublet of doublets
Et	ethyl
E	electrophile
Fc	ferrocenyl
Fc'	ferrocendiyl
FT-IR	Fourier Transform Infrared
Fu	furyl
LEP	Lever electronic parameters
m	medium (IR)
m	multiplet (NMR)
Me	methyl
MS	mass-spectrometry
NHC	*N*-Heterocyclic carbene
NMR	Nuclear Magnetic Resonance
Nu	nucleophile
Ph	phenyl
ppm	parts per million
rt	room temperature
s	singlet (NMR)
s	strong (IR)
TEP	Tolman electronic parameter
Th	Thienyl
TLC	thin layer chromatography
TOF	turnover frequency
vs	very strong (IR)

w	Weak (IR)

Chapter 1: Introduction

1.1: General Overview; Carbene Complexes

Carbene ligands have been useful tools in organometallic chemistry for more than four decades. Since the first stable and correctly characterized carbene complex in 1964,[1] the metal-carbon double bond has been thoroughly studied and applied by various research groups and industries around the globe. Carbene complexes have found wide application mainly as precursors in metal-facilitated organic reactions, and to a lesser extent, as homogeneous catalysts.[2] This is due to the versatile nature of the carbene carbon, for example, Fischer carbenes are well known to be very electrophilic while Schrock carbenes are nucleophilic.[3]

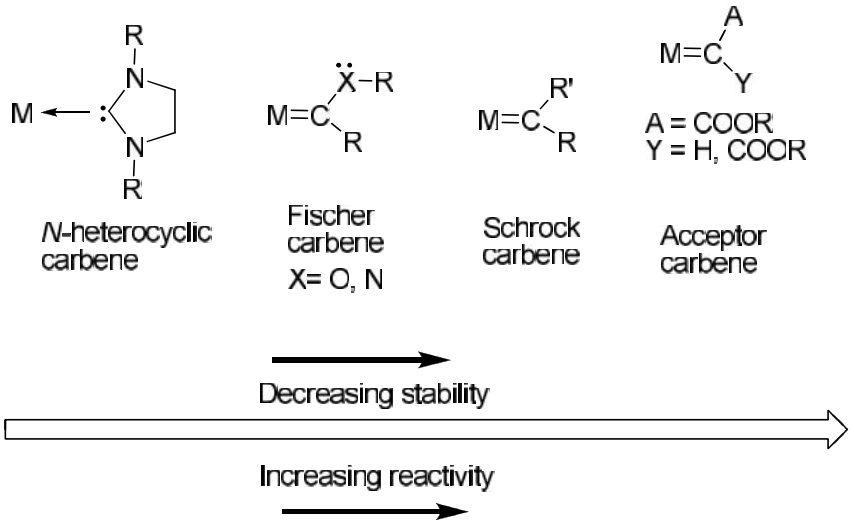

Figure 1.1: Classes of metallocarbenoid structures and reactivity.[4]

The stability of a carbene complex (as well as its ease of isolation and application) is determined by the types of carbene carbon atom substituents, which in turn determines the type of carbene complex (Figure 1.1). Generally speaking, four main classes of carbene complexes have been defined, namely *N*-heterocyclic carbene (NHC) complexes, Fischer, Schrock and acceptor carbene complexes[5,6]. NHCs are singlet carbenes, stabilized by two flanking nitrogen atoms through a π-push σ-pull system whereby the σ-electron withdrawing effect of the nitrogen atom stabilizes the σ-orbital while the electron pair's donor ability stabilizes the vacant π-orbital, resulting in a robust carbene ligand which can be isolated even when not complexed to a metal center. Acyclic Fischer carbenes are stabilized by only one heteroatom accounting for their relative ease of isolation,[7]consequently, the free carbene is not stable enough to isolate. Triplet Schrock carbenes usually contain alkyl or aryl carbene substituents, with no stabilizing heteroatoms, and are therefore less stable than either Fischer carbenes or NHCs. Acceptor carbenes are the least stable because the carbene carbon is bonded to acceptor ligands (e.g, esters, carboxylic acids, etc). Acceptor carbene complexes are often implied as key stoichiometric intermediates in a broad range of carbon-carbon bond formation reactions,[8,9] however, due to its unstable nature, examples of a fully characterized acceptor carbene complex are rare.[4]

Chapter 1: Introduction

1.1.1: Fischer carbene complexes

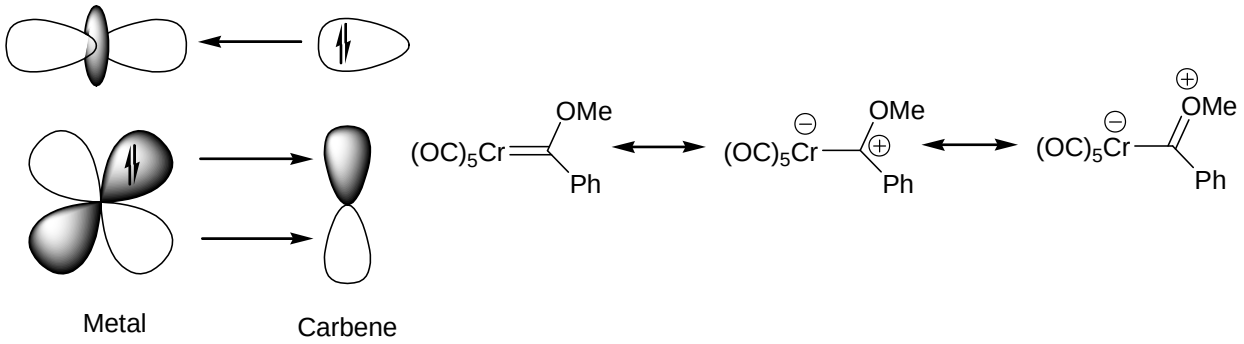

Scheme 1.1: Metal-carbon bonding in Fischer carbene complexes.

As a result of the relative stability of Fischer carbene complexes, their chemistry in synthesis and application has been thoroughly reviewed by different research groups.[6,10,11] Fischer carbene complexes can be simply defined as transition metal-carbon double bond complexes featuring strong π-acceptors and an electrophilic carbene carbon atom bound to the metal. The metal-carbon bond is formed by mutual donor-acceptor interactions of two closed shell fragments (Scheme 1.1):[5] the dominant bonding interaction arises from carbene-mental σ-donation and simultaneous metal-carbene π-back donation.

Fischer carbene complexes are most commonly prepared from non-carbene complex precursors or by modification of pre-existing carbene complexes.

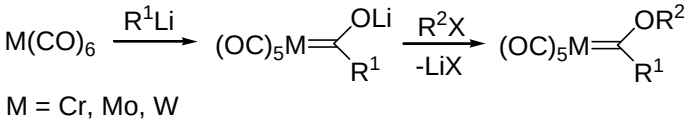

Scheme 1.2: Fischer route to Group 6 metal alkoxycarbene complexes.

The "Fischer route" is the original and still most general entry to access Fischer-type carbenes. This route involves the sequential addition of a carbon nucleophile and an electrophile across a metal-coordinated carbonyl ligand to yield the Fischer alkoxycarbene complex.[12] The air-stable, low oxidation state Group 6 metal hexacarbonyl precursors are commonly employed as metal precursors, preventing side-reactions of the lithiated substrates with coligands other than the carbonyl ligands, and yielding stable alkoxycarbene products.

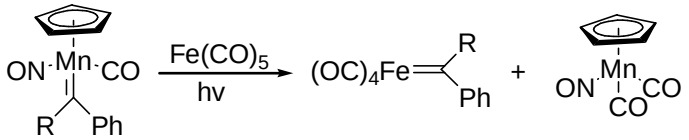

Scheme1.3: The first report of a carbene ligand transfer between metal ions.[13]

Chapter 1: Introduction

The second most common synthetic methodology to prepare Fischer carbene complexes is *via* the metal-metal exchange route. The carbene ligand is stoichiometrically transferred from a pre-existing Fischer carbene metal complex to another metal ion.[13] This route has been used recently to gain access to late transition metal Fischer carbene complexes for applications in stoichiometric organic syntheses.[14]

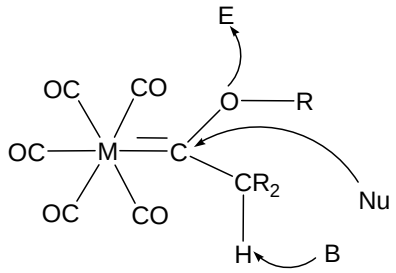

Figure 1.2: Reactivity of Fischer carbene complexes.

Fischer carbene complexes can undergo reactions at several sites as indicated in Figure 1.2 above. Carbyne complexes can be formed from the coordination of electrophiles (E) to the alkoxy substituent of the carbene complex. The electrophilic carbene carbon is prone to nucleophilic attacks (Nu), and alkyl carbene complexes can be deprotonated by bases (B) depending on the acidity of the α-CH group. Additionally, the carbonyl ligands around the metal atom can also be replaced by neutral 2-electron donor ligands.

1.1.2: Late transition metal Fischer carbene complexes

The first reported example of a late transition metal Fischer carbene complex was by Fischer in the early 1970's (Scheme 1.3).[13] Since then, the interest in the chemistry of late-transition metal complexes has significantly increased due to the versatile applications of late-transition metals in catalysis and biological studies. Late transition metal carbenes can be accessed via several different routes such as the Aldol-type condensation of isocyanides and aldehydes,[15] the reversible reaction of Group 8 (Fe, Ru) or Group 9 (Co, Rh) carbonyl complexes with zirconium hydrides,[16] stoichiometric metal-metal exchange (transmetallation) between Group 6 (Cr, Mo, W) carbene complexes and late transition metal complexes,[17]amongst others.[18–20]

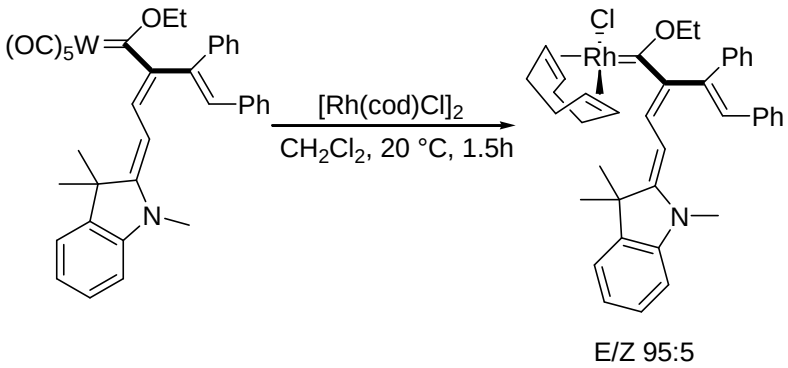

Scheme 1.4: The first explicitly characterized transmetallated Fischer carbene.[21]

Chapter 1: Introduction

The transmetallation/carbene transfer route is the simplest route to isolate a late transition metalcarbene complex in high yields. One of the earliest stable transmetallated Fischer carbene complex from a Group 6 to a late transition metal was reported by Sierra and co-workers in 1998,[22] but was only fully characterized in 2001 (Scheme 1.4).[23,21] Examples of late transition metal Fischer carbene complexes obtained from metal-metal exchange processes include iron, rhodium, iridium, nickel, palladium, platinum, copper, silver, and gold.[17,21,24–26] Gold carbene complexes are stabilized by aurophilic interactions, which can be simply defined as the aggregation of gold complexes via formation of weak gold-gold bonds.[27] Some examples of more unstable gold Fischer carbene complexes have been used for carbene ligand dimerization reactions.[28]

Late transition metals bonded to carbene ligands open up more avenues in the study and application of these complexes because of the consequent reduced stability and inferred increased reactivity of the carbene complex, compared to other organometallic ligands. More focus is given to the rhodium-containing Fischer carbene complexes because in addition to their applications in organic syntheses (such as carbene ligand dimerization, stoichiometric cyclization, benzannulation, etc),[21,26] these complexes can potentially also be used for catalytic reactions. However, examples of rhodium(I) Fischer carbene isolated via transmetallation are rare,[23,25,26] leaving room for exploration in this aspect.

1.2: Fischer Carbenes in Catalysis

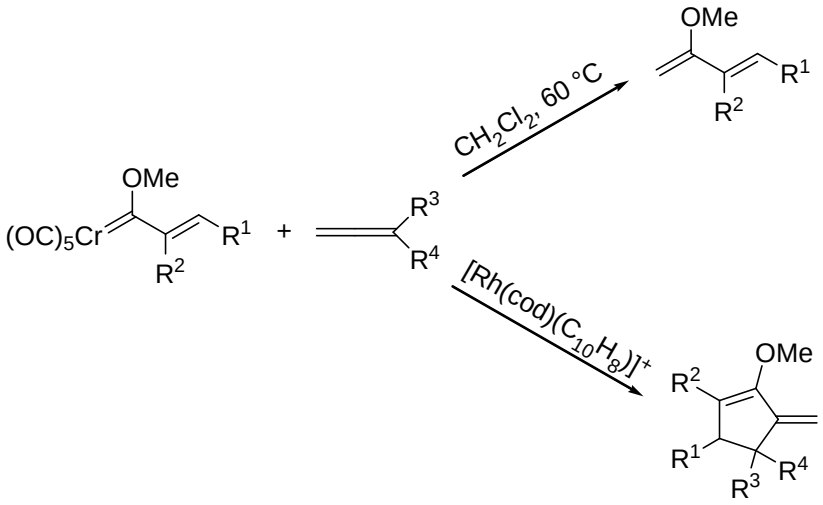

Scheme 1.5: Reactivity of Fischer alkenylcarbene complex with allenes.

Examples of catalytic processes mediated by Fischer carbenes are much more limited than for any of the other classes of carbenes. The most common example of the use of Fischer carbenes in catalysis involves the application of Group 6 (Cr, W) Fischer carbene complexes as metal-containing precursors in organic synthesis, in the presence of a late-transition metal catalyst.[21,29] Studies suggest that a late-transition metal carbene complex is always formed during the catalyzed process and in fact acts as precursor for the organic synthesis.[26] Fischer carbene complexes are also prone to nucleophilic attack on the electrophilic carbene carbon by allenes or alkynes in the presence or absence of a late transition metal catalyst(Scheme 1.5).[29,30]

Chapter 1: Introduction

The catalytic mechanism for the organic syntheses suggest that during the group 6 to late transition metal carbene transfer process, both the mono- and biscarbene complexes form, and it is the biscarbene complex which undergoes self-dimerization to form the consequent alkene product (Scheme 1.6).

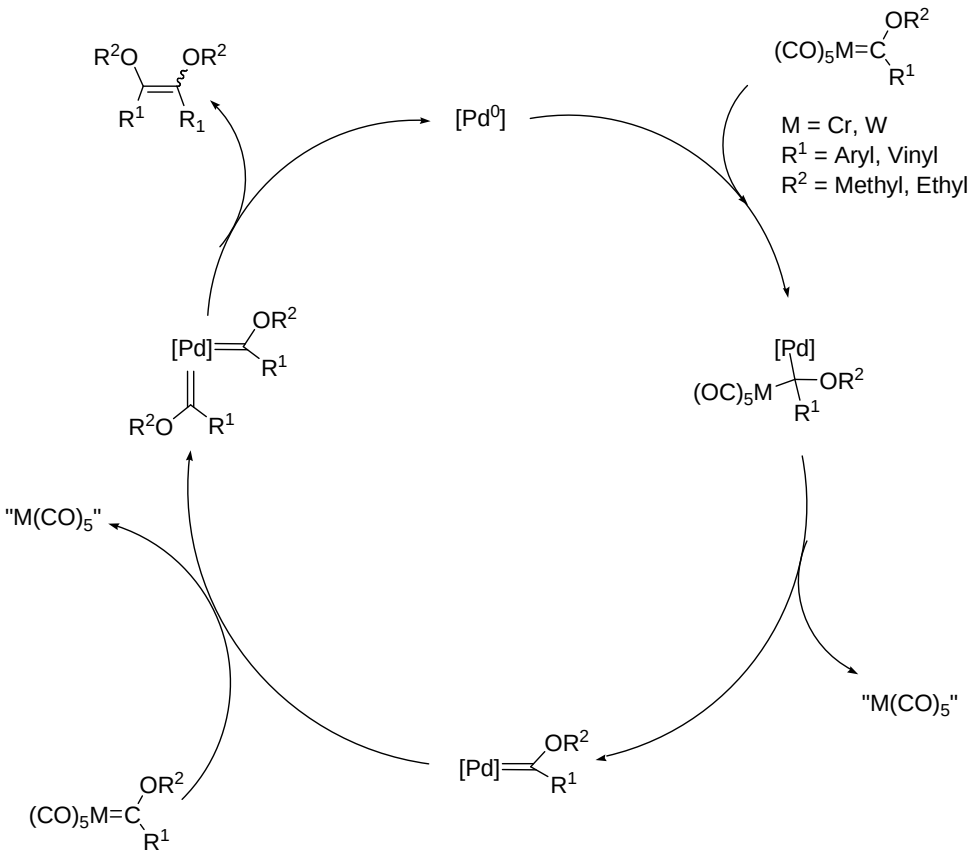

Scheme 1.6: Proposed catalytic cycle from Cr^0- and W^0- to Pd^0 carbene complexes.[31]

The mechanism suggests that the metal-metal exchange process occurs to facilitate the new carbon-carbon bond formation due to the increased reactivity of the transmetallated late transition metal Fischer carbene complex. In addition, specific neutral alkenes can be selectively isolated and the synthetic potential of Fischer carbenes can be expanded by varying the substituents around the carbene carbon.[32] Studies also show that to circumvent the limited self-dimerisation of chromium carbenes, nickel and rhodium carbenes can be used as they cyclo-add to substituted allenes, providing the opportunity for the fine tuning of the chemo- and regioselectivity of the products formed.[33] It should be noted that no methyl-carbene complexes have been applied in literature for organic synthesis to avoid the potential β-hydride elimination.[34]

Chapter 1: Introduction

1.3: Hydroformylation

1.3.1: Overview

Hydroformylation is an important homogeneously catalyzed industrial and commercial process for the production of aldehydes from alkenes.[2] During this process, alkene isomers and branched aldehydes may also form in the presence of a catalyst, in addition to the commercially preferred linear aldehydes. Linear aldehydes are the more preferred products of hydroformylation because they are industrially applicable as precursors for the production of plasticizers, acetic acid, detergents, as ingredients in flavours and perfumes, etc.[35,36] To this effect, the ideal catalyst would demonstrate high activity (high conversion of substrate olefin and high turnover numbers), as well as good chemoselectivity (facilitate only the conversion of starting material to either linear or branched aldehydes without any alkene isomerization to form internal alkenes), as well as good regioselectivity (maximum formation of linear aldehydes instead of branched aldehydes) to allow for minimal compound separation after the catalysis.

1.3.2: Rhodium-catalyzed hydroformylation

Rhodium-containing hydroformylation catalysts are relatively more stable and require milder reaction conditions than other metal-catalysts, and generally give better reactivity rates and chemoselectivity towards the formation of aldehydes.[37]

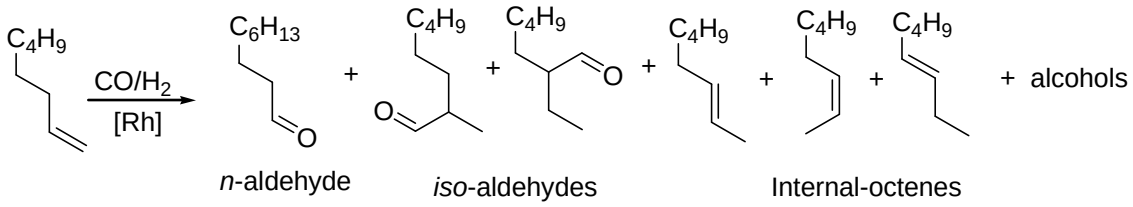

Scheme 1.7: Rhodium-catalyzed hydroformylation of 1-octene.

Before the discovery of Wilkinson's catalyst,[38] different transition metals were applied as catalysts for the hydroformylation of terminal olefins, including mixed transition metal catalysts such as rhodium-cobalt salts. Wilkinson and co-workers found that through the addition of phosphorous ligands, rhodium-catalyzed hydroformylation can be performed under mild conditions, but too many phosphorous ligands can deactivate the catalysts, so it is ideal to replace one phosphorous ligand with a carbonyl ligand to yield the catalyst *trans*-carbonylbis(triphenylphosphine)rhodium(I) chloride.

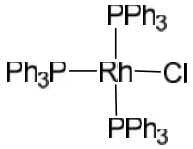

Figure 1.3: Commercially available Wilkinson's catalyst.

Chapter 1: Introduction

Since this revelation was made, many variations of Wilkinson's catalyst have been thoroughly studied to increase the rate and selectivity during the hydroformylation process.[39–41] The catalytic activity of rhodium can also be investigated in terms of the "reusability" of the catalysts. This is studied in biphasic systems wherein the water-soluble catalyst remains in one phase and the products in another, availing the catalyst to be reused without losing its homogeneous catalytic activity and selectivity and allowing for a facile catalyst separation.[42]

To find application in catalysis, the proposed, rationally designed auxiliary ligand has to be stable enough upon coordination to the metal centre, to be included in the catalytic coordination sphere.Thus, optimizing said ligand becomes a very important and interesting aspect for the catalytic reaction. For the catalyzed hydroformylation reaction, sufficient electron density around the rhodium metal center is required for maximum conversion of terminal olefins to the more preferred linear aldehydes.[41]

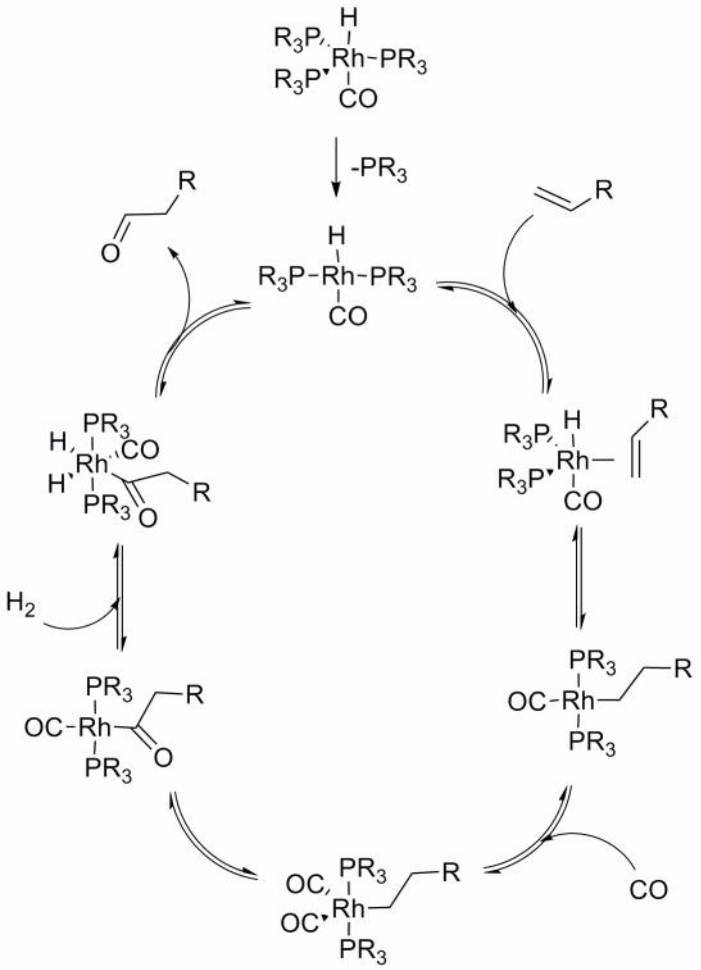

Scheme 1.8: Wilkinson's hydroformylation catalytic cycle.[43]

From the catalytic conversion of terminal alkenes to aldehydes, it is well understood that the modulation of the steric and electronic properties of the commonly-used phosphine ligands has been directed towards the optimization of both the activity and the selectivity of these rhodium-based

Chapter 1: Introduction

catalysts. Specifically, an increase in the *n*/*iso* ratio of the aldehydes has been found due to a high steric demand around the rhodium-center when excess phosphines were employed, or when phosphines with stronger π-acceptor properties were used.[39,44] The status quo with regards to rhodium carbene (NHC) complex catalysts for hydroformylation will be discussed in Chapter 5.

1.4: Aim

The chemistry of group 6 Fischer carbene complexes has been thoroughly studied and can be controlled and manipulated. However, examples of isolated group 8 transition metal, and specifically rhodium(I) Fischer carbene complexes, are rare,[23,25] although they have been implicated as the catalytically active intermediates in the cyclization of allenes and alkynes with Group 6 Fischer alkenylcarbene complexes. This constitutes one of the few examples of the catalytic use of Fischer carbene complexes. The use of rhodium(I) Fischer carbene complexes in the catalytic hydroformylation of alkenes is, however, unexplored in the literature.

The Fischer method will be used to synthesize Group 6 heteroaryl and ferrocenylcarbene complexes and the metal-metal exchange process will be used to obtain the rhodium(I) ferrocenylcarbene complexes. The general aim of this project is to:

a) Synthesize group 6 Fischer carbene complexes
b) Synthesize via transmetallation novel rhodium(I) carbene complexes and fully characterize by means of spectroscopic and electrochemical techniques.
c) Screening of the new rhodium(I) carbene complexes as hydroformylation catalyst precursors.

Chapter 1: Introduction

1.5: References

1 E. O. Fischer; A. Maasbol, *Angew. Chemie - Int. Ed.*, 1964, **3**, 580–581.

2 W. Gil and A. M. Trzeciak, *Coord. Chem. Rev.*, 2011, **255**, 473–483.

3 M. a. Esteruelas, A. I. González, A. M. López and E. Oñate, *Organometallics*, 2003, **22**, 414–425.

4 K. P. Kornecki, J. F. Briones, V. Boyarskikh, F. Fullilove, J. Autschbach, K. E. Schrote, K. M. Lancaster, H. M. L. Davies and J. F. Berry, *Science*, 2013, **342**, 351–354.

5 P. de Frémont, N. Marion and S. P. Nolan, *Coord. Chem. Rev.*, 2009, **253**, 862–892.

6 J. W. Herndon, *Coord. Chem. Rev.*, 2014, **272**, 48–144.

7 B. van der Westhuizen, P. J. Swarts, I. Strydom, D. C. Liles, I. Fernández, J. C. Swarts and D. I. Bezuidenhout, *Dalt. Trans.*, 2013, **42**, 5367–5378.

8 C. M. Che, J. S. Huang, F. W. Lee, Y. Li, T. S. Lai, H. L. Kwong, P. F. Teng, W. S. Lee, W. C. Lo, S. M. Peng and Z. Y. Zhou, *J. Am. Chem. Soc.*, 2001, **123**, 4119–4129.

9 E. Nakamura, N. Yoshikai and M. Yamanaka, *J. Am. Chem. Soc.*, 2002, **124**, 7181–7192.

10 D. I. Bezuidenhout, S. Lotz, D. C. Liles and B. van der Westhuizen, *Coord. Chem. Rev.*, 2012, **256**, 479–524.

11 H. G. Raubenheimer, *Dalt. Trans.*, 2014, **43**, 16959–16973.

12 E. O. Fischer and A. Maasböl, *Chem. Ber.*, 1967, **100**, 2445–2456.

13 E. O. Fischer and H.-J. Beck, *Angew. Chemie Int. Ed. English*, 1970, **9**, 72–73.

14 K. H. Dötz and J. Stendel, *Chem. Rev.*, 2009, **109**, 3227–3274.

15 Y. Motoyama, K. Shimozono, K. Aoki and H. Nishiyama, *Organometallics*, 2002, **21**, 1684–1696.

16 P. T. Barger and J. E. Bercaw, *Organometallics*, 1984, **3**, 278–284.

17 S.-T. Liu and K. Rajender Reddy, *Chem. Soc. Rev.*, 1999, **28**, 315–322.

18 W. P. Fehlhammer, K. Bartel and W. Petri, *J. Organomet. Chem.*, 1975, **87**, C34–C36.

19 K. R. Grundy and W. R. Roper, *J. Organomet. Chem.*, 1975, **91**, C61–C64.

Chapter 1: Introduction

20 G. Erker, R. Lecht, Y.-H. Tsay and C. Krüger, *Chem. Ber.*, 1987, **120**, 1763–1765.

21 I. Göttker-Schnetmann, R. Aumann and K. Bergander, *Organometallics*, 2001, **20**, 3574–3581.

22 M. a. Sierra, M. J. Mancheno, E. Saez and J. C. Del Amo, *J. Am. Chem. Soc.*, 1998, **120**, 6812–6813.

23 I. Göttker-Schnetmann and R. Aumann, *Organometallics*, 2001, **20**, 346–354.

24 I. Fernández, M. J. Mancheño, R. Vicente, L. a. López and M. a. Sierra, *Chem. - A Eur. J.*, 2008, **14**, 11222–11230.

25 J. Barluenga, R. Vicente, L. a. López and M. Tomás, *J. Organomet. Chem.*, 2006, **691**, 5654–5659.

26 J. Barluenga, R. Vicente, L. a. López, E. Rubio, M. Tomás and C. Álvarez-Rúa, *J. Am. Chem. Soc.*, 2004, **126**, 470–471.

27 H. Schmidbaur, *Chem. Soc. Rev.*, 1995, **24**, 391–400.

28 M. Fañanás-Mastral and F. Aznar, *Organometallics*, 2009, **28**, 666–668.

29 J. Barluenga, R. Vicente, L. a. López and M. Tomás, *J. Am. Chem. Soc.*, 2006, **128**, 7050–7054.

30 J. Barluenga, R. Vicente, L. a. López and M. Tomás, *Tetrahedron*, 2005, **61**, 11327–11332.

31 M. P. López-Alberca, I. Fernández, M. J. Mancheño, M. Gómez-Gallego, L. Casarrubios and M. a. Sierra, *European J. Org. Chem.*, 2011, **6**, 3293–3300.

32 J. Barluenga, R. Vicente, P. Barrio, L. A. López, M. Tomás and J. Borge, *J. Am. Chem. Soc.*, 2004, **126**, 14354–14355.

33 J. Barluenga, P. Barrio, L. Riesgo, L. a. López and M. Tomás, *Tetrahedron*, 2006, **62**, 7547–7551.

34 J. C. Del Amo, M. J. Mancheño, M. Gómez-Gallego and M. a. Sierra, *Organometallics*, 2004, **23**, 5021–5029.

35 C. M. Fairchild, *Anal. Chem.*, 1967, **39**, 22A–34A.

36 M. G. Mura, L. De Luca, M. Taddei, J. M. J. Williams and A. Porcheddu, *Org. Lett.*, 2014, **16**, 2586–2589.

37 N. C. Antonels, J. R. Moss and G. S. Smith, *J. Organomet. Chem.*, 2011, **696**, 2003–2007.

38 D. Evans, J. A. Osborn and G. Wilkinson, *J. Chem. Soc. A Inorganic, Phys. Theor.*, 1968, 3133–3142.

39 A. Van Rooy, P. C. J. Kamer, P. W. N. M. Van Leeuwen, K. Goubitz, J. Fraanje, N. Veldman and A. L. Spek, *Organometallics*, 1996, **15**, 835.

Chapter 1: Introduction

40 A. C. Chen, L. Ren, A. Decken and C. M. Crudden, *Organometallics*, 2000, **19**, 3459–3461.

41 M. Sparta, K. J. Børve and V. R. Jensen, *J. Am. Chem. Soc.*, 2007, **129**, 8487–8499.

42 S. Siangwata, N. Baartzes, B. C. E. Makhubela and G. S. Smith, *J. Organomet. Chem.*, 2015, **796**, 26–32.

43 S. A. Decker and T. R. Cundari, *Organometallics*, 2001, **20**, 2827–2841.

44 C. A. Tolman, *Chem. Rev.*, 1977, **77**, 313–348.

Chapter 2: Group 6 Fischer carbene complexes

2.1: Background

The first heteroatom stabilized carbene complex was incorrectly reported by King in 1963 as a dinuclear complex without a carbene ligand (Figure 2.1 (a)),[1] a year before Fischer reported his now-famed pentacarbonyl tungsten methoxycarbene complex (Figure 2.1 (b)). Fischer found that the heteroatom (X) lone electron pair stabilizes the $p_{carbene}$-p_x π-bonding with electrophilic carbene carbon atom.[2] Although King's complex was later correctly characterized by Casey in 1970, who proved it to be the first synthesized heteroatom stabilized carbene complex (Figure 2.1 (c)),[3] all credit is still given to Fischer for the discovery.

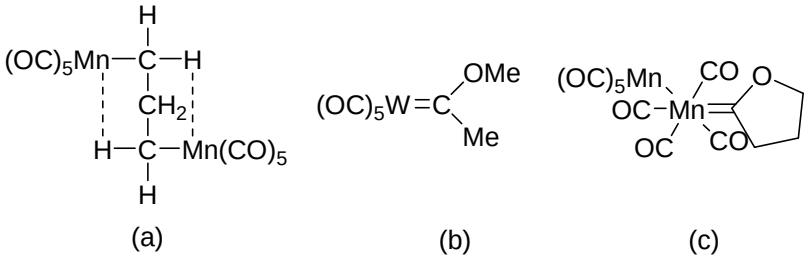

Figure 2.1: (a) King's incorrectly characterized dimanganese complex, (b) the first reported Fischer carbene complex, and (c) the corrected cyclic Fischer carbene complex structure of (a).

One of the earliest examples of a characterized Fischer carbene complex contained a phenyl ring as carbene substituent, which was shown to play a part in the π-delocalization network around the carbene carbon (see Figure 2.2).[4] This finding initiated the interest in the study of (hetero)aryl substituted carbenes.

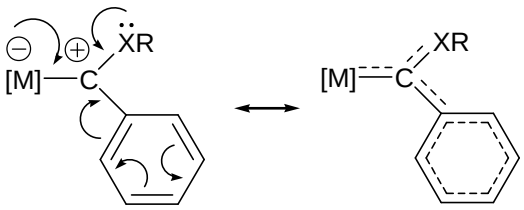

Figure 2.2: π-delocalized network around a Fischer carbene carbon atom.

The strong electron withdrawing character of the metal-pentacarbonyl fragment bound to the carbene carbon results in the electrophilic character of the carbene carbon atom which is a target for nucleophilic reagents. The metallic moiety introduces an electron deficiency which extends to other positions of the unsaturated carbene ligand, more so in aryl- than alkenylcarbene complexes.[5] This observation in turn speaks to the above mentioned π-delocalized network around arylcarbenes, which is limited in alkenylcarbenes. Depending on the nature of the nucleophile and steric boundaries around the carbene carbon, other positions can undergo nucleophilic attack for the diastereoselective and enantioselective synthesis of a number of functionalized organic molecules (Figure 2.3).

Chapter 2: Group 6 Fischer carbene complexes

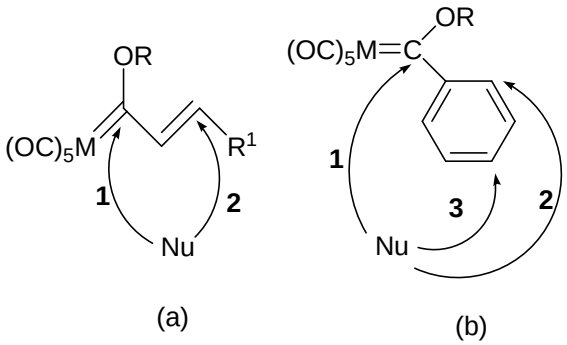

1: 1,2-addition; **2:** 1,4-addition; **3:** 1,6-addition

Figure 2.3: Nucheophilic attacks on alkenyl (a) and aryl (b) Fischer carbene complexes.

2.1.1: Heteroaryl Fischer carbene complexes

Aryl or heteroaryl substituted Fischer carbene complexes are more stable than their alkyl or alkenyl counterparts. This is due to the ability of the aryl or heteroaryl substituent to act as either an electron withdrawing or donating substituent to the carbene carbon atom. For instance, a *para*- substituted phenyl ring (for example *p*-NMe_2Ph or *p*-CF_3Ph) can either (respectively) donate electrons towards or withdraw from the carbene carbon atom. In the case of the stable $W(CO)_5C(Ph)Ph$ carbene complex, the unsubstituted phenyl substituent donates electron density to the carbene carbon.[4] To investigate the extent to which heteroaryl ligands stabilize the carbene carbon, Connor and Jones synthesized the first heteroaryl Fischer carbene complexes in 1971 (Figure 2.4). From this study, it was concluded that the heteroatom's donor ability towards stabilizing the carbene carbon increases in the order O<S<NMe by employing vibrational spectroscopic data to investigate kinetic and potential energy matrices.[6] In this study, a finite set of rules was defined for metal carbonyl complexes including those of the form $ML(CO)_5$, after which a series of calculations were carried out to consequently deduce values of λ, which were used to evaluate the respective energies of the complexes, and thus a stability-energy relationship was established.[7]

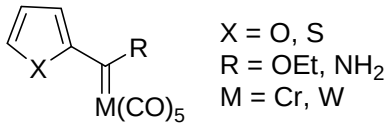

Figure 2.4: Group 6 heteroaryl monocarbene complexes.

The stability trend established by Connor has been attested to by the electrochemical studies done on Fischer carbenes over the last decade.[8–11] From the cyclic voltammetry studies, it has been shown that the electron-poor carbene double bond is reduced (Scheme 2.1(a)) while the carbene metal is oxidized (Scheme 2.1(b)).[12]

Chapter 2: Group 6 Fischer carbene complexes

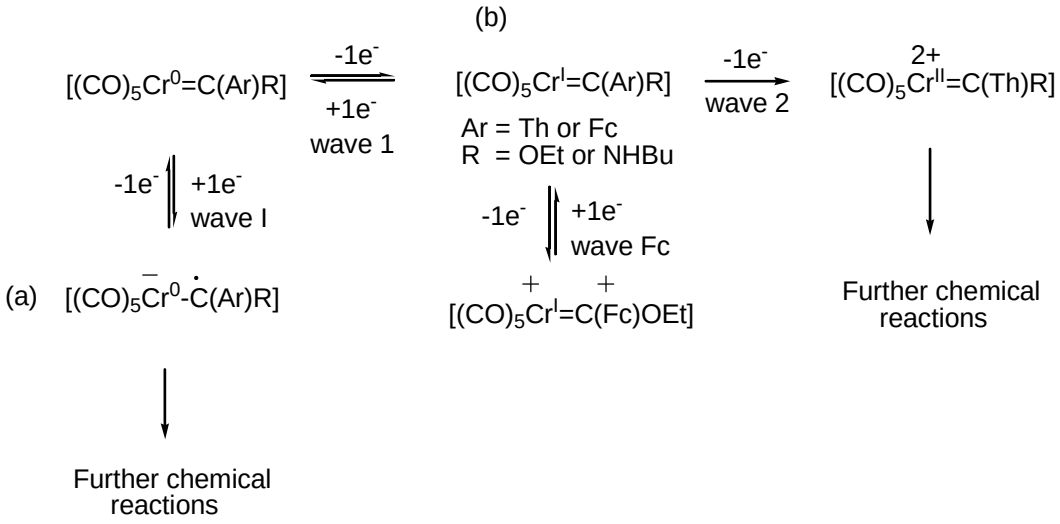

Scheme 2.1: Electrochemical reactions associated with selected chromium carbene complexes.[12]

It is noteworthy that the oxidation of the carbene metal was found to occur in either a 1 or 2-electron transfer reaction for chromium[10,12] or tungsten[13] respectively. More electron-donating heteroaryl substituents (ie. more carbene-stabilizing substituents) result in an increased ease of oxidation of the metal redox couple, and decreased ease of the metal-carbene bond reduction. Thus, Fischer carbene complexes containing the strongly donating ferrocenylcarbene substituent result in a more electron-rich Cr=C functionality than either thienyl or furyl substituents, due to their increased stability.[14,15]

2.1.2: Preparatory methods

The most common synthesis method towards Fischer carbene complexes is the so-called Fischer route,[16] which involves the addition of an organolithium reagent to a metal carbonyl to give an acyl metalate. This is followed by O-alkylation of the acylate by a strong alkylating agent such as trialkyloxonium salts, flourosulfonates or alkyl triflouromethanesulfonates (Scheme 2.1).

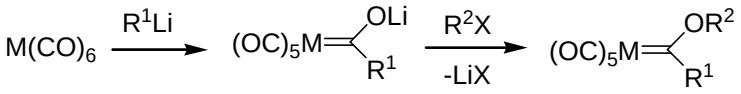

M = Cr, Mo, W
R^1 = alkyl, aryl, vinyl
R^2 = Et, Me

Scheme 2.2: The classic synthetic route for the preparation of Fischer carbene complexes.

The use of a lithiated organometallic compound as organolithium reagent provides access to bimetallic carbene complex formation (Scheme 2.2).[17] Bimetallic carbene complexes paves the way towards push-pull systems where the electron withdrawing metal carbonyl fragment can be further activated by a second electron withdrawing organometallic moiety that acts as an electron sink (Figure 2.5 (a)), for

Chapter 2: Group 6 Fischer carbene complexes

example a π-aryl metal carbonyl group. Alternatively, a donating organometallic fragment such as a ferrocenyl group (Figure 2.5(b)), can facilitate electron donation (as electron reservoir) to the electron poor metal carbonyl group.[17,18]

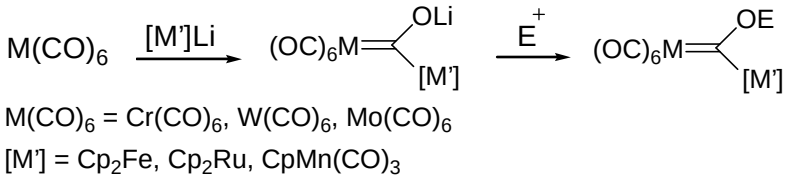

Scheme 2.3: Synthesis of bimetallic monocarbene complexes.[17]

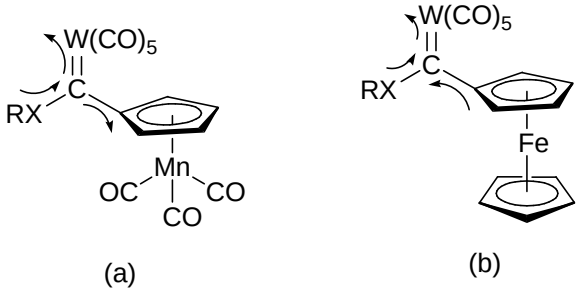

Figure 2.5: Metal substituent effect in bimetallic carbene complexes depicting electron donation towards (a) and withdrawal from (b) the carbene carbon atom.

2.2: Aim

The aim of this chapter is the synthesis of known mono- and bisalkoxycarbene complexes of chromium and tungsten, containing thienyl, furyl and ferrocenyl substituents, as precursors for the transmetallation reaction to late transition metals in subsequent chapters (Figure 2.6, complexes **1**-**11**). Simple aminolysis of the alkoxycarbene ligands of the thienyl- and ferrocenylcarbene complexes of tungsten and chromium respectively yielded the corresponding aminocarbene complexes (**12** and **13**) (see Figure2.6). The aminocarbene complexes of thienyl and ferrocenyl complexes were later synthesized to test their effect on transmetallation (Chapter 3). However, all attempts at transmetallation with aminocarbene complex precursors were unsuccessful. The complexes were thereafter characterized using NMR and infrared spectroscopy for to confirm their identity and purity as compared to previous literature findings.

Chapter 2: Group 6 Fischer carbene complexes

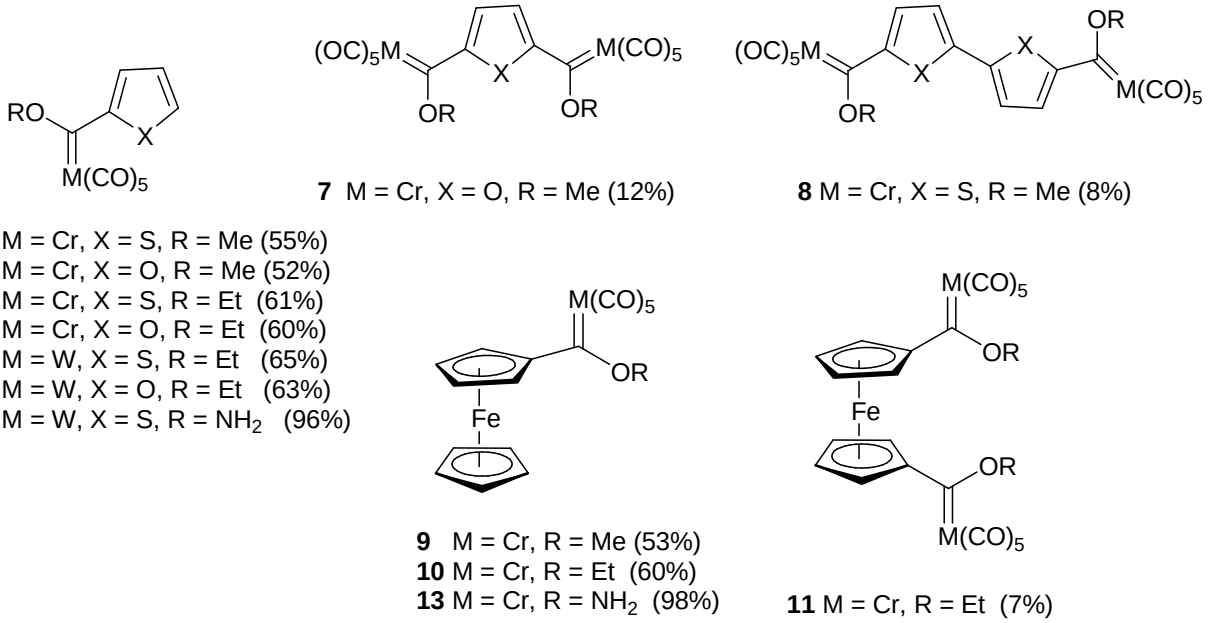

1 M = Cr, X = S, R = Me (55%)
2 M = Cr, X = O, R = Me (52%)
3 M = Cr, X = S, R = Et (61%)
4 M = Cr, X = O, R = Et (60%)
5 M = W, X = S, R = Et (65%)
6 M = W, X = O, R = Et (63%)
12 M = W, X = S, R = NH_2 (96%)

7 M = Cr, X = O, R = Me (12%)

8 M = Cr, X = S, R = Me (8%)

9 M = Cr, R = Me (53%)
10 M = Cr, R = Et (60%)
13 M = Cr, R = NH_2 (98%)

11 M = Cr, R = Et (7%)

Figure 2.6: Thienyl, furyl and ferrocenyl mono- and biscarbene complexes of chromium(0) and tungsten(0) pentacarbonyl prepared in this chapter.

2.3: Results and Discussions

2.3.1: Synthesis

The Fischer method was adapted for the syntheses of the desired alkoxy monocarbene complexes.[12] In a number of cases, the use of excess lithiating agent resulted in the formation of the corresponding biscarbene complexes as side-products in low yield (complexes **7**, **8** and **11**).

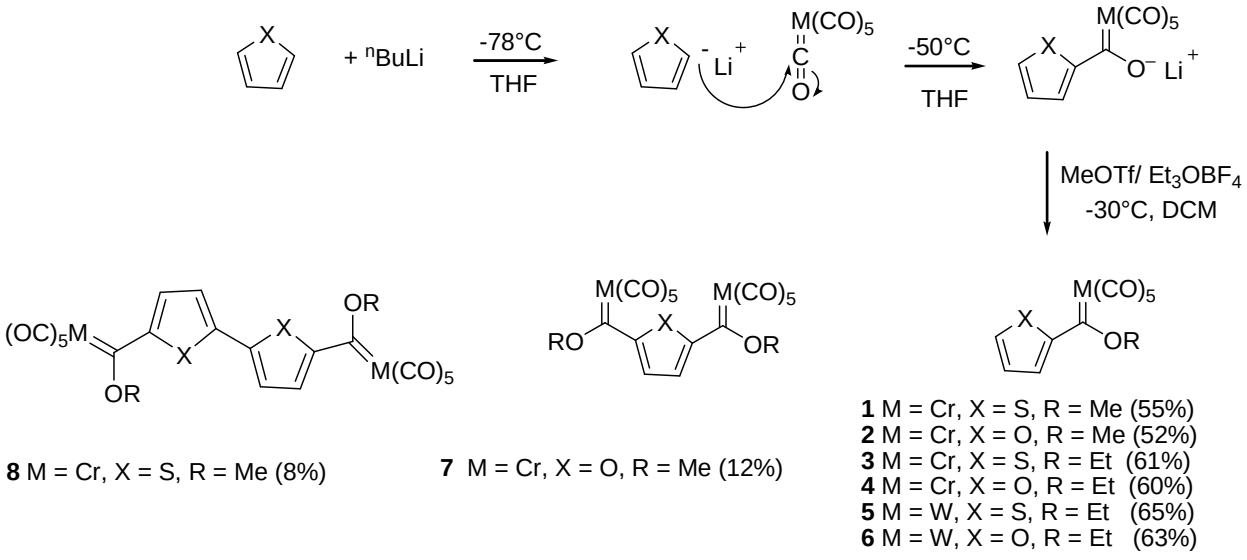

8 M = Cr, X = S, R = Me (8%)

7 M = Cr, X = O, R = Me (12%)

1 M = Cr, X = S, R = Me (55%)
2 M = Cr, X = O, R = Me (52%)
3 M = Cr, X = S, R = Et (61%)
4 M = Cr, X = O, R = Et (60%)
5 M = W, X = S, R = Et (65%)
6 M = W, X = O, R = Et (63%)

Scheme 2.3: Syntheses of complexes **1 – 8**

Chapter 2: Group 6 Fischer carbene complexes

Deprotonation of the α-proton of the heteroarene (thiophene or furan) is achieved by the slow addition of ^{n}BuLi to a solution of the heteroarene in THF at -78°C and stirring the mixture for 30 minutes at that low temperature. After addition of the metal hexacarbonyl to the reaction mixture at -50°C, the resulting nucleophilic α-carbon of the lithiated heteroaryl ring attacks an electron-deficient carbon of the metal hexacarbonyl to form a metal acylate. The THF solvent was removed from the reaction mixture *in vacuo* and the residue thereafter dissolved in dichloromethane (DCM). Alkylation was then achieved by adding methyl trifluoromethanesulfonate or triethyloxonium salt to the metal acylate at -30°C, resulting in the methoxy- or ethoxycarbene complexes, respectively. The desired neutral product was purified and removed from unreacted starting reagents and side-products by column chromatography in yields ranging from 52 – 65% for the monocarbene complexes **1** – **6**. The biscarbene complexes **7** and **8** were obtained in trace amounts (7 – 12%).

The same procedure was followed to obtain the ferrocenylcarbene complexes **9** – **11.** The stronger base ^{t}BuLi was used for the deprotonation of the cyclopentadienyl proton. The use of ^{n}BuLi was avoided as it favours dilithiation of the ferrocene, resulting in the ferrocenyl biscarbene complex being the major product.[12] The biscarbene complexes formed in yields too low to allow for full spectroscopic characterization.

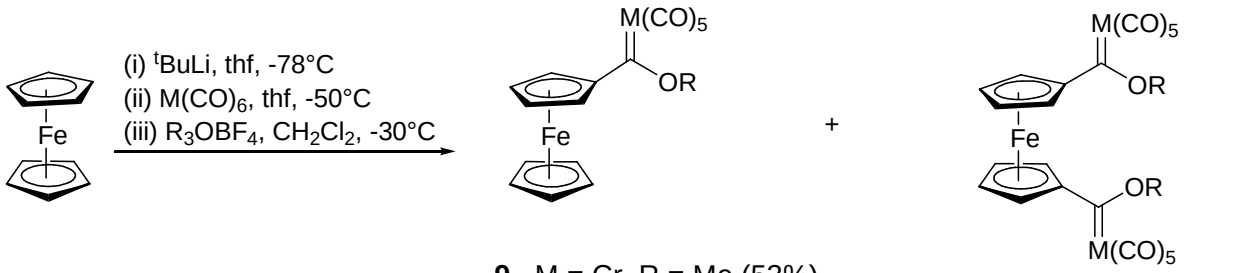

Scheme 2.4: Syntheses of complexes **9** - **11**.

Complexes **12** and **13** were synthesized by the simple aminolyses of complexes **6** and **10** respectively (Scheme 2.5).[8,10] Through a dark red solution of the ethoxycarbene complex precursor in diethyl ether, was bubbled ammonia gas at room temperature until a colour change to yellow was observed. The diethyl ether solvent was dried *in vacuo* to give a bright yellow crystalline solid in high yield (**12**, 89%, **13**, 92%).

Chapter 2: Group 6 Fischer carbene complexes

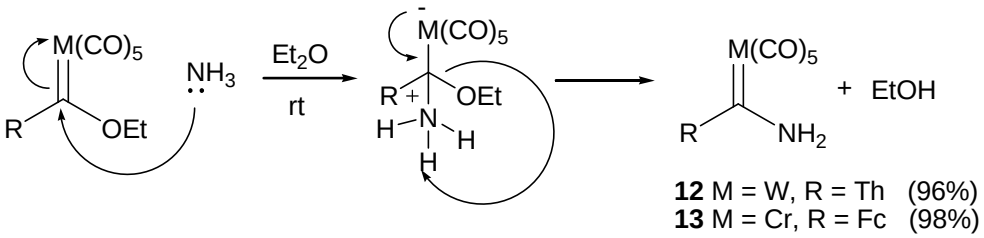

Scheme 2.5: Syntheses of aminocarbene complexes **12** and **13**.

2.3.2: Spectroscopic characterization

The synthesized mono- and biscarbene complexes were characterized in solution using ^{1}H and ^{13}C NMR and infrared spectroscopy, and compared to the reported spectroscopic data for these known compounds as confirmation of product identity.[6,12,15,19–22]

2.3.2.1: NMR Spectroscopy

When coordinated to the metal carbene fragment, the heteroaryl ring proton resonances are shifted downfield due to the electron withdrawing nature of the metal pentacarbonyl moiety. As depicted in Figure 2.7, the π-resonance effect extends throughout the heteroaryl ring .[23] As a result, different metal carbonyl fragments display different chemical shifts for the ring protons of the heterocyclecarbene substituents. The same conclusion can be made for the ferrocenylcarbene complexes, where the electron donor property of the ferrocenyl substituent will result in a more shielded carbene carbon as attested to by the lowered ^{13}C NMR carbene resonance in comparison to those of the furyl and thienyl substituted carbene complexes.

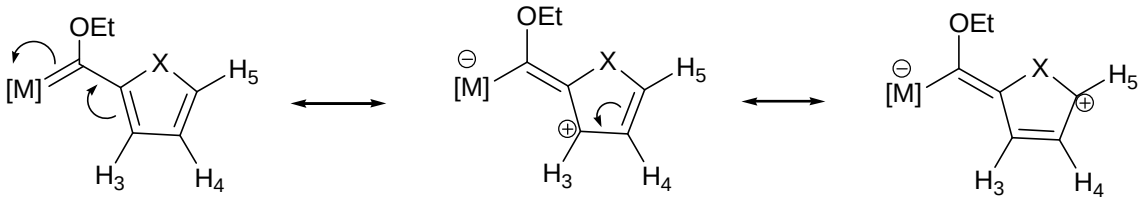

Figure 2.7: π-resonance effects in monocarbene complexes.

The identities of complexes **1 – 13** were confirmed by NMR spectroscopy.[11,12,15] From the ^{1}H NMR spectrum of complex **10** shown in Figure 2.8 below, it can be seen that the substituted cyclopentadienyl ring of the ferrocenyl group is in a symmetrical environment, so that only two proton resonances are observed for the substituted Cp'-ring. This feature was observed for all the Group 6 ferrocenylcarbene

Chapter 2: Group 6 Fischer carbene complexes

carbonyl complexes reported in this chapter. Similarly, the ^{13}C NMR spectra of these complexes also attest to the symmetry of the ferrocenyl carbon resonances.

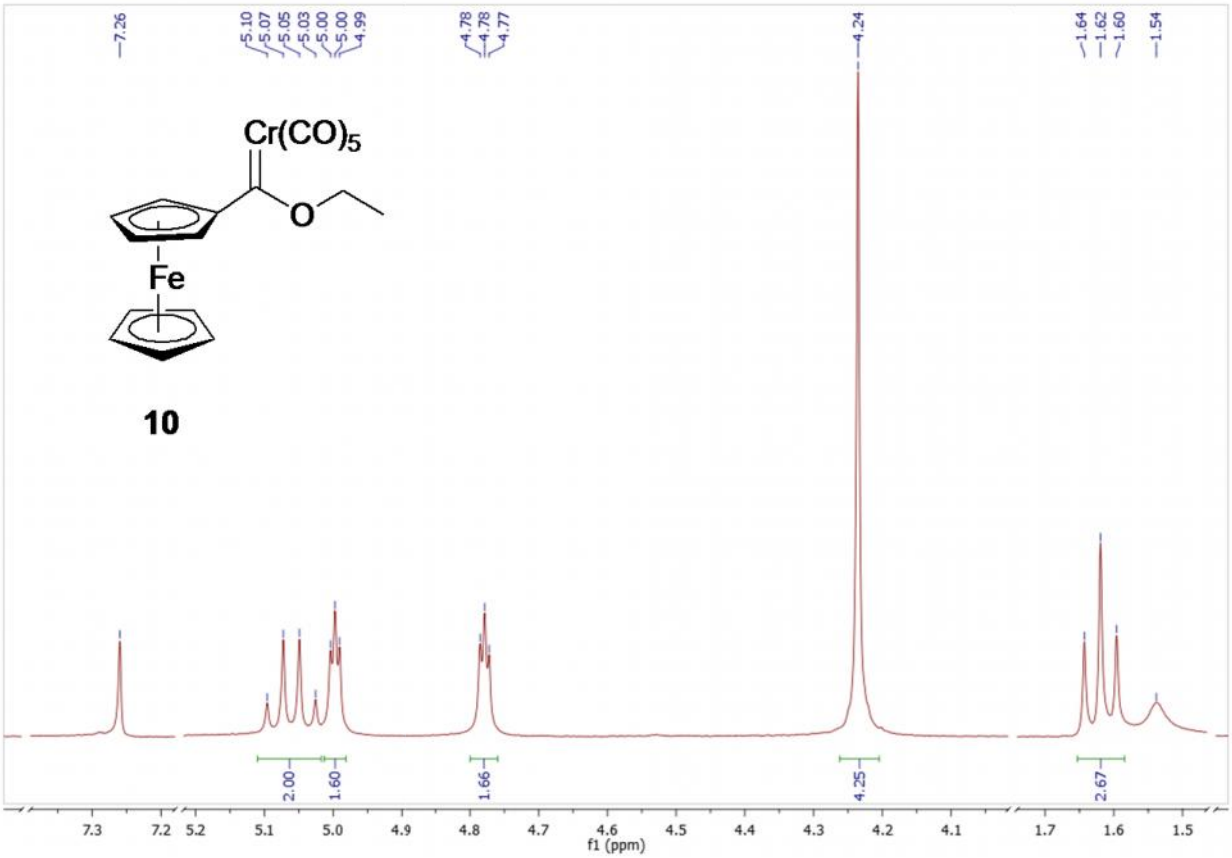

Figure 2.8: ^{1}H NMR spectrum of complex **10**.

2.3.2.2: IR Spectroscopy

Contrary to the M-C stretching frequencies, the C-O stretching vibrational frequencies can be seen as being independent of other vibrations in the molecule, thus the vibrational frequencies and bond orders of the C-O bond can be correlated.[24] The M-C bond order increases with an increase in metal-carbonyl back-bonding. The C-O bond consequently lengthens, shifting the carbonyl stretching vibration to a lower frequency on the IR spectrum. The weak π-acceptor properties of the carbene ligand, compared to the carbonyl ligands, result in increased back-bonding ability of the metal towards the carbonyl ligands with lower wavenumbers of the ν_{CO} bands observed for the carbene complexes compared to the corresponding metal carbonyl precursors.

Chapter 2: Group 6 Fischer carbene complexes

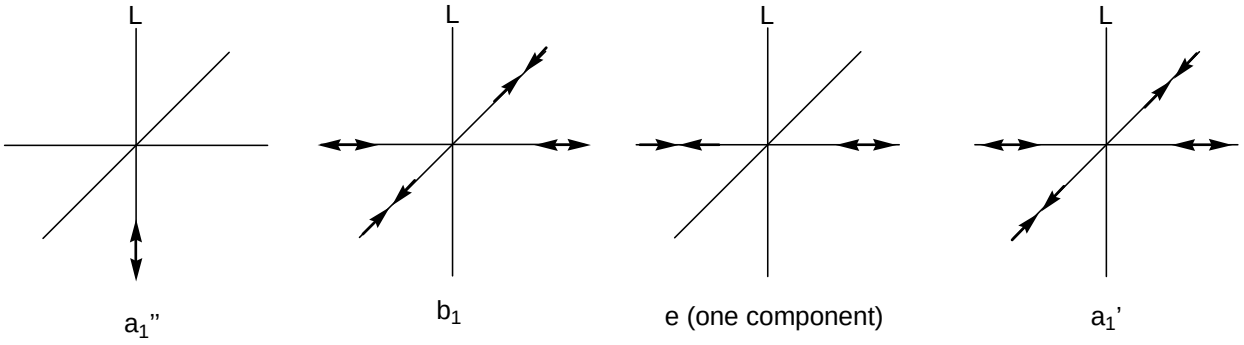

Figure 2.9: IR-active normal modes observed for metal carbonyls with the general formula $M(CO)_5L$.

The Group 6 Fischer carbene complexes $[M(CO)_5(carbene)]$ display a pseudo-C_{4v} symmetry, with the infrared active modes depicted in Figure 2.9 above.[24] The general band pattern observed is an band for the a_1'' vibration mode at higher frequencies, followed by b_1 and a_1', and an intense e-band. The formerly IR-inactive b_1-mode often appears as a weak feature due to the lifting of the section rules by the asymmetry of the carbene ligand. The IR modes on the spectrum are usually labeled as in Figure 2.10 below.[24]

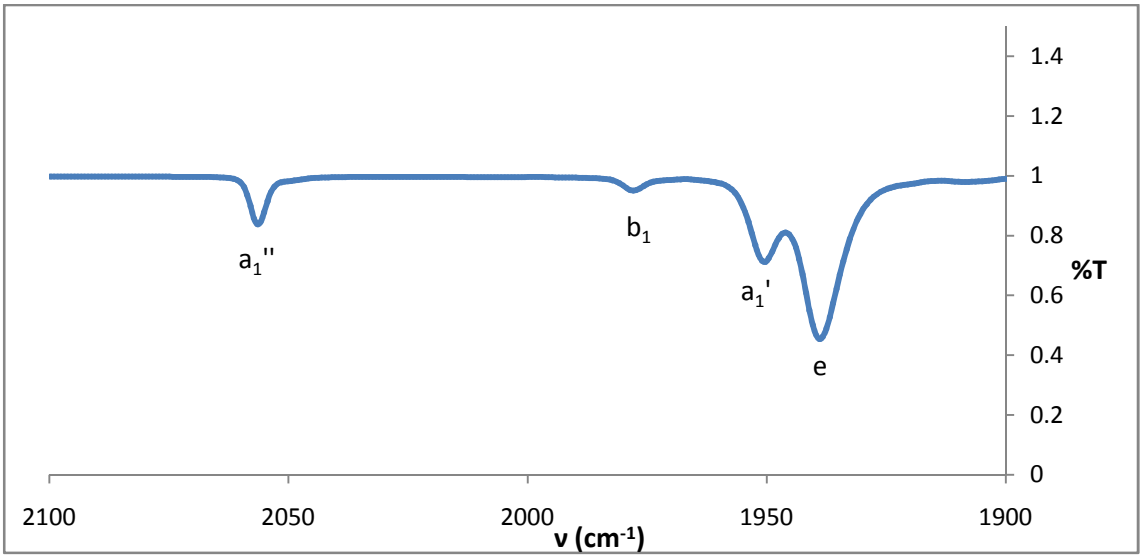

Figure 2.10: IR spectrum in the carbonyl region of complex **10**.

Chapter 2: Group 6 Fischer carbene complexes

2.4: Conclusion

A series of known alkoxy- and aminocarbene complexes of chromium and tungsten were successfully synthesized and characterized via spectroscopic methods. Structure determinations for all complexes were confirmed by comparison with spectroscopic data previously reported in literature. These complexes were synthesized as precursors for further reactions in later chapters.

2.5: Experimental

The preparation, purification and reactions of the complexes described were carried out under an atmosphere of dry, oxygen-free dinitrogen or argon gas, using standard Schlenk techniques. Silica gel 60 (particle size 0.0063-0.200 mm) was used as resin for all separation in column chromatography. Anhydrous tetrahydrofuran, diethyl ether and *n*-hexane were distilled over sodium metal and dichloromethane over CaH_2. All other reagents are commercially available and were used as received. All NMR spectra were obtained in chloroform-d_1 solutions. Infrared spectra of the alkoxycarbene complexes were measured in solvent hexane and the aminocarbene complexes in solvent dichloromethane.

Complexes **1 – 13** were prepared according to literature procedures, thus spectroscopic data have been reported in previous studies.[6,11–13,15]

$[Cr(CO)_5\{C(OMe)(2\text{-thienyl})\}]$ (1)[6]

Yield = 1.12 g, 55%. ^{1}H NMR (300 MHz, $CDCl_3$) δ 8.30 (d, ^3J(HH) = 3.9 Hz, 1H, Th-H_α), 7.74 (d, ^3J(HH) = 4.9 Hz, 1H, Th-H_γ), 7.27 (dd, ^3J(HH) = 5.2 Hz, ^3J(HH) = 4.1 Hz, 1H, Th-H_β), 4.88 (s, 3H, OCH_3). $^{13}C\{^1H\}$ NMR (75 MHz, $CDCl_3$) δ 319.1 ($C_{carbene}$), 223.5 (CO_{trans}), 217.4 (CO_{cis}), 155.6 (Th-C_{ipso}), 141.6 (Th-C_α), 135.4 (Th-C_γ), 129.4 (Th-C_β), 66.6 (OCH_3). IR (hexane) ν(CO/cm^{-1}): 2059 (a''$_1$), 1984 (b_1), 1959 (a'$_1$), 1948 (e).

$[Cr(CO)_5\{C(OMe)(2\text{-furyl})\}]$ (2)[6]

Yield = 1.05 g, 52%. ^{1}H NMR (300 MHz, $CDCl_3$) δ 7.84 (s, br, 1H, Fu-H_γ), 7.00 (s, br, 1H, Fu-H_α), 6.59 (d, br, ^3J(HH) = 5.2 Hz, 1H, Th-H_β), 4.82 (s, 3H, OCH_3). $^{13}C\{^1H\}$ NMR (75 MHz, $CDCl_3$) δ 313.3 ($C_{carbene}$), 224.2

Chapter 2: Group 6 Fischer carbene complexes

(CO_{trans}), 217.2 (CO_{cis}), 164.4 (Fu-C_{ipso}), 150.3 (Fu-C_γ), 113.4 (Fu-C_α), 113.0 (Fu-C_β), 66.3 (OCH_3). IR (hexane) ν(CO/cm^{-1}): 2062 (a''_1), 1993 (b_1), 1963 (a'_1), 1947 (e).

$[Cr(CO)_5\{C(OEt)(2\text{-thienyl})\}]$ (3)[12]

Yield = 1.36 g, 61%. ^{1}H NMR (300 MHz, $CDCl_3$) δ 8.26 (d, ^3J(HH) = 3.6 Hz, 1H, Th-H_α), 7.70 (d, ^3J(HH) = 4.6 Hz, 1H, Th-H_γ), 7.22 (dd, ^3J(HH) = 3.9 Hz, ^3J(HH) = 4.9 Hz, 1H, Th-H_β), 5.18 (q, ^3J(HH) = 7.0 Hz, 2H, $O\underline{CH_2}CH_3$), 1.68 (t, ^3J(HH) = 7.0 Hz, 3H, $OCH_2\underline{CH_3}$). $^{13}C\{^1H\}$ NMR (75 MHz, $CDCl_3$) δ 316.8 ($C_{carbene}$), 223.6 (CO_{trans}), 217.4 (CO_{cis}), 155.8 (Th-C_{ipso}), 141.4 (Th-C_α), 135.2 (Th-C_γ), 129.4 (Th-C_β), 76.4 ($O\underline{CH_2}CH_3$), 15.5 ($OCH_2\underline{CH_3}$). IR (hexane) ν(CO/cm^{-1}): 2059 (a''_1), 1983 (b_1), 1958 (a'_1), 1947 (e).

$[Cr(CO)_5\{C(OEt)(2\text{-furyl})\}]$ (4)[12]

Yield = 0.95 g, 60%. ^{1}H NMR (300 MHz, $CDCl_3$) δ 7.84 (s, br, 1H, Fu-H_γ), 6.99 (s, br, 1H, Fu-H_α), 6.58 (s, br, 1H, Th-H_β), 5.16 (q, ^3J(HH) = 7.1 Hz, 2H, $O\underline{CH_2}CH_3$) 1.65 (t, ^3J(HH) = 6.9 Hz, 3H, $OCH_2\underline{CH_3}$). $^{13}C\{^1H\}$ NMR (75 MHz, $CDCl_3$) δ 313.3 ($C_{carbene}$), 224.3 (CO_{trans}), 217.2 (CO_{cis}), 164.4 (Fu-C_{ipso}), 150.3 (Fu-C_γ), 113.3 (Fu-C_α), 112.7 (Fu-C_β), 76.1 ($O\underline{CH_2}CH_3$), 15.6 ($OCH_2\underline{CH_3}$). IR (hexane) ν(CO/cm^{-1}): 2052 (a''_1), 1985 (b_1), 1960 (a'_1), 1949 (e).

$[W(CO)_5\{C(OEt)(2\text{-thienyl})\}]$ (5)[13]

Yield = 1.52g, 65%. ^{1}H NMR (300 MHz, $CDCl_3$) δ 8.16 (dd, ^3J(HH) = 4.1 Hz, ^4J(HH) = 1.0 Hz, 1H, Th-H_α), 7.82 (dd, ^3J(HH) = 5.0 Hz, ^4J(HH) = 1.0 Hz, 1H, Th-H_γ), 7.22 (dd, ^3J(HH) = 5.0 Hz, ^3J(HH) = 4.1 Hz, 1H, Th-H_β), 5.00 (q, ^3J(HH) = 7.1 Hz, 2H, $O\underline{CH_2}CH_3$), 1.66 (t, ^3J(HH) = 7.1 Hz, 3H, $OCH_2\underline{CH_3}$). $^{13}C\{^1H\}$ NMR (75 MHz, $CDCl_3$) δ 291.1 ($C_{carbene}$), 202.9 (CO_{trans}), 198.0 (CO_{cis}), 158.7 (Th-C_{ipso}), 141.9 (Th-C_α), 136.3 (Th-C_γ), 129.3 (Th-C_β), 78.9 ($O\underline{CH_2}CH_3$), 15.3 ($OCH_2\underline{CH_3}$). IR (dcm) ν(CO/cm^{-1}): 2069 (a''_1), 1988 (b_1), 1963 (a'_1), 1948 (e).

$[W(CO)_5\{C(OEt)(2\text{-furyl}\}]$ (6)[10]

Yield = 1.43g, 63%. ^{1}H NMR (300 MHz, $CDCl_3$) δ 7.88 (dd, ^3J(HH) = 3.6 Hz, ^4J(HH) = 0.7 Hz, 1H, Fu-H_γ), 7.15 (dd, ^3J(HH) = 3.7 Hz, ^4J(HH) = 0.6 Hz, 1H, Fu-H_α), 6.62 (dd, ^3J(HH) = 3.7 Hz, ^3J(HH) = 1.7 Hz, 1H, Fu-H_β), 4.96 (q, ^3J(HH) = 7.1 Hz, 2H, $O\underline{CH_2}CH_3$), 1.64 (t, ^3J(HH) = 7.1 Hz, 3H, $OCH_2\underline{CH_3}$). $^{13}C\{^1H\}$ NMR (75 MHz, $CDCl_3$) δ 285.2 ($C_{carbene}$), 203.7 (CO_{trans}), 197.7 (CO_{cis}), 166.5 (Fu-C_{ipso}), 150.3 (Fu-C_γ), 115.2 (Fu-C_α), 113.8 (Fu-C_β), 78.7 ($O\underline{CH_2}CH_3$), 15.4 ($OCH_2\underline{CH_3}$). IR (dcm) ν(CO/cm^{-1}): 2072 (a''_1), 1979 (b_1), 1960 (a'_1), 1945 (e).

$[Cr(CO)_5\{C(OMe)(2,5\text{-furyl})C(OMe)\}Cr(CO)_5]$ (7)[6,10]

Chapter 2: Group 6 Fischer carbene complexes

Yield = 0.08 g, 12%. ^{1}H NMR (300 MHz, $CDCl_3$) δ 7.22 (s, 2H, Fu-$H_{\alpha,\alpha'}$), 4.92 (s, 6H, OCH_3). $^{13}C\{^{1}H\}$ NMR (75 MHz, $CDCl_3$) δ 315.4 ($C_{carbene}$), 224.4 (CO_{trans}), 216.8 (CO_{cis}), 162.5 (Fu'-C_{ipso}), 118.8 (Fu'-$C_{\alpha,\alpha'}$), 67.0 (OCH_3). IR (hexane) ν(CO/cm^{-1}): 2054 (a''_1), 1995 (b_1), 1962 (a'_1), 1955 (e).

$[Cr(CO)_5\{C(OMe)(2,5\text{-thienyl})(2,5\text{-thienyl})C(OMe)\}Cr(CO)_5]$ (8)[20]

Yield = 0.09g, 8%. ^{1}H NMR (300 MHz, $CDCl_3$) δ 8.19 (d, ^{3}J(HH)=4.4 Hz, 2H, Th'-H_{α}, Th'-$H_{\alpha'}$), 7.47 (d, ^{3}J(HH) = 4.3 Hz, 1H, Th'-H_{β}, Th'-$H_{\beta'}$), 4.85 (s, 6H, OCH_3). $^{13}C\{^{1}H\}$ NMR (75 MHz, $CDCl_3$) δ 321.1 ($C_{carbene}$), 222.0 (CO_{trans}), 218.5 (CO_{cis}), 158.4 (Th',Th'-C_{ipso}), 154.0 (Th',Th'-$C_{\alpha,\alpha'}$), 152.3 (Th',Th'-$C_{\gamma,\gamma'}$), 148.1 (Th',Th'-$C_{\beta,\beta'}$), 67.1 (OCH_3). IR (hexane) ν(CO/cm^{-1}): 2055 (a''_1), 1990 (b_1), 1962 (a'_1), 1951 (e).

$[Cr(CO)_5\{C(OMe)(ferrocenyl)\}]$ (9)[12,19,22]

Yield = 0.98 g, 53%. ^{1}H NMR (300 MHz, $CDCl_3$) δ 5.00 (s, br, 2H, FeCp'-$H_{\alpha,\alpha'}$), 4.79 (s, br, 2H, FeCp'-$H_{\beta,\beta'}$), 4.69 (s, 3H, OCH_3) 4.25 (s, 5H, FeCp). $^{13}C\{^{1}H\}$ NMR (75 MHz, $CDCl_3$) δ 333.4 ($C_{carbene}$), 223.3 (CO_{trans}), 217.7 (CO_{cis}), 93.9 (FeCp'-C_{ipso}), 75.0 (FeCp'), 72.6 (FeCp'), 70.9 (FeCp), 6646 (OCH_3). IR (hexane) ν(CO/cm^{-1}): 2056 (a''_1), 1978 (b_1), 1950 (a'_1), 1939 (e).

$[Cr(CO)_5\{C(OEt)(ferrocenyl)\}]$ (10)[19]

Yield = 1.26 g, 60%. ^{1}H NMR (300 MHz, $CDCl_3$) δ 5.06 (q, ^{3}J(HH) = 7.0 Hz, 2H, $O\underline{CH_2}CH_3$), 5.00 (d, br, ^{3}J(HH) = 3.9 Hz, 2H, FeCp'-$H_{\alpha,\alpha'}$), 4.78 (d, br, ^{3}J(HH) = 4.1 Hz, 2H, FeCp'-$H_{\beta,\beta'}$), 4.24 (FeCp), 1.62 (t, ^{3}J(HH) = 7.0 Hz, 3H, $OCH_2\underline{CH_3}$). $^{13}C\{^{1}H\}$ NMR (75 MHz, $CDCl_3$) δ 330.2 ($C_{carbene}$), 223.3 (CO_{trans}), 217.7 (CO_{cis}), 94.0 (FeCp'-C_{ipso}), 75.8 ($O\underline{CH_2}CH_3$) 74.9 (FeCp'-$C_{\alpha,\alpha'}$), 72.6 (FeCp'-$C_{\beta,\beta'}$), 70.9 (FeCp), 15.8 ($OCH_2\underline{CH_3}$). IR (hexane) ν(CO/cm^{-1}): 2056 (a''_1), 1977 (b_1), 1949 (a'_1), 1937 (e).

$[Cr(CO)_5\{C(OEt)(fc')C(OEt)\}Cr(CO)_5]$(11)[22]

Yield = 0.11 g, 7%. ^{1}H NMR (300 MHz, $CDCl_3$) δ 5.09 (q, ^{3}J(HH) = 7.0 Hz, 4H, $O\underline{CH_2}CH_3$), 5.01 (s, br, 4H, Fc'-$H_{\alpha,\alpha',\alpha'',\alpha'''}$), 4.75 (s, br, 4H, Fc'-$H_{\beta,\beta',\beta'',\beta'''}$), 65 (t, ^{3}J(HH) = 7.0 Hz, 6H, $OCH_2\underline{CH_3}$). $^{13}C\{^{1}H\}$ NMR (75 MHz, $CDCl_3$) δ 306.2 ($C_{carbene}$), 223.6 (CO_{trans}), 217.1 (CO_{cis}), 99.2 (FeCp'-C_{ipso}), 77.4 ($O\underline{CH_2}CH_3$), 76.2 (FeCp'-$C_{\alpha,\alpha'\alpha'',\alpha'''}$), 72.7 (FeCp'-$C_{\beta,\beta',\beta'',\beta'''}$), 15.5 ($OCH_2\underline{CH_3}$). IR (hexane) ν(CO/$cm^{-1}$): 2054 ($a''_1$), 1979 ($b_1$), 1938 ($a'_1$ overlap with e).

Chapter 2: Group 6 Fischer carbene complexes

$[W(CO)_5\{C(NH_2)(2\text{-thienyl})\}]$ (12)[13]

Yield = 1.50g, 96%. ^{1}H NMR (300 MHz, $CDCl_3$) δ 8.58 (s, br, 1H, NH_2), 8.11 (s, br, 1H, NH_2), 7.74 (dd, ^3J(HH) = 5.0 Hz, ^4J(HH) = 1.0 Hz, 1H, Th-H_α), 7.68 (dd, ^3J(HH) = 3.9 Hz, ^4J(HH) = 1.0 Hz, 1H, Th-H_γ), 7.25 (dd, ^3J(HH) = 5.0 Hz, ^3J(HH) = 4.0 Hz, 1H, Th-H_β). $^{13}C\{^1H\}$ NMR (75 MHz, $CDCl_3$) δ 244.2 ($C_{carbene}$), 202.9 (CO_{trans}), 198.7 (CO_{cis}), 153.9 (Fu-C_{ipso}), 133.5 (Fu-C_α), 133.0 (Th-C_γ), 129.4 (Th-C_β). IR (dcm) ν(NH/ cm^{-1}): 2301, ν(CO/cm^{-1}): 2063 (a''_1), 1973 (b_1), 1925 (e) overlap with (a'_1).

$[Cr(CO)_5\{C(NH_2)(\text{ferrocenyl})\}]$ (13)[15,19]

Yield = 1.20 g, 98%. ^{1}H NMR (300 MHz, $CDCl_3$) δ 8.25 (s, br, 1H, NH_2), 8.13 (s, br, 1H, NH_2), 4.76 (s, br, 2H, FeCp'-$H_{\alpha,\alpha'}$), 4.68 (s, br, 2H, FeCp'-$H_{\beta,\beta'}$), 4.26 (FeCp). $^{13}C\{^1H\}$ NMR (75 MHz, $CDCl_3$) δ 279.1 ($C_{carbene}$), 223.1 (CO_{trans}), 218.5 (CO_{cis}), 88.2 (FeCp'-C_{ipso}), 73.5 (FeCp'-$C_{\beta,\beta'}$), 70.8 (FeCp), 70.2 (FeCp'-$H_{\beta,\beta'}$). IR (hexane) ν(NH/cm^{-1}): 2240. ν(CO/cm^{-1}): 2053 (a''_1), 1971 (b_1), 1931 (a'_1 overlap with e).

2.5: References

1 R. B. King, *J. Am. Chem. Soc.*, 1963, **85**, 1922–1926.

2 E. O. Fischer, *Angew. Chem.*, 1974, 651–682.

3 C. P. Casey, *J. Chem. Soc. Chem. Commun.*, 1970, 1220.

4 C. P. Casey and T. J. Burkhardt, *J. Am. Chem. Soc.*, 1973, **95**, 5833–5834.

5 J. Barluenga, J. Flórez and F. J. Fañanás, *J. Organomet. Chem.*, 2001, **624**, 5–17.

6 J. A. Connor and E. M. Jones, *J. Chem. Soc. A Inorganic, Phys. Theor.*, 1971, 1974.

7 F. A. Cotton and C. S. Kraihanzel, *J. Am. Chem. Soc.*, 1962, **84**, 4432–4438.

8 I. Hoskovcová, J. Roháčová, L. Meca, T. Tobrman, D. Dvořák and J. Ludvík, *Electrochim. Acta*, 2005, **50**, 4911–4915.

9 M. A. Sierra, M. Gómez-Gallego and R. Martínez-Álvarez, *Chem. - A Eur. J.*, 2007, **13**, 736–744.

10 B. van der Westhuizen, P. J. Swarts, L. M. van Jaarsveld, D. C. Liles, U. Siegert, J. C. Swarts, I. Fernández and D. I. Bezuidenhout, *Inorg. Chem.*, 2013, **52**, 6674–6684.

Chapter 2: Group 6 Fischer carbene complexes

11 D. I. Bezuidenhout, I. Fernández, B. Van Der Westhuizen, P. J. Swarts and J. C. Swarts, *Organometallics*, 2013, **32**, 7334–7344.

12 B. van der Westhuizen, P. J. Swarts, I. Strydom, D. C. Liles, I. Fernández, J. C. Swarts and D. I. Bezuidenhout, *Dalton Trans.*, 2013, **42**, 5367–5378.

13 B. van der Westhuizen, J. Matthäus Speck, M. Korb, D. I. Bezuidenhout and H. Lang, *J. Organomet. Chem.*, 2014, **772-773**, 18–26.

14 D. I. Bezuidenhout, B. Van Der Westhuizen, P. J. Swarts, T. Chatturgoon, O. Q. Munro, I. Fernández and J. C. Swarts, *Chem. - A Eur. J.*, 2014, **20**, 4974–4985.

15 B. Van Der Westhuizen, J. M. Speck, M. Korb, J. Friedrich, D. I. Bezuidenhout and H. Lang, *Inorg. Chem.*, 2013, **52**, 14253–14263.

16 E. O. Fischer; A. Maasbol, *Angew. Chem. - Int. Ed.*, 1964, **3**, 580–581.

17 M. A. Sierra, *Chem. Rev.*, 2000, **100**, 3591–3637.

18 D. I. Bezuidenhout, S. Lotz, D. C. Liles and B. van der Westhuizen, *Coord. Chem. Rev.*, 2012, **256**, 479–524.

19 J. A. Connor and J. P. Lloyd, *J. Chem. Soc., Dalton Trans.*, 1972, 1470–1476.

20 S. Lotz, N. A. van Jaarsveld, D. C. Liles, C. Crause, H. Görls and Y. M. Terblans, *Organometallics*, 2012, **31**, 5371–5383.

21 S. Aoki, T. Fujimura and E. Nakamura, *J. Am. Chem. Soc.*, 1992, **114**, 2985.

22 D. I. Bezuidenhout, W. Barnard, B. van der Westhuizen, E. van der Watt and D. C. Liles, *Dalton Trans.*, 2011, **40**, 6711–6721.

23 R. J. Abrahams, J. Fischer and P. Loftus, *Introduction to NMR Spectroscopy*, John Wiley and Sons, Somerset, New Jersey, 1st edn., 1989.

24 D. M. Adams, *Metal-Ligand and Relative Vibrations: A Critical Survey of the Infrared and Raman Spectra of Metallic and Organometallic Compounds*, Edinburg University Press, London, 1967.

Chapter 3: Synthesis of Rhodium(I) Fischer carbene complexes *via* a transmetallation approach

3.1: Overview

The concept of rhodium Fischer carbene complexes is of interest due to the unique steric and electronic properties of Fischer carbene ligands (and consequent implied reactivity of the resultant metal carbene complexes), and paves the way for versatile applications of these complexes. The study of rhodium(I) Fischer carbene complexes was initiated in 2001 with the implication of rhodium Fischer carbene formation as intermediate during the template organic synthesis reactions (3+2 cyclization reactions) involving Group 6 carbene complexes in the presence of a rhodium catalyst.[1] Experimental proof for the existence of these intermediate was supplied by the isolation and NMR characterization of the first rhodium(I) Fischer carbene complex shortly thereafter (Figure 3.1 (a)).[2] A few years later, Barluenga and co-workers reported the new examples of rhodium(I) Fischer carbene complexes as shown in Figure 3.1 (b),[3] and mixed Fischer-rhodium-NHC biscarbene complexes (Figure 3.1(c)).[4] However, these are the only three literature reports to date that describe the isolation of rhodium(I) Fischer carbene complexes accessed *via* a carbene transfer reaction. Other synthetic methods towards the preparation of these types of complexes, like thermally induced addition reactions,[5] have been previously employed, but lacks the relative simplicity of the transmetallation method.

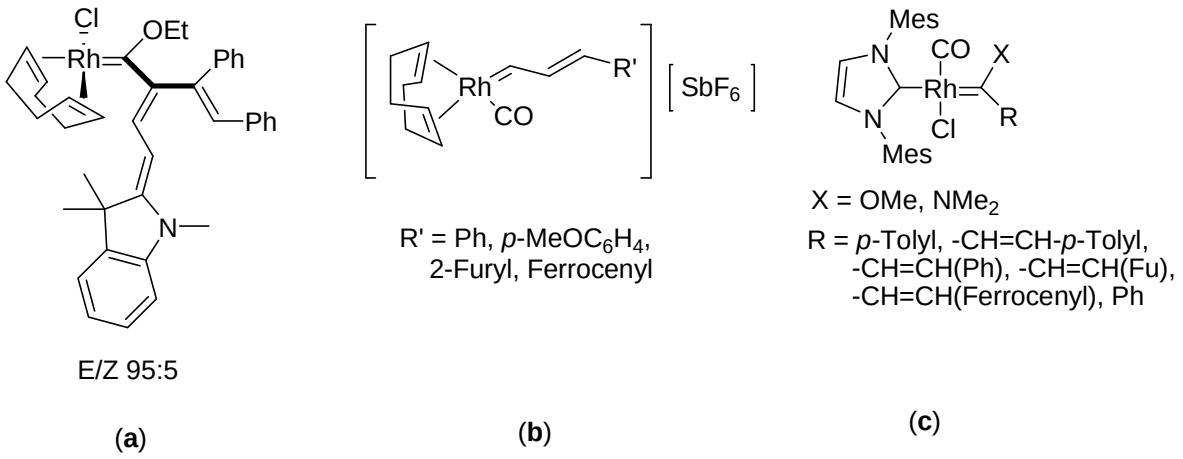

Figure 3.1: The only examples of Rh(I) Fischer carbenes in literature to date obtained *via* carbene ligand transfer as isolated by Aumann *et al.* (**a**) and Barluenga *et al.* {(**b**) and (**c**)}.

All three reports (Figure 3.1), however, state that the synthesized rhodium carbene complexes are thermally unstable. As a result, the carbene ligand dissociates from the rhodium metal and self-dimerizes to form the corresponding organic alkene with regeneration of the corresponding rhodium dimer precursor (Scheme 3.1).[4] This carbene dissociation is a consequence of the increased reactivity of the carbene complex brought about by the late transition metal, wherein the Group 8 metal complex fails to π-back donate to the carbene carbon as extensively as the low oxidation state Group 6 transition metal.

Chapter 3: Synthesis of Rhodium(I) Fischer carbene complexes *via* a transmetallation approach

Considering the effect of the Wanzlick equilibrium on this system, which states that a free singlet carbene exists in an unfavourable equilibrium with its corresponding dimer,[6] late transition metal Fischer carbene complexes accessed *via* carbene transfer are not readily isolated. In the case of mixed Fischer-rhodium-NHC biscarbene rhodium complexes, only the Fischer carbene ligand undergoes dimerization while the NHC ligand remains intact and attached to the rhodium metal. This in turn attests to the stability and robust nature of the metal-carbon bond in *N*-heterocyclic carbene complexes.[7] To circumvent the carbene ligand dissociation, it therefore becomes essential to utilize Group 6 Fischer carbene complexes bearing electron-donating carbene substituents to stabilize the electrophilic carbene carbon.

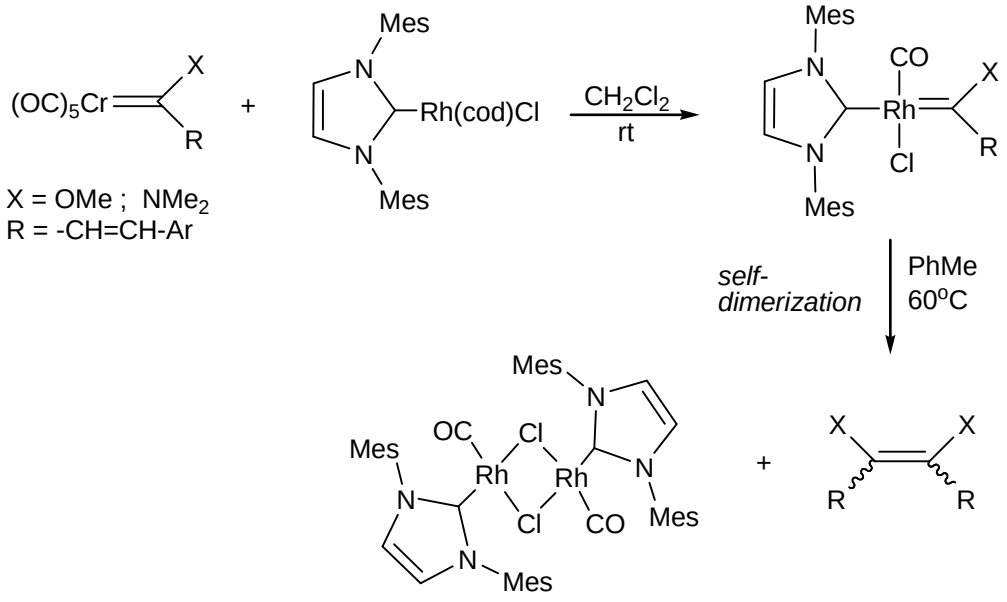

Scheme 3.1: Preparation of mixed biscarbene-rhodium(I) complexes *via* carbene transfer reactions, and subsequent thermal self-dimerization.

3.2: AIM

In this chapter, the aim is to synthesize novel rhodium(I) Fischer carbene complexes utilizing the monocarbene complexes prepared in chapter 2 as precursors. The variation of the alkoxycarbene ligand with aminocarbene substituents will be done by aminolysis reactions, and the 1,5-cyclooctadiene (cod) coligand will be substituted by carbonyl ligands to expand the range of complexes prepared and characterized by NMR, FT-IR, single crystal XRD and mass spectroscopic, and electrochemical methods, with more π-accepting coligands.

Chapter 3: Synthesis of Rhodium(I) Fischer carbene complexes *via* a transmetallation approach

3.2.1: Synthetic strategy

The synthesis of the proposed rhodium(I) Fischer carbene complexes were to be achieved following a metal-metal exchange process (transmetallation) between a Group 6 carbene complex and a rhodium(I)1,5-cyclooctadienyl chloride dimer (Scheme 3.2). The Fischer carbene group 6 metal complex and the rhodium(I) precursor are dissolved in dichloromethane and stirred at room temperature for the amount of time required for product formation. The reaction is monitored by thin layer chromatography (TLC) to indicate the formation of products and the eventual disappearance of starting reagents. Under ideal conditions, the Group 6 Fischer carbene reacts with the $[RhCl(cod)]_2$[8] whereby the carbene ligand is transferred to the rhodium metal resulting in a 100% product yield while the chromium/ tungsten pentacarbonyl decomposition product remains immobile on the TLC plate.

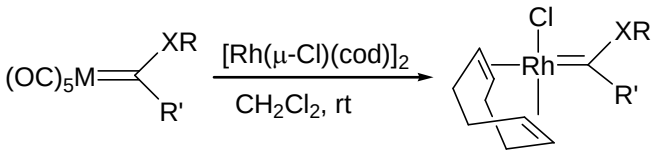

M = Cr, W

XR = OMe, OEt, NH_2

R' = 2-thienyl, 2-furyl, Ferrocenyl

Scheme 3.2: Proposed rhodium(I) Fischer carbene complexes to be prepared from their Group 6 metal precursors.

3.3: Results and Discussions

The synthetic procedure followed in all attempts at transmetallation is as outlined in Scheme 3.2, employing strictly inert synthetic techniques.

3.3.1: Transmetallation from 2-thienyl and 2-furylalkoxy- and aminocarbene complexes of Group 6.

All attempts at synthesizing the rhodium(I) carbene complexes from chromium or tungsten aminocarbene complexes **12** and **13** proved unsuccessful, due to the formation of unidentified side products. Attempts to purify the transmetallated aminocarbene complexes resulted in decomposition of the target compounds during column chromatography. As a result, this synthetic route was discontinued.

Chapter 3: Synthesis of Rhodium(I) Fischer carbene complexes *via* a transmetallation approach

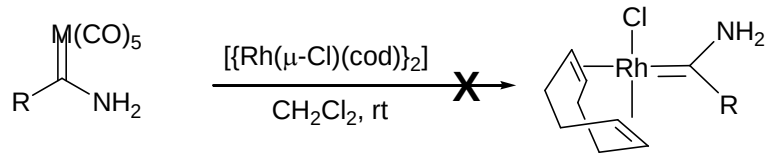

12 M = W, R = 2-thienyl
13 M = Cr, R = ferrocenyl

Scheme 3.3: Attempted syntheses of rhodium(I) aminocarbene complexes *via* carbene transfer reactions from complexes **12** and **13**.

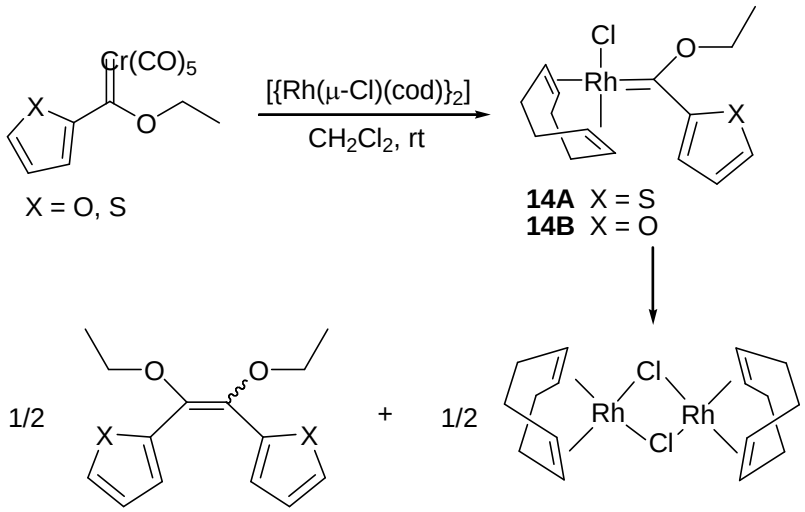

Scheme 3.4: Transmetallation of 2-thienyl or 2-furyl chromium(0) ethoxycarbene complexes and rhodium(I) metal precursors, and subsequent alkene formation.

Transmetallation reactions for the transfer of 2-thienyl and 2-furylalkoxycarbene ligands to rhodium metal showed initial positive results with product formation clearly indicated on the TLC plate along with the self-dimerization products and some traces of the starting material. In addition, ^{1}H and ^{13}C NMR characterization also indicated the formation of the expected rhodium(I) carbene complexes. However, in solution at room temperature, the resulting carbene complexes were found to be unstable with decomposition/self-dimerization occurring to form the corresponding alkene and $[Rh(cod)Cl]_2$ precursor (Scheme 3.4).

For this reason, no NMR spectra of the pure rhodium(I)carbene complexes **14A** and **14B** could be obtained without the presence of the self-dimerization products. In contrast to the previous examples of rhodium(I) carbene complexes prepared by transmetallation, self-dimerization of these thermally unstable complexes occurs at room temperature, and not at 60 °C (as reported for the rhodium(I) carbene complexes of Barluenga[4]), indicating the instability of the rhodium(I) 2-thienyl or 2-furyl alkoxycarbene complexes in comparison to the rhodium(I) carbene complexes illustrated in Scheme 3.1.[4] The NMR spectra (^{1}H and ^{13}C) of the fraction isolated after column chromatography, where continued decomposition in solution results in a mixture of the reaction product [Rh(cod)Cl{C(OEt)(2-thienyl)} **14A**]

Chapter 3: Synthesis of Rhodium(I) Fischer carbene complexes *via* a transmetallation approach

(Figure 3.2), and the decomposition products $[Rh(cod)Cl]_2$ and the self-dimerized alkene $[C(OEt)(2\text{-thienyl})]_2$ are given in Figure 3.2 and Figure 3.3 below.

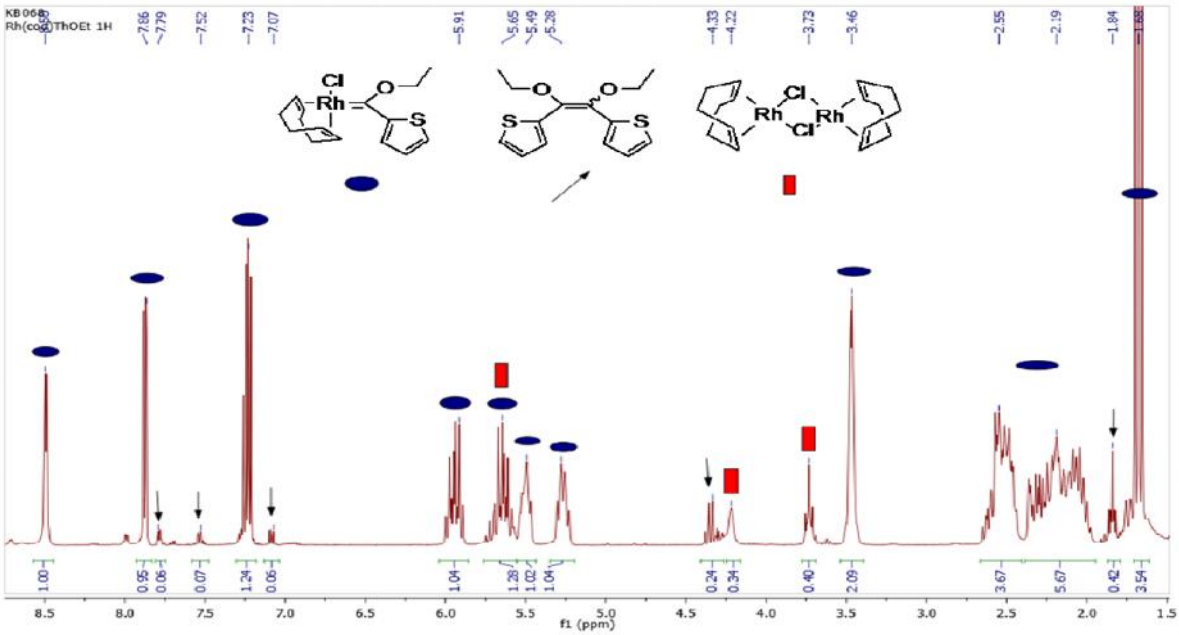

Figure 3.2: ^{1}H NMR spectrum of 2-thienylethoxycarbenerhodium(I) complex **14A** and decomposition products in $CDCl_3$.

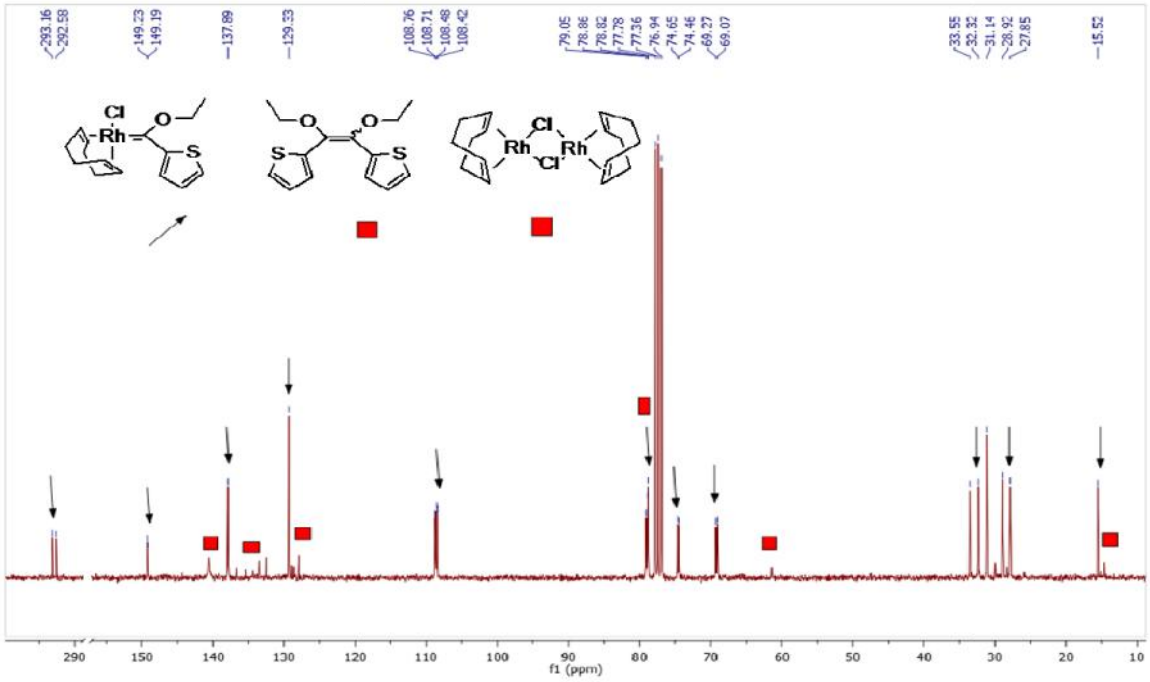

Figure 3.3: ^{13}C NMR spectrum of 2-thienylethoxycarbenerhodium(I) complex **14A** and decomposition products in $CDCl_3$.

Chapter 3: Synthesis of Rhodium(I) Fischer carbene complexes *via* a transmetallation approach

As observed in the ^{13}C NMR spectrum above, unambiguous assignment of the complex and decomposition resonances are non-trivial, as decomposition continues during data collection. This ligand-dissociation problem was also observed during the attempted characterization of complex **14B**, thus the NMR spectra could be excluded here.

This observed self-dimerization of the electrophilic2-thienylcarbene and 2-furylcarbene rhodium(I) carbene complexes (**14A** and **14B**) prompted the necessity of a more stabilizing alkoxycarbene ligand substituent. Ferrocenyl Fischer carbene complexes have previously been discussed to be the most stable of the carbene complexes synthesized in this project (Chapter 2), due to the strongly electron donating ability of the ferrocenyl moiety. As a result, transmetallation from a ferrocenylcarbene Group 6 complex were reasoned to be able to afford a more stable rhodium(I) carbene complex for better characterization, ligand modification and practical application.

3.3.2: Syntheses and characterization of complexes 15 – 18.

In this section, we discuss the syntheses and isolation of complexes **15** – **18** as depicted in Figure 3.4 below.

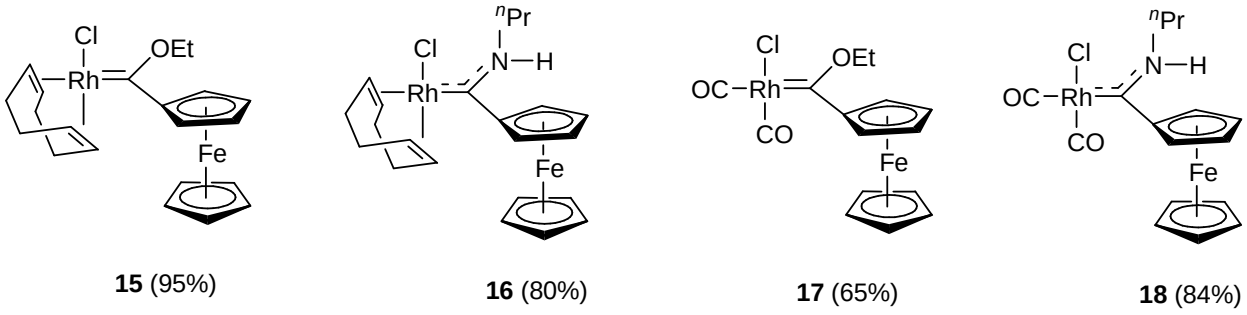

15 (95%) **16** (80%) **17** (65%) **18** (84%)

Figure 3.4: Successfully synthesized and isolated rhodium(I) Fischer carbene complexes in this chapter.

Complex **15** was synthesized *via* transmetallation wherein the carbene ligand is transferred from the chromium(0) ferrocenylcarbene complex to the rhodium(I) precursor to form the desired product, which was subsequently used as a precursor for the syntheses of complexes **16** – **18** as outlined in scheme 3.5 below. The dicarbonyl complexes **17** and **18** were prepared from **15** and **16**, respectively, whereby the cod (1,5-cyclooctadiene) ligand is substituted by carbonyl ligands when carbon monoxide gas is bubbled through a solution of the precursor (complex **15** or **16**) under inert conditions.

Chapter 3: Synthesis of Rhodium(I) Fischer carbene complexes *via* a transmetallation approach

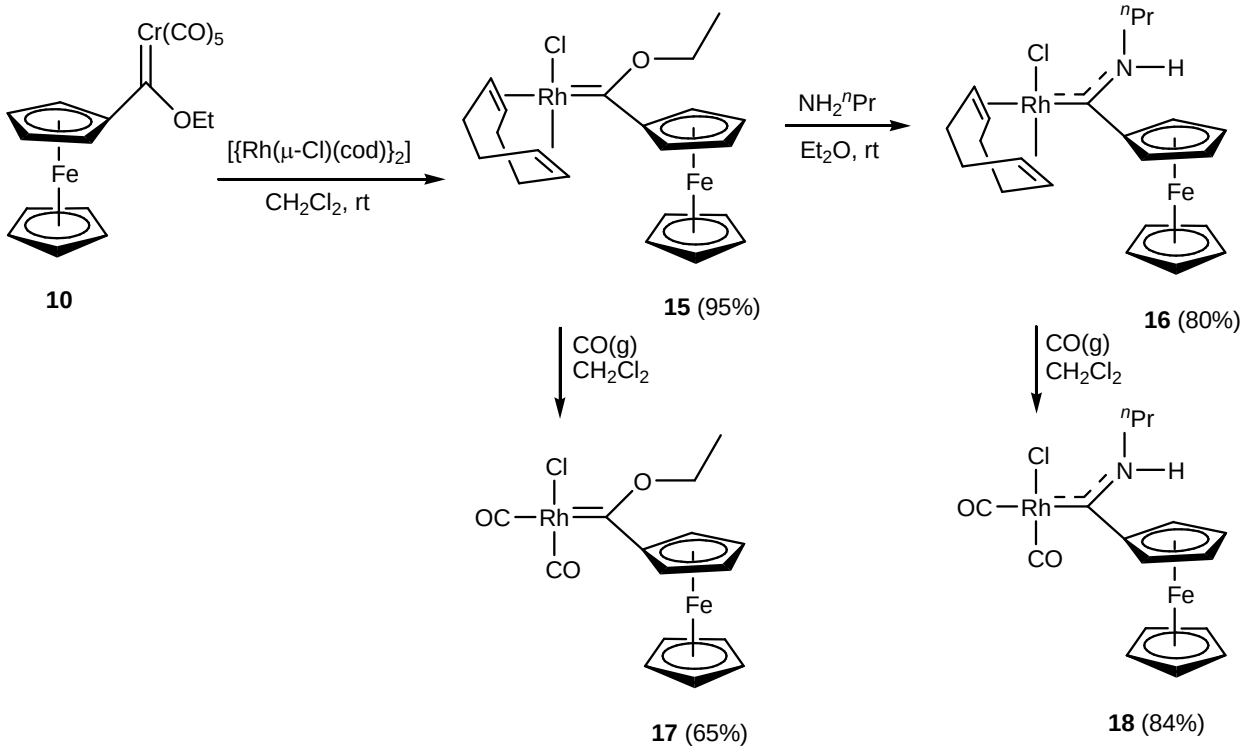

10

15 (95%)

16 (80%)

17 (65%)

18 (84%)

Scheme 3.5: Synthetic routes towards the isolation of complexes **15** – **18**.

3.3.2.1: 1,5-cyclooctadienechlorido{(ferrocenyl)ethoxycarbene}rhodium(I) complex 15.

For the synthesis of complex **15**, the procedure outlined in Scheme 3.5 was utilized where the ferrocenylethoxycarbenechromium(0) complex **10** was reacted with 0.5 equivalent of the precursor $[Rh(cod)Cl]_2$. The target product was successfully isolated with 95% yield. In literature, transmetallation reaction times of 1 – 4 hours were reported,[2,4] however for the ferrocenyl carbene complex the reaction period was increased significantly (14 days) for maximum yields (95% with no evidence of any alkene formation). Presumably, this is due to the increased stability of the precursor carbene complex and stronger metal-carbene carbon bond. During the metal-metal exchange process, the key step is the carbene ligand dissociation, and higher reaction temperatures were avoided to prevent self-dimerization of the carbene ligand (Scheme 3.1).

NMR spectroscopy indicated that the Rh(cod)-moiety is less electron withdrawing than the $Cr(CO)_5$-moiety with its π-accepting carbonyl ligands, as attested by the upfield shift of the carbene carbon signal in the carbon NMR spectrum. The complete loss of symmetry for all protons and carbons is clearly evident (Figure 3.5) due to the lack of symmetry of the Rh(cod)Cl moiety which infers the different interactions of the complex's protons and carbons with the highly electronegative chlorido ligand. The effect of the chloride ligand results consistently in the ethoxy CH_2 proton signal split into two doublet of

Chapter 3: Synthesis of Rhodium(I) Fischer carbene complexes *via* a transmetallation approach

quartets (5.97 ppm ^{2}J(HH) = 10.4, ^{3}J(HH) = 7.2 Hz and 5.51 ppm, ^{2}J(HH) = 10.4 Hz, ^{3}J(HH) = 7.1 Hz), and the cyclooctadiene CH protons split into four multiplets whereby the two protons with closer proximity to the chlorine atom resonate at significantly higher chemical shifts (5.38–5.32 ppm, (m) and 5.21–5.14 ppm (m)) than the other two (3.38–3.32 ppm (m) and 3.24–3.17 ppm (m)). For the ferrocenyl proton chemical shifts, resonances in the range 4.65 – 4.83 ppm is observed, with the exception of one proton resonance, which is shifted significantly downfield (5.41 ppm) presumably due to its close proximity to both the chlorido ligand as well as the ethoxy O-atom.

Similarly, the ^{13}C NMR spectrum (Figure 3.6) also displays individual resonances for all the carbon atoms, attesting to the above mentioned asymmetry of the complex. The carbene carbon resonance (309.2 ppm) appears as a doublet with a coupling constant of 43.2 Hz. This carbene signal is reminiscent of that reported by Barluenga (313 – 304 ppm and 35.4 – 32.1 Hz)[4] and from this comparison it was reasoned that the slight upfield shift and greater coupling constant observed are due to the electron donating ability of the ferrocenyl substituent in contrast to the alkenylcarbene ligand. Interestingly enough, the long distance coupling of the ferrocenyl *ipso*-carbon to the rhodium metal with a coupling constant of 2.1 Hz was also observed.

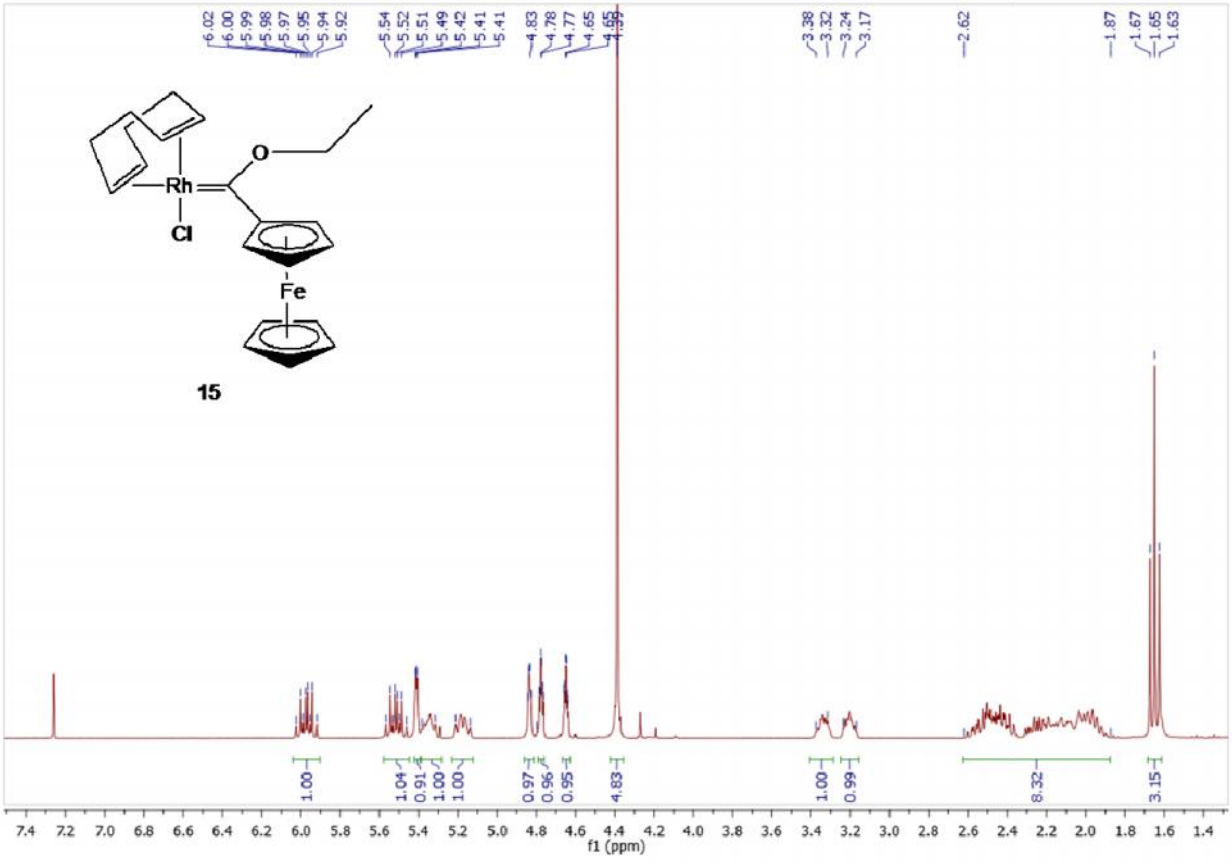

Figure 3.5: ^{1}H NMR spectrum of **15** in $CDCl_3$

Chapter 3: Synthesis of Rhodium(I) Fischer carbene complexes *via* a transmetallation approach

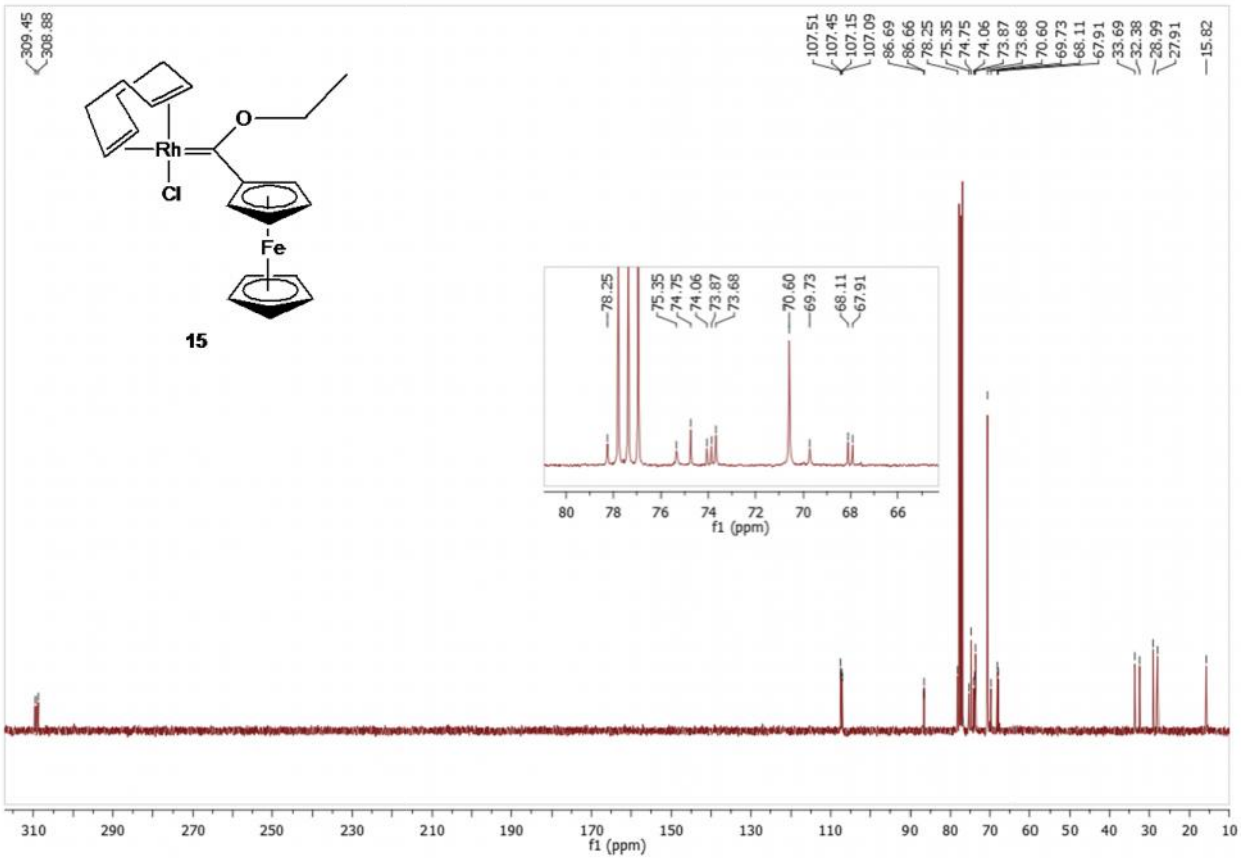

Figure 3.6: ^{13}C NMR spectrum of **15** in $CDCl_3$

Single crystals suitable for X-ray diffraction were grown by the slow diffusion of distilled hexanes into a concentrated solution of **15** in dichloromethane, and the crystal structure of **15** was determined (Figure 3.7). The complex display a *pseudo*-square planar geometry at the rhodium(I) center as a result of the distortion of the cyclooctadiene ligand, with a Rh–$C_{carbene}$ bond distance of 1.958(2) Å. The Rh–$C_{carbene}$ bond length is comparable to that reported for a previously isolated Rh(I) Fischer carbene complex wherein the bond length was 2.011(4) Å.[4]

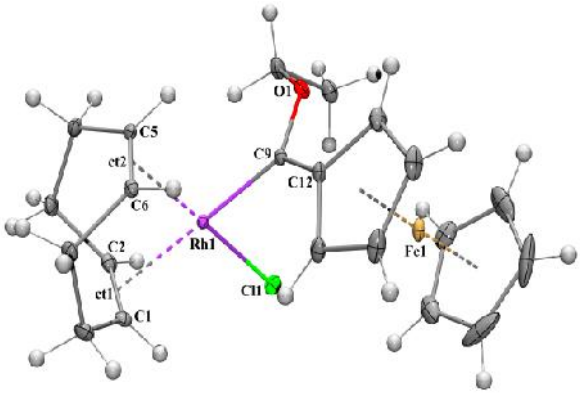

Figure 3.7: Crystal structure of **15**

Chapter 3: Synthesis of Rhodium(I) Fischer carbene complexes *via* a transmetallation approach

3.3.2.2: 1,5-cyclooctadienechlorido{(ferrocenyl)-*n*-propylaminocarbene}rhodium(I) complex 16.

To compare with a more donating carbene ligand, the ethoxycarbene substituent was replaced with an *n*-propylamino-substituent by direct aminolysis of the alkoxycarbene with the primary amine in diethyl ether for the synthesis of complex **16** (Scheme 3.5).[9] The reaction mixture was washed several times with distilled hexanes and the product was isolated in high yields (**16**, 80%).

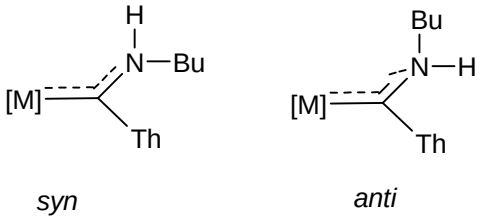

syn *anti*

Figure 3.8: Depiction of *syn*- and *anti*-isomers of products formed during the aminolysis of an alkoxycarbene complex.[10]

From the ^{1}H NMR spectrum (Figure 3.9), only one NH proton signal is observed (8.08 ppm), indicating the presence of only one of two possible isomers (*syn*- or *anti*-isomer as depicted in Figure 3.8) when a primary amine-carbene substituent is utilized.[11,12] In this case, only the *anti*-isomer is obtained due to the availability of the nitrogen lone pair for donation towards the carbene carbon, resulting in an increased $C_{carbene}$–N bond order,[13] and due to the restricted rotation around the $C_{carbene}$-N bond brought about by the steric bulk of the ferrocenyl substituent. The significant upfield shift for the carbene carbon resonance from 309.2 ppm for the ethoxycarbene complex **15** to 257.9 ppm for the aminocarbene complex **16** (Figure 3.10) attests to the increased electron donating effect of the amino-substituent in comparison to the alkoxy-substituent, due to the greater availability of the N-lone pair for stabilization of the empty carbene p-orbital than the O-lone pairs.

Chapter 3: Synthesis of Rhodium(I) Fischer carbene complexes *via* a transmetallation approach

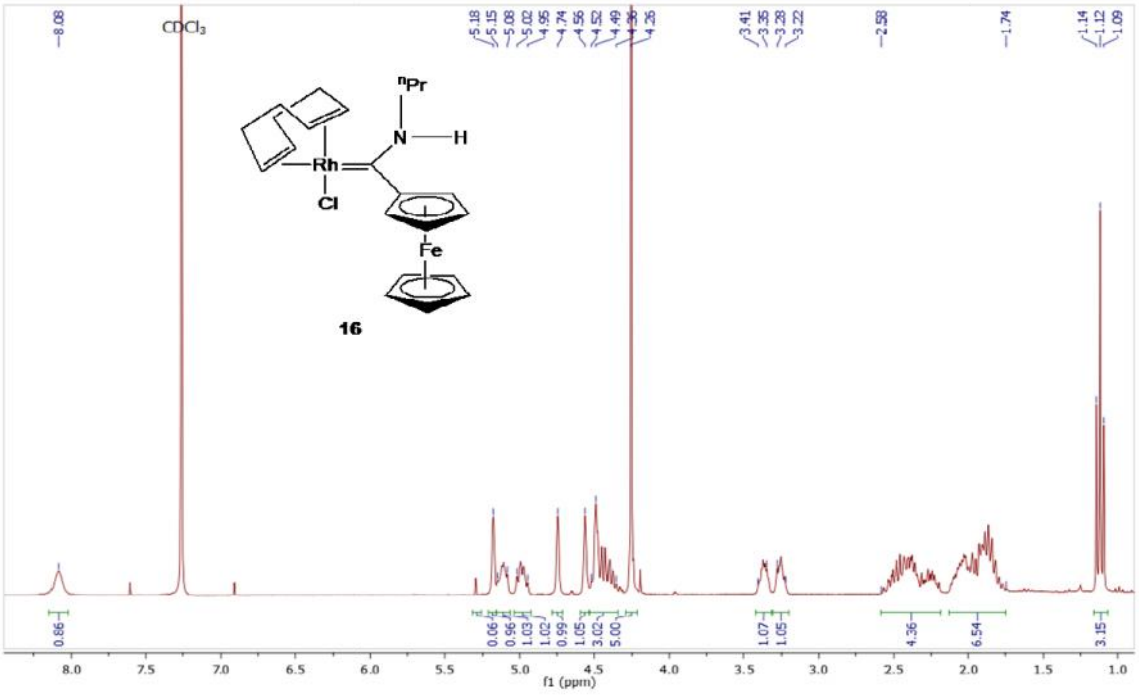

Figure 3.9: ^{1}H NMR spectrum of **16** in $CDCl_3$

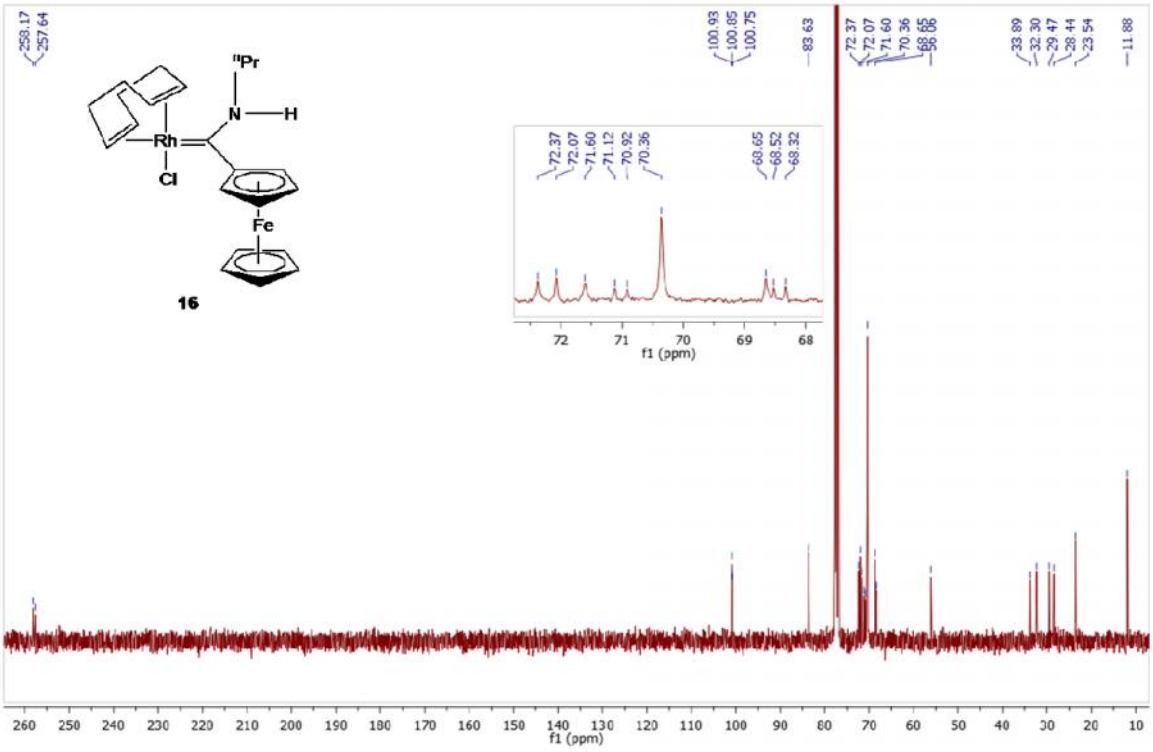

Figure 3.10: ^{13}C NMR spectrum of **16** in $CDCl_3$

Chapter 3: Synthesis of Rhodium(I) Fischer carbene complexes *via* a transmetallation approach

Single crystals suitable for X-ray diffraction were grown by the slow diffusion of distilled hexanes into a solution of **16** in dichloromethane, and the crystal structure as shown in Figure 3.11 displays a *pseudo*-square planar arrangement of ligands at the rhodium(I) center, with a Rh–$C_{carbene}$ bond distance of 2.0178(13) Å.

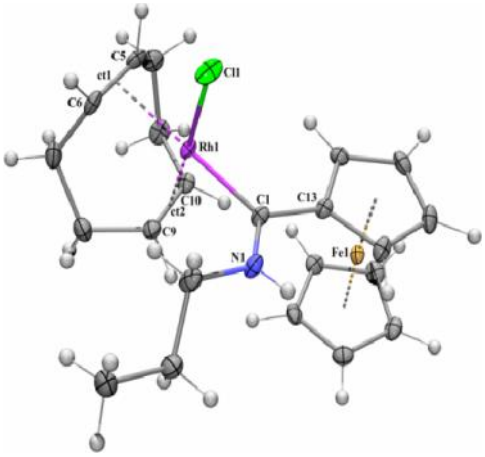

Figure 3.11: Crystal structure of **16**

3.3.2.3: *cis*-(dicarbonyl)chlorido{(ferrocenyl)ethoxycarbene}rhodium(I) complex 17.

The substitution of the cyclooctadiene ligand was effected, in an effort to investigate the effect of other π-acceptor ligands in the metal coordination sphere with regards to the activity and selectivity of the prepared complexes as hydroformylation catalysts. To this end, carbon monoxide gas was bubbled through a dichloromethane solution of **15** for the synthesis of the dicarbonylcarbene complex **17**, $[Rh(CO)_2Cl\{C(OEt)Fc\}]$ (65%) as depicted in Scheme 3.5. The near-immediate colour change from dark red to deep purple indicated completion, during which point the product was crystallized out of solution as a dark purple powder. The relative reduction in the yield is due to product loss during extensive washing in an effort to isolate the product as a powder or solid.

The ^{1}H NMR spectrum (Figure 3.12) shows the restoration of the symmetry of the carbene ligand (due to the loss of the cyclooctadiene ligand) as seen for the precursor chromium(0) ferrocenylcarbene complex **10** (Chapter 2) prior to transmetallation. However, the asymmetry of the Cp' (substituted cyclopentadienyl ring of Fc) is reflected in the observance of five separate resonances for the Cp' ring in the ^{13}C NMR spectrum of **17** (Figure 3.13). There is also a significant upfield shift in the $C_{carbene}$ resonance peak (289 ppm) brought about by the π-acceptor effect of the carbonyl ligands. There are two distinctively different peaks for the two carbonyls with significantly different coupling constants indicative of the properties of the ligands *trans* to these carbonyl ligands. The C_{CO} doublet *trans* to the electrophilic carbene carbon has a smaller coupling constant (^{1}J(Rh-C) = 50 Hz) than that of the C_{CO} doublet *trans* to the chlorido ligand (^{1}J(Rh-C) = 77 Hz).

Chapter 3: Synthesis of Rhodium(I) Fischer carbene complexes *via* a transmetallation approach

FT-IR (Fourier transform infrared) spectroscopy was also employed as a characterization method to attest to the presence of the carbonyl ligands in the rhodium(I) coordination sphere. Two carbonyl vibration bands were observed at 2001 cm^{-1} and 2084 cm^{-1}.

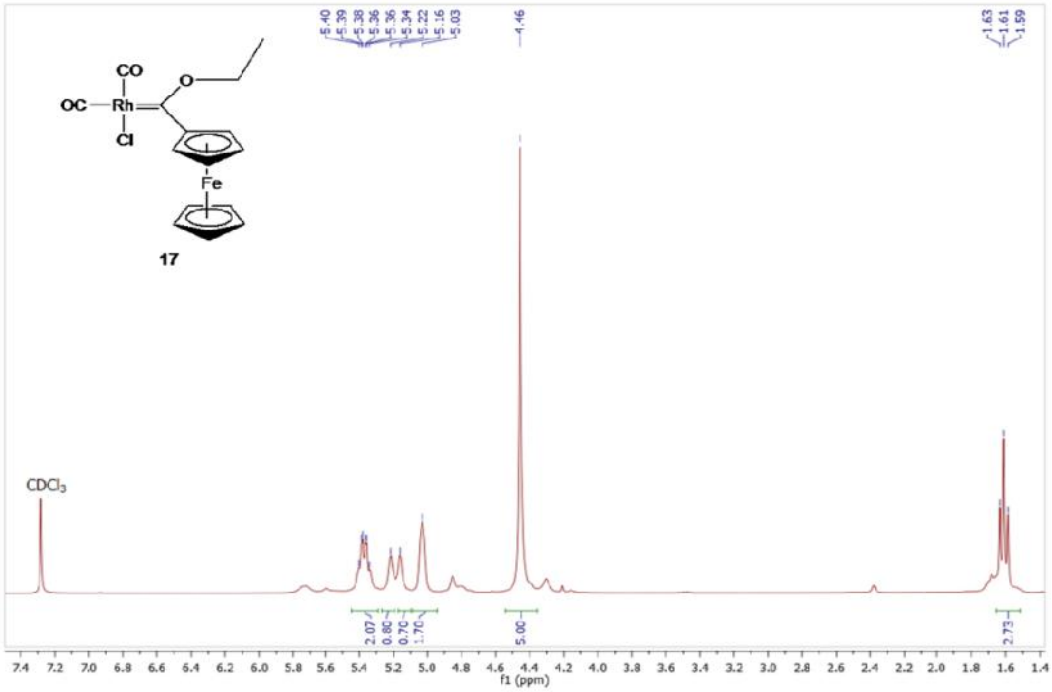

Figure 3.12: ^{1}H NMR spectrum of **17** in $CDCl_3$

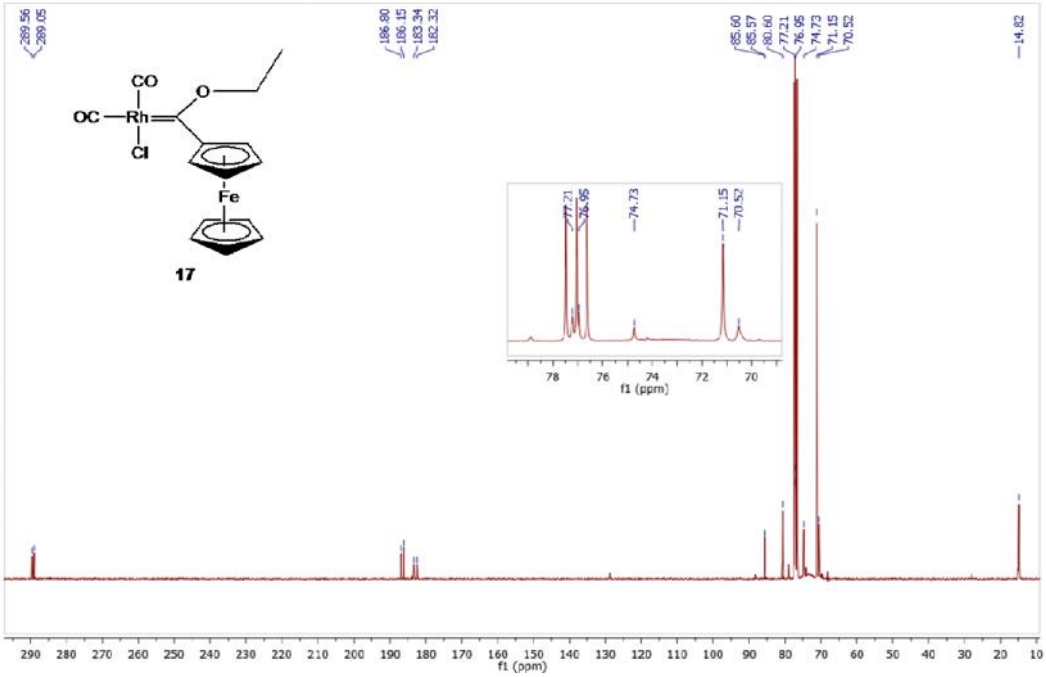

Figure 3.13: ^{13}C NMR spectrum of **17** in $CDCl_3$

Chapter 3: Synthesis of Rhodium(I) Fischer carbene complexes *via* a transmetallation approach

3.3.2.4: *cis*-(dicarbonyl)chlorido{(ferrocenyl)-*n*-propylaminocarbene}rhodium(I) complex 18.

Carbon monoxide gas was bubbled through a dichloromethane solution of **16** for the synthesis of the dicarbonylcarbene complex **18**, [Rh(CO)$_2$Cl{C(NHPr)Fc}] (84%) as depicted in Scheme 3.5. No visible colour change was observed in solution so FT-IR spectroscopy was employed to follow the substitution of the cod ligand by carbonyl ligands.

From the ^{1}H NMR spectrum of **18** (Figure 3.14), the retention of the *anti*-geometry around the C-N bond is maintained even with the reduced steric bulk around the rhodium(I) metal's coordination sphere. The lack of symmetry (from **16**) around the substituted cyclopentadienyl ring is also maintained, presumably due to restricted rotation brought about by the increased C-N bond order for the amino substituent in comparison to its ethoxy counterpart. The broadened, low intensity chemicals shifts observed in the spectrum is a result of the low solubility of the carbene complex in the chloroform-d_1 solvent. The $C_{carbene}$ signal (238 ppm) in the ^{13}C NMR spectrum (Figure 3.15) is shifted upfield compared to the carbene resonance of the precursor rhodium(I) cod aminocarbene complex **16** (258 ppm), and significantly upfield compared to the dicarbonylethoxycarbene complex **18** (289 ppm).

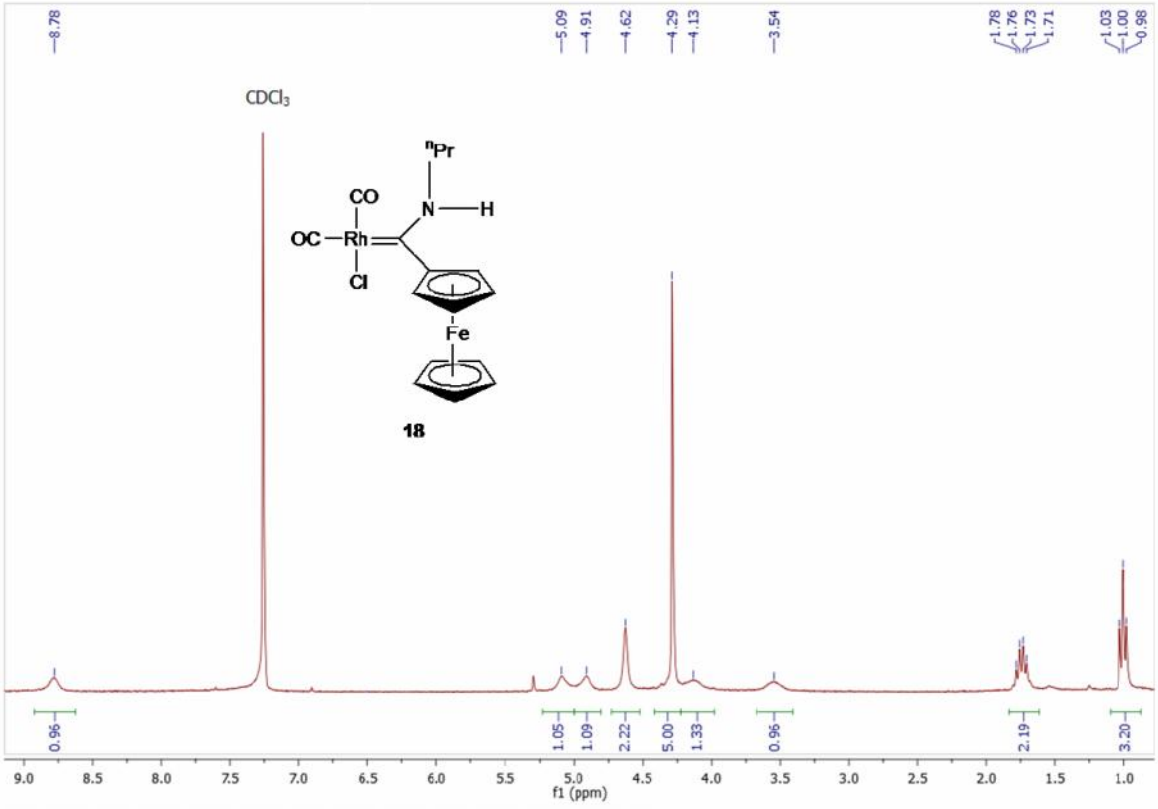

Figure 3.14: ^{1}H NMR spectrum of **18** in $CDCl_3$

Chapter 3: Synthesis of Rhodium(I) Fischer carbene complexes *via* a transmetallation approach

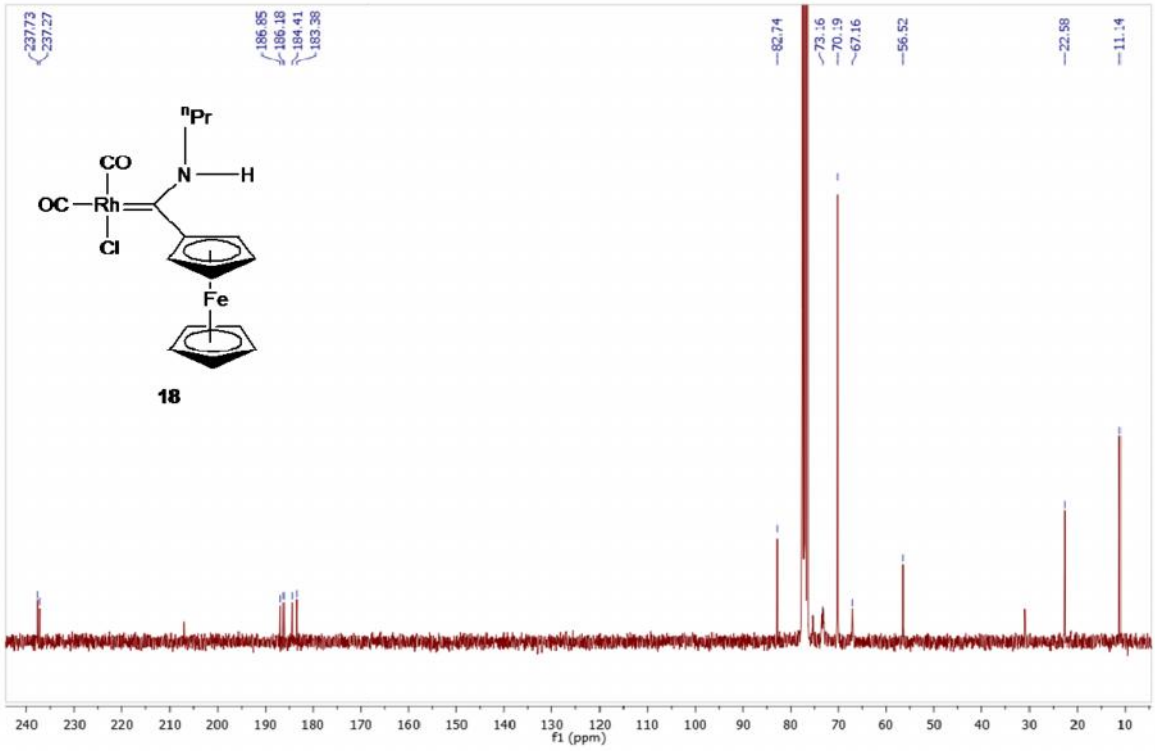

Figure 3.15: ^{13}C NMR spectrum of **18** in $CDCl_3$

Single crystals suitable for X-ray diffraction were grown by the slow diffusion of distilled hexanes into a concentrated solution of **18** in dichloromethane, and the crystal structure as shown in Figure 3.16 displays a square planar at the rhodium(I) center. The *anti*-conformation around the $C_{carbene}$-N bond of the aminocarbene ligand of **18** is retained, with the H-atom on the amino moiety orientated towards the Fc-substituent (see Figure 3.16).

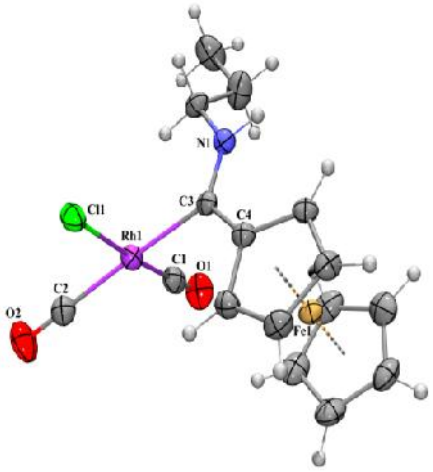

Figure 3.16: Crystal structure of **18**

Chapter 3: Synthesis of Rhodium(I) Fischer carbene complexes *via* a transmetallation approach

3.3.3: A comparative view

Table 3.1: Selected bond lengths (Å) and angles (°) for the complexes **15**, **16** and **18**.

Bond lengths	15	16	18
Rh-$C_{carbene}$	1.958(2)	2.018(1)	2.061(2)
$C_{carbene}$-O/N	1.322(3)	1.308(2)	1.305(3)
$C_{carbene}$-$C_{ipso\text{-}Fc}$	1.448(3)	1.467(2)	1.470(3)
Rh-Cl	2.375(1)	2.391(1)	2.374(1)
Rh-$Y^{a,b}$ or Rh-CO_{trans}	2.005(1)[a]	1.988(1)[b]	1.826(2)
Rh-$Y^{c,d}$ or Rh-CO_{cis}	2.166(1)[c]	2.104(1)[d]	1.932(3)
Bond angles			
$C_{carbene}$-Rh-Cl	94.90(7)	87.61(4)	88.12(6)
O/N-$C_{carbene}$-$C_{ipso\text{-}Fc}$	109.3(2)	115.6(1)	116.1(2)

[a]Y= midpoint of C(5)–C(6). [b]Y = midpoint of C(1)–C(6).[c]Y= midpoint of C(1)–C(2). [d]Y = midpoint of C(9)–C(10).

The Rh–$C_{carbene}$ bond length is comparable to those reported for previously isolated Rh(I) Fischer carbene complexes (1.930–2.113 Å). The increased Rh–$C_{carbene}$ distance of the aminocarbene complex compared to the ethoxy-analogue **15** (1.958(2) Å), is indicative of the greater carbene carbon stabilization from the N-heteroatom compared to the O-carbene substituent, and resultant decreased π-back bonding required from the rhodium metal towards the carbene carbon atom.

Likewise, the short $C_{carbene}$–N bond distances (1.3083(18) Å for **16**; 1.305(5) Å for **18**) and less acute N–$C_{carbene}$–C_{Fc} bond angles (115.56(12)° for **16**, 116.1(2)° for **18**) compared to the O–$C_{carbene}$–C_{Fc} bond angle (109.3(2) Å for **15**), also attest to the increased $C_{carbene}$-N bond order (Table 3.1). Additionally, the effect of the π-acidic carbonyl ligands in **18** (Rh–$C_{carbene}$ distance = 2.061(2) Å) on the π-back donation of the metal to the carbene carbon in **16** (Rh–$C_{carbene}$ distance = 2.0178(13) Å). In like manner, the Rh–CO bond lengths of the carbonyl ligands *trans* to the chlorido-ligand are all significantly shorter (1.799(2) – 1.832(6) Å), than that of the Rh–CO bond length of the CO *trans* to the carbene ligand in **18** (1.932(3) Å). The steric bulk of the coligand *cis* to the carbene influences the rotational freedom of the ferrocenyl moiety.

The spectroscopic data for complexes **15**– **18** as summarized in Table 3.2 for comparative purposes, clearly verify the presence of the carbene and the CO ligands, with Rh-$C_{carbene}$ doublet resonances for the ethoxycarbene complex **15**, 309 ppm, and for the aminocarbene complexes **16** and **18** the values are 258 and 238 ppm, respectively. These values are slightly upfield from those reported by Barluenga and co-workers (307 – 314 ppm for the alkoxycarbene complexes and 243 – 245 ppm for the aminocarbene complexes).[4] Presumably the upfield shift is due to the increased donating ability of the ferrocenylcarbene ligand compared to the alkenylcarbenes. In the case of the two dicarbonylcarbene complexes **17** and **18**, the ν_{av}(CO) could be used to estimate and compare the stereoelectronic properties of the ferrocenylethoxycarbene ligand and the ferrocenylaminocarbene ligand with each other, and

Chapter 3: Synthesis of Rhodium(I) Fischer carbene complexes *via* a transmetallation approach

known imidazolylidene-based NHCs. This was done by calculating the TEP (Tolman electronic parameter); which is a measure of the electron donating or withdrawing ability of a ligand as determined by the FT-IR frequency of the A_1 C-O vibrational mode of a complex with the general formula $[Ni(CO)_3L]$, where L is the ligand under study.[14] TEPs were calculated using the simple linear regression model (TEP = $0.8001\nu_{av}(CO) + 420$ cm^{-1}) reported by Glorius[15] to correlate $\nu_{av}(CO)$ of $[RhCl(carbene)(CO)_2]$ with the TEPs for the $[LNi(CO)_3]$ system originally described by Tolman,[14] and expanded for $[IrCl(carbene)(CO)_2]$; wherein it was stated that the most commonly used *N*-heterocyclic carbenes are more strongly donating than the strongest tertiary phosphines as investigated by Tolman;[16,17] and later expanded for $[RhCl(carbene)(CO)_2]$.[18]

Table 3.2: Spectroscopic data for complexes **15– 18**.

Com-plex	$^{13}C\delta(C_{carbene})^a$, ($^1J$(RhC) and ^2J(PC) (Hz))	$^{13}C\ \delta(CO)^a$, (^1J(RhC)and ^2J(PC) (Hz))	IR^b $\nu(CO)$ (cm^{-1})	$IR^b\nu_{av}(CO)$, TEP^e (cm^{-1})
15	309 (d, 43)	-	-	-
16	258 (d, 40)	-	-	-
17	289 (d, 38)	187 (d, 50)^c 183 (d, 77)^d	2001^d 2084^c	2042 2054^e
18	238 (d, 35)	187 (d, 51)^c 184 (d, 78)^d	1995^d 2077^c	2036 2049^e

*^{a}Recorded in $CDCl_3$. ^{b}Recorded in CH_2Cl_2. ^{c}CO-ligand trans to carbene. ^{d}CO-ligand trans to Cl. ^{e}Calculated using the linear regression model TEP = $0.8001\nu_{av}(CO)$**Rh** + 420 cm^{-1}.*[15]

The TEPs calculated for **17** (2054 cm^{-1}) and **18** (2049 cm^{-1}) demonstrate, to the best of our knowledge, for the first time the comparable donor strength of both ferrocenyl Fischer carbene ligands with known saturated and unsaturated NHCs with TEPs ranging between 2055 – 2049 cm^{-1},[17]and also indicate the greater donor character of the aminocarbene *versus* the alkoxycarbene ligands.

Chapter 3: Synthesis of Rhodium(I) Fischer carbene complexes *via* a transmetallation approach

3.4: Conclusion

Rhodium(I) ferrocenyl Fischer ethoxy- and aminocarbene complexes **15** – **18** were successfully synthesized and fully characterized. The restricted rotation of the ferrocenyl ligand brought about by the steric bulk around the rhodium metal coordination sphere results in the lack of symmetry as observed in the NMR spectra for all complexes. Said restricted rotation also results in the formation of only the *anti*-aminocarbene isomers in the cases of complexes **16** and **18**, as attested to by both NMR and single crystal X-ray diffraction studies. The aminocarbene complex **18** was found to be more stable than its ethoxy analogue, however, this was not the case when comparing the Rh(I) cod complexes; ethoxy analogue (**15**) with the aminocarbene complex **16**. Calculated TEP-values for **17** and **18** indicate the strongly donating effect of the ferrocenylcarbene substituent; and to a greater extent for the aminocarbene ligand of **18** compared to the alkoxy-analogue **17**.

3.5: Experimental

3.5.1: [Rh(cod)Cl{C(OEt)Fc}] (15)

A mixture of $[Cr(CO)_5\{C(OEt)Fc\}]$ **10** (1.67 g, 3.84 mmol) and $[Rh(cod)Cl]_2$ (0.946 g, 1.92 mmol) in CH_2Cl_2 (30 mL) was stirred for 14 days at room temperature. The formation of unknown byproducts can be observed by TLC if the temperature is increased. The resulting dark red solution was reduced in volume *in vacuo* and then added to a silica chromatography column. Elution with CH_2Cl_2 gave a deep red band which was collected and evaporated to dryness. The product, a dark red oil, was dissolved in 3 mL of CH_2Cl_2 and treated with *n*-hexane (5 mL) to precipitate a crystalline red solid. Yield = 0.89 g,95%. Mp: 110–111 °C.^{1}H NMR (300 MHz, $CDCl_3$) δ 5.97 (dq, ^2J(HH) = 10.4, ^3J(HH) = 7.2 Hz, 1H, O$\underline{CH_2}CH_3$), 5.51 (dq, ^2J(HH) = 10.4 Hz, ^3J(HH) = 7.1 Hz, 1H, O$\underline{CH_2}CH_3$), 5.41 (dd, ^3J(HH) = 1.3 Hz, ^4J(HH) = 1.3 Hz, 1H, FeCp'), 5.38–5.32 (m, 1H, cod –$\underline{CH}$), 5.21–5.14 (m, 1H, cod –$\underline{CH}$), 4.83 (dd, ^3J(HH) = 1.3 Hz, ^4J(HH) = 1.3 Hz, 1H, FeCp'), 4.79–4.76(m, 1H, FeCp'), 4.66–4.64 (m, 1H, FeCp'), 4.39 (s, 5H, FeCp), 3.38–3.32 (m, 1H, cod –$\underline{CH}$), 3.24–3.17 (m, 1H, cod -$\underline{CH}$), 2.60–1.90 (m, 8H, cod-$\underline{CH_2}$), 1.65 (t, ^3J(HH) = 7.1 Hz, 3H, $OCH_2\underline{CH_3}$).$^{13}C\{^1H\}$ NMR (75 MHz, $CDCl_3$) δ 309.2 (d, ^1J(RhC) = 43.2 Hz, $C_{carbene}$), 107.5 (d, ^1J(RhC) = 4.6 Hz, cod-$\underline{CH}$), 107.1 (d, ^1J(RhC) = 4.5 Hz, cod-$\underline{CH}$), 86.7 (d, ^2J(RhC) = 2.1 Hz, FeCp'-C_{ipso}), 78.3 (O$\underline{CH_2}CH_3$), 75.4 (FeCp'), 74.8 (FeCp'), 73.8 (d, ^1J(RhC) = 14.9 Hz, cod-$\underline{CH}$), 73.7 (FeCp'), 70.6 (FeCp), 69.7 (FeCp'), 68.0 (d, ^1J(RhC) = 14.9 Hz, cod-$\underline{CH}$), 33.7 (cod-$\underline{CH_2}$), 32.4 (cod-$\underline{CH_2}$), 29.0 (cod-$\underline{CH_2}$), 27.9 (cod-$\underline{CH_2}$), 15.8 ($OCH_2\underline{CH_3}$).

Anal.Calcd. For $C_{21}H_{26}OClFeRh$: C 51.62, H 5.36. Found: C 51.99, H 4.94. ESI-HRMS (15V, positive mode, *m/z*): calcd. for $[M\text{-}Cl]^+$ 453.0388; found, 453.0357.

Chapter 3: Synthesis of Rhodium(I) Fischer carbene complexes *via* a transmetallation approach

3.5.2: [Rh(cod)Cl{C(NH^{n}Pr)Fc}] (16)

To a dark red solution of **15** (0.149 g, 0.30 mmol) in 10 mL of Et_2O, $^nPrNH_2$ (0.05 mL, 0.60 mmol) was added dropwise at room temperature. The mixture was stirred for 2 hours, during which period the yellow-orange product **16** slowly precipitated out of solution. The solvent was decanted and the solid obtained washed with *n*-hexane(20 mL) and dried *in vacuo*. Yield =0.120 g,75%. Mp (decomp.): 164–167 °C. ^{1}H NMR (300 MHz, $CDCl_3$) δ 8.08 (s, br, 1H, NHCH$_2$CH$_2$CH$_3$), 5.18 (s, br, 1H, FeCp'), 5.15–5.08 (m, 1H, cod-CH), 5.02–4.95 (m, 1H, cod-CH), 4.74 (s, br, 1H, FeCp'), 4.56 (s, br, 1H, FeCp'), 4.49 (s, br, 1H, FeCp'), 4.52–4.36 (m, 3H, NHCH$_2$CH$_2$CH$_3$), 4.26 (s, 5H, FeCp), 3.41–3.35 (m, 1H, cod-CH), 3.28–3.22 (m, 1H, cod-CH), 2.56–1.77 (m, 10H, cod-CH$_2$, NHCH$_2$CH$_2$CH$_3$), 1.12 (t, ^3J(HH) = 7.4 Hz, 3H, NHCH$_2$CH$_2$CH$_3$). ^{13}C{^{1}H} NMR (75 MHz, $CDCl_3$) δ 257.9 (d, ^1J(RhC) = 40.1 Hz, $C_{carbene}$), 100.9 (d, ^1J(RhC) = 6.1 Hz, cod-CH), 100.8 (d, ^1J(RhC) = 7.3 Hz, cod-CH), 83.6 (FeCp'-C_{ipso}), 72.4 (FeCp'), 72.1 (FeCp'), 71.6 (FeCp'), 71.0 (d, ^1J(RhC) = 15.2 Hz, cod-CH), 70.4 (FeCp), 68.7 (FeCp'), 68.4 (d, ^1J(RhC) = 15.0 Hz, cod-CH), 56.1 (NHCH$_2$CH$_2$CH$_3$), 33.9 (cod-CH$_2$), 32.3 (cod-CH$_2$), 29.5 (cod-CH$_2$), 28.4 (cod-CH$_2$), 23.5 (NHCH$_2$CH$_2$CH$_3$), 11.9 (NHCH$_2$CH$_2$CH$_3$. (IR, CH_2Cl_2, ν(NH), cm^{-1}): 3320. Anal. Calcd. For $C_{22}H_{29}NClFeRh$: C 50.53, H 5.49, N 2.64. Found: C 51.18, H 5.23, N 2.19. ESI-HRMS (15V, positive mode, *m/z*): calcd. for [M-Cl]$^+$ 466.0704; found, 466.0718.

3.5.3: [Rh(CO)$_2$Cl{C(OEt)Fc}] (17)

Carbon monoxide gas was bubbled for 5 min through a stirred solution of **15** (0.139 g, 0.28 mmol) in CH_2Cl_2 (5 mL) in the absence of light and at -10 °C. Immediate colour change from deep red to dark purple was observed. The flow of CO was stopped and purple needle-like crystals of the product were grown by slow diffusion of *n*-hexane (5 mL) into the concentrated CH_2Cl_2 reaction mixture at -30 °C. Yield = 0.079 g, 65%. Mp (decomp.): 120–122 °C.^{1}H NMR (300 MHz, $CDCl_3$) δ 5.35 (q, br, ^3J(HH) = 6.8 Hz, 2H, OCH$_2$CH$_3$), 5.20 (s, br, 1H, FeCp'), 5.14 (s, br, 1H, FeCp'), 5.01 (s, br, 2H, FeCp'), 4.44 (s, 5H, FeCp), 1.59 (t, ^3J(HH) = 7.1 Hz, 3H, OCH$_2$CH$_3$). ^{13}C{^{1}H} NMR (75 MHz, $CDCl_3$) δ 289.3 (d, ^1J(RhC) = 37.9 Hz, $C_{carbene}$), 186.5 (d, ^1J(RhC) = 49.5 Hz, CO), 182.8 (d, ^1J(RhC) = 77.4 Hz, CO), 85.6 (d, ^1J(RhC) = 2.1 Hz FeCp-C_{ipso}), 80.6 (OCH$_2$CH$_3$), 77.2 (FeCp'), 77.0 (FeCp'), 74.7 (FeCp'), 71.2 (FeCp), 70.5 (FeCp'), 14.8 (OCH$_2$CH$_3$). (IR, CH_2Cl_2, ν(CO), cm^{-1}): 2001, 2084. Anal. Calcd. For $C_{15}H_{14}O_3ClFeRh$: C 41.28, H 3.23. Found: C 41.39, H 2.88. ESI-MS (15V, positive mode, *m/z*): calcd. for [M-Cl-CO]$^+$372.9398; found, 372.9282.

3.5.4: [Rh(CO)$_2$Cl{C(NH^{n}Pr)Fc}] (18)

The complex **[Rh(CO)$_2$Cl{C(NH^{n}Pr)Fc}] 18** was prepared similarly from **16** (0.105 g, 0.21 mmol), but at room temperature. In this case, no visible colour change was observed upon CO bubbling. Slow addition of *n*-hexane to the reaction mixture allowed a dark orange powder, which was washed with *n*-hexane (10 mL) and dried *in vacuo*. Yield = 0.08 g, 84%. Mp (decomp): 138–139 °C.^{1}H NMR (300 MHz, $CDCl_3$) δ 8.78 (s, br, 1H, NHCH$_2$CH$_2$CH$_3$), 5.09 (s, br, 1H, FeCp'), 4.91 (s, br, 1H, FeCp'), 4.62 (s, br, 2H, FeCp'), 4.29 (s, 5H, FeCp), 4.13 (s, br, 1H, NHCH$_2$CH$_2$CH$_3$), 3.54 (s, br, 1H, NHCH$_2$CH$_2$CH$_3$), 1.81–1.68 (m, 2H, NHCH$_2$CH$_2$CH$_3$), 1.01 (t, ^3J(HH) = 7.4 Hz, 3H, NHCH$_2$CH$_2$CH$_3$). ^{13}C{^{1}H} NMR (75 MHz, $CDCl_3$) δ 237.8 (d, ^1J(RhC) = 34.7 Hz, $C_{carbene}$), 186.9 (d, ^1J(RhC) = 51.3 Hz, CO), 184.2 (d, ^1J(RhC) = 78.2 Hz, CO), 83.0 (FeCp'-

Chapter 3: Synthesis of Rhodium(I) Fischer carbene complexes *via* a transmetallation approach

C_{ipso}), 73.6 (FeCp'), 70.5 (FeCp), 67.5 (FeCp'), 56.9 ($NH\underline{CH_2}CH_2CH_3$), 22.9 ($NHCH_2\underline{CH_2}CH_3$), 11.5 ($NHCH_2CH_2\underline{CH_3}$). (IR, CH_2Cl_2, ν(CO) and ν(NH), cm^{-1}): 1995, 2077, 3315. Anal. Calcd. For $C_{16}H_{18}NO_2ClFeRh$: C 42.66, H 4.03, N 3.11. Found: C 42.55, H 3.83, N 3.41. ESI-HRMS (15V, positive mode, *m/z*): calcd. for $[M\text{-}Cl\text{-}CO]^+$385.9714; found, 385.9647.

3.6: References

1 I. Göttker-Schnetmann and R. Aumann, *Organometallics*, 2001, **20**, 346–354.

2 I. Göttker-Schnetmann, R. Aumann and K. Bergander, *Organometallics*, 2001, **20**, 3574–3581.

3 J. Barluenga, R. Vicente, L. A. López, E. Rubio, M. Tomás and C. Álvarez-Rúa, *J. Am. Chem. Soc.*, 2004, **126**, 470–471.

4 J. Barluenga, R. Vicente, L. A. López and M. Tomás, *J. Organomet. Chem.*, 2006, **691**, 5654–5659.

5 G. Erker, M. Mena, U. Hoffmann, B. Menjon and J. L. Petersen, *Organometallics*, 1991, **10**, 291–298.

6 H. W. Wanzlick, *Angew. Chem.-Int. Ed. English*, 1962, **1**, 75–80.

7 P. de Frémont, N. Marion and S. P. Nolan, *Coord. Chem. Rev.*, 2009, **253**, 862–892.

8 G. Giordano, R. H. Crabtree, R. M. Heintz, D. Forster, D. and D. E. Morris in *Inorganic Syntheses*, ed. R. J. Angelici, Wiley & Sons, Inc., New york, 28th edn., 1991, pp. 88 – 89.

9 D. I. Bezuidenhout, D. C. Liles, P. H. van Rooyen and S. Lotz, *J. Organomet. Chem.*, 2007, **692**, 774 – 783.

10 B. van der Westhuizen, P. J. Swarts, I. Strydom, D. C. Liles, I. Fernández, J. C. Swarts and D. I. Bezuidenhout, *Dalton Trans.*, 2013, **42**, 5367–5378.

11 D. I. Bezuidenhout, W. Barnard, B. van der Westhuizen, E. van der Watt and D. C. Liles, *Dalton Trans.*, 2011, **40**, 6711–6721.

12 B. van der Westhuizen, J. Matthäus Speck, M. Korb, D. I. Bezuidenhout and H. Lang, *J. Organomet. Chem.*, 2014, **772-773**, 18–26.

13 B. van der Westhuizen, P. J. Swarts, L. M. van Jaarsveld, D. C. Liles, U. Siegert, J. C. Swarts, I. Fernández and D. I. Bezuidenhout, *Inorg. Chem.*, 2013, **52**, 6674–6684.

14 C. A. Tolman, *Chem. Rev.*, 1977, **77**, 313–348.

15 T. Dröge and F. Glorius, *Angew. Chem.- Int. Ed.*, 2010, **49**, 6940–6952.

16 A. R. Chianese, X. Li, M. C. Janzen, J. W. Faller and R. H. Crabtree, *Organometallics*, 2003, **22**, 1663–1667.

17 R. A. Kelly III, H. Clavier, S. Giudice, N. M. Scott, E. D. Stevens, J. Bordner, I. Samardjiev, C. D. Hoff, L. Cavallo and S. P. Nolan, *Organometallics*, 2008, **27**, 202–210.

18 S. Wolf and H. Plenio, *J. Organomet. Chem.*, 2009, **694**, 1487–1492.

Chapter 4: Ligand substitution in the coordination sphere of the Rh(I) carbene complexes

4.1: Overview

The importance of optimizing the ligand structure of homogeneous rhodium(I) complexes for the industrially important hydroformylation reaction is well-known, where sufficient electron density on the rhodium(I) center is required for maximum conversion of terminal olefins to the more preferred linear aldehydes as desired hydroformylation product for most applications.[1] As the donor/acceptor properties of various phosphorous ligands are well understood,[2,3] the modulation of the steric and electronic properties of the commonly-used phosphine ligands has been directed towards the optimization of both the activity and the selectivity of these rhodium-based catalysts. Wilkinson and co-workers determined that the changes in electronegativity of the rhodium(I) coordination sphere vastly affected the chemo- and regioselectivities of the products formed during hydroformylation (see Figure 4.1).[4] Specifically, an increase in the *n*/*iso* ratio of the aldehydes has been found due to a high steric demand around the rhodium-center when excess phosphines were employed, or when phosphines with stronger π-acceptor properties were used.[1]

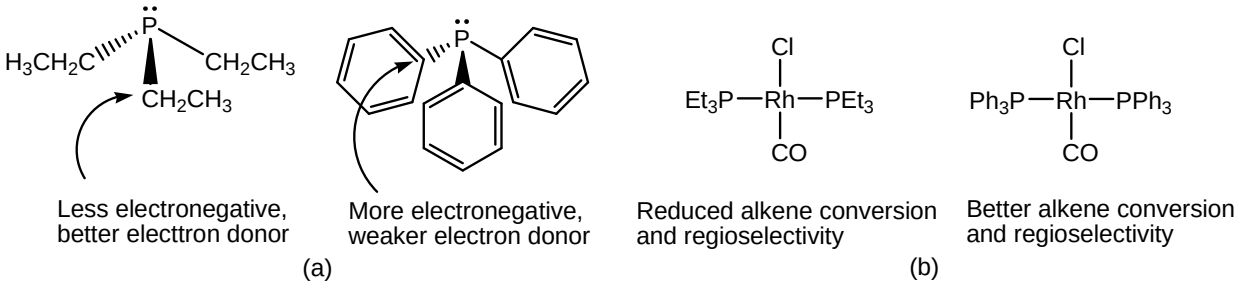

Figure 4.1: Selected pnictogen ligand properties (a) and their resultant effect in the rhodium-catalyzed hydroformylation of 1-pentene (b).

This observation prompted the replacement of one of the carbonyl ligands in the previously discussed $[Rh(CO)_2Cl\{C(OEt)Fc\}]$ (**15**) in Chapter 3 with a range of phosphine ligands resulting in carbene complexes with varied electronic properties and catalytic activities.

The approach to monitor changes in the carbonyl stretching frequencies of carbonyl complexes via infrared spectroscopy is the classic method to evaluate the electron donating properties of ligands.[5,6] However the electrochemical approach, where the redox potentials are determined by cyclic voltammetry, is a more sensitive tool for determining the electronic environment surrounding the central rhodium(I) metal.[7] The redox potentials of Ru(III/II) metal complexes have been used to establish the Lever electronic parameters (LEP), which reflect the donor capacity of the ligands bound to the Ru-metal.[8] LEP uses the Ru(III/II) reduction potential as an electrochemical standard for the prediction of metal-centered redox potentials of various complexes. Although correlations between LEPs and TEPs are rare,[3,9,10] correlations between ν(CO) in $[Rh(CO)_2Cl(carbene)]$ and the Rh(I/II) redox potentials have been

Chapter 4: Ligand substitution in the coordination sphere of the Rh(I) carbene complexes

reported.[11] The redox potentials do not directly provide information on the electron-donating capacity of a given ligand, but represent the energy difference between the reduced metal complex and the oxidized metal complex.

4.2: Aim

In this chapter, the aim is to synthesize novel rhodium(I) Fischer carbene complexes utilizing the monocarbene complexes [Rh(cod)Cl{C(OEt)Fc}] (**15**) and [Rh(cod)Cl{C(NH^{i}Pr)Fc}] (**16**) prepared in Chapter 3 as precursors.

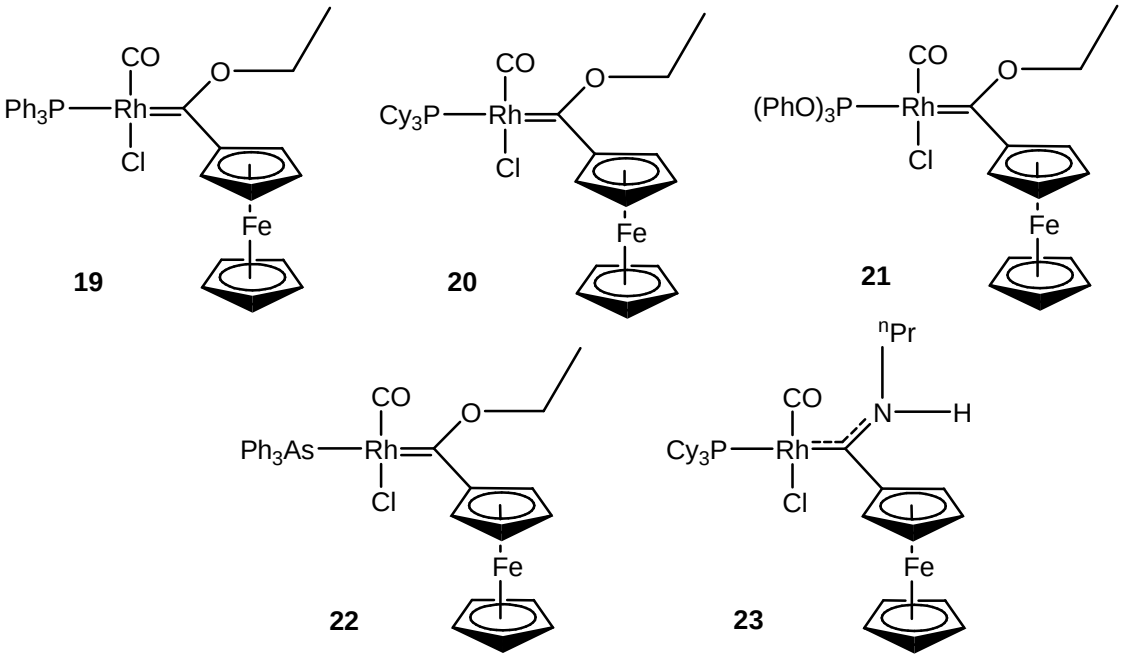

Figure 4.2: Carbonyl-substituted ethoxy- and aminocarbene complexes of rhodium(I)

The syntheses of the desired complexes will be achieved by the replacement of the *trans* carbonyl ligand in complex **17** with pnictogen ligands after the 1,5-cyclooctadiene (cod) co-ligand is substituted by carbonyl ligands to expand the range of complexes prepared and characterized by NMR, FT-IR, single crystal XRD and mass spectroscopic, and electrochemical methods. The variation of the alkoxycarbene ligand with an aminocarbene substituent will be achieved by employing the aminocarbene analogue **16** as the monocarbene complex precursor.

4.2.1: Synthetic strategy

The synthesis of the proposed rhodium(I) Fischer carbene complexes **19** – **23** were to be achieved following a ligand substitution reaction as outlined in Scheme 4.1 and Scheme 4.2. The Fischer carbene complex **15** or **16** (for the syntheses of complexes **19** – **22** or complex **23**, respectively) is dissolved in dichloromethane and carbon monoxide gas is bubbled through the solution for two minutes. An

Chapter 4: Ligand substitution in the coordination sphere of the Rh(I) carbene complexes

equimolar amount of the phosphine or arsine ligand is added to the solution at low temperature in the absence of light until the carbon monoxide gas evolution ceases. The reaction is monitored by FT-IR spectroscopy to indicate the formation of products and the eventual disappearance of starting reagents, indicated by the disappearance of one of the carbonyl stretching frequencies in the FT-IR spectrum as it is replaced by the phosphine, phosphite or arsine ligand.

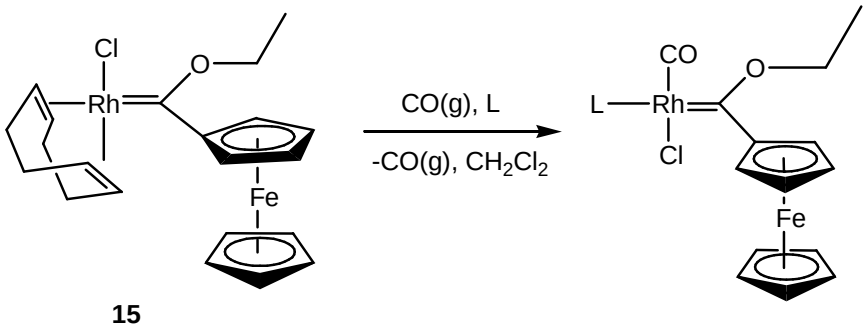

15

19 L = PPh_3 (90%)
20 L = PCy_3 (67%)
21 L = $P(OPh)_3$ (63%)
22 L = $AsPh_3$ (63%)

Scheme 4.1: The synthetic route towards the isolation of rhodium(I) Fischer carbene complexes **19** – **22**.

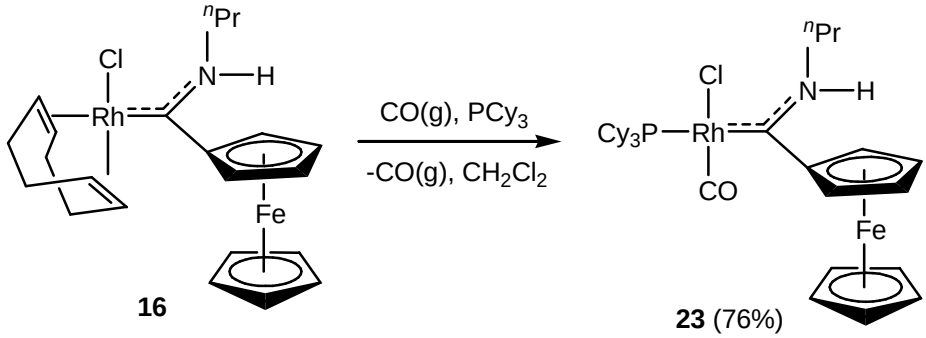

16

23 (76%)

Scheme 4.2: Synthesis of complex **23**.

4.3: Results and Discussions

4.3.1: Syntheses and characterization of complexes 19 – 23.

The synthetic procedure followed in all attempts at ligand modification is outlined in Schemes 4.1 and 4.2, employing strictly inert synthetic techniques. In this section, the syntheses and full spectroscopic and electrochemical characterization of carbene complexes **19** – **23** (Figure 4.2) are discussed as well as the electrochemical characterization of complexes **15** – **18** reported in Chapter 3.

Chapter 4: Ligand substitution in the coordination sphere of the Rh(I) carbene complexes

4.3.1.1: Carbonylchloridotriphenylphosphine{(ferrocenyl)ethoxycarbene}rhodium(I) complex 19

After addition of the equimolar amount of the triphenylphosphine ligand for the synthesis of complex **19**, the reaction proceeds rapidly to form the desired product. Prolonged reaction times should be avoided, as decomposition occurs to result in the formation of the *trans*-chlorocarbonyl(*bis*-triphenylphosphine) rhodium(I) complex reported by Wilkinson and co-workers.[12] The dichloromethane solvent was removed *in vacuo* immediately after the no more CO(g) was evolved, and the colour changed from purple to a slightly red-purple colour. The desired Fischer carbene complex **19** was isolated with 90% yield. The reaction was monitored by FT-IR (1965 cm^{-1}) and ^{31}P NMR (27.4 ppm) spectroscopic methods. The low carbonyl stretching frequency is indicative of the decreased π-acidity of the phosphine coligand in comparison to the CO coligand in the dicarbonyl complex **17** (2001 cm^{-1}).

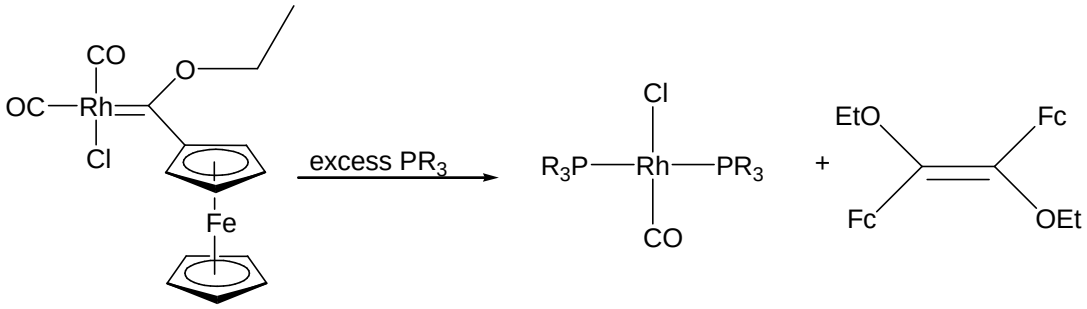

Scheme 4.3: Decomposition of rhodium(I) Fischer carbene complexes.

From the ^{31}P NMR spectrum shown in Figure 4.3 below, only one doublet signal appears at 27.4 ppm with a coupling constant of J_{Rh-P} = 99.9 Hz, which confirms the coordination of the phosphine ligand to the rhodium metal center and sample purity. Trace amounts of Wilkinson's complex is observed as indicated by the doublet at 29 ppm, on the spectrum in Figure 4.3, however the free triphenylphosphine ligand (δ ^{31}P = -6 ppm[13]) or the notoriously persistent triphenylphosphine oxide (δ ^{31}P = 23 ppm[14]) are not present as contaminants.

The lack of any other signals anywhere else on the spectrum is the first proof that the complex is pure of all possible unwanted phosphorus-containing material such as the above-mentioned.

The hindered rotation of the ferrocenyl and ethoxycarbene substituents, as observed in complex **15**, is maintained for complex **19** (and in all the other carbene complexes **20** - **23**), as both the ^{1}H (Figure 4.4) and ^{13}C (Figure 4.5) NMR spectra indicate no symmetry for the ferrocenyl and ethoxy protons and carbons respectively. The ^{1}H NMR spectrum (Figure 4.4) again demonstrates the purity of the sample, as only the isolated product resonances are observed. Importantly, no alkene formation resulting from the dimerization of the carbene ligand is apparent. However, the dimerisation products start to appear after prolonged periods (see Scheme 4.3), as indicated in the ^{13}C NMR spectrum (Figure 4.5). The spectrum

Chapter 4: Ligand substitution in the coordination sphere of the Rh(I) carbene complexes

shows a general downfield shift of all signals compared to that of complex **19** with the carbene carbon signal resonating at 300 ppm (289 ppm for complex **15**). The carbene carbon signal is split into a doublet of doublets as the carbon atom couples with the rhodium atom (^{1}J = 40 Hz) and to the phosphorus atom (^{2}J = 110 Hz). Similarly, the carbonyl carbon resonates at 188 ppm (dd, ^{1}J = 16 Hz, ^{2}J = 81 Hz). Surprisingly, the same coupling pattern is also observed for the *ipso*-carbon of the ferrocenyl substituent (87 ppm), with a Rh-C coupling constant of ^{2}J = 8.2 Hz and a P-C coupling constant of ^{3}J = 2.3 Hz, even though the Fc *ipso*-carbon atom is not directly bonded to the Rh-metal atom. Similarly, complexes **20** – **23** also display long-range ^{2}J (Rh-C) coupling for the of the ferrocenyl-substituted carbon atom with the rhodium atom, and ^{3}J(P-C) coupling for the relevant complexes **20** and **21**.

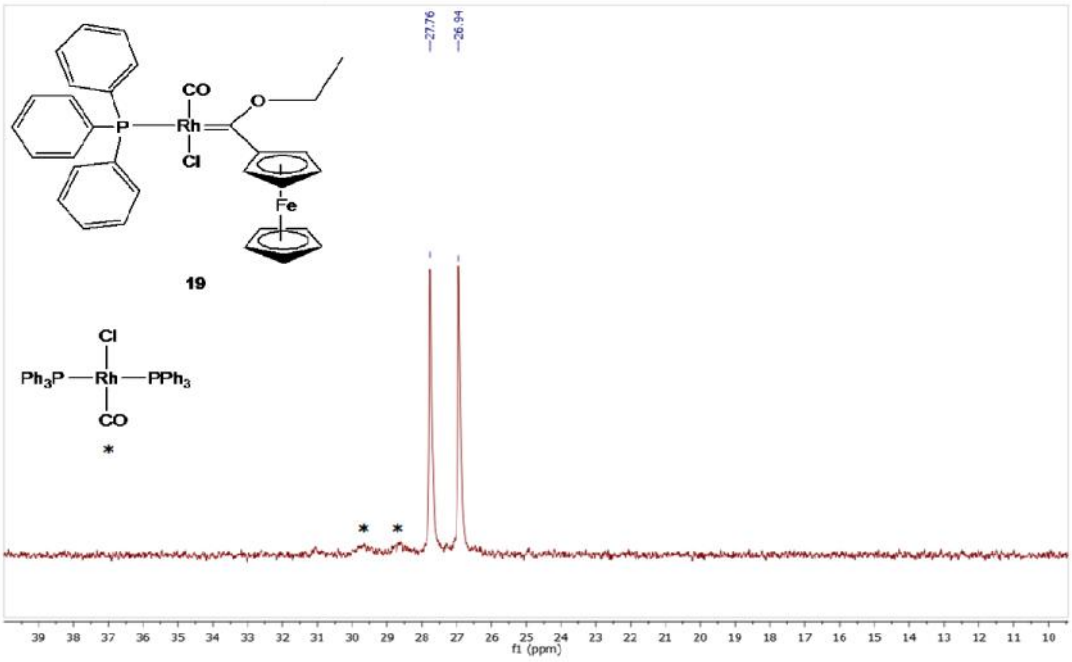

Figure 4.3: ^{31}P NMR spectrum of carbene complex **19** in $CDCl_3$ with wilkinson's catalyst indicated by *

Chapter 4: Ligand substitution in the coordination sphere of the Rh(I) carbene complexes

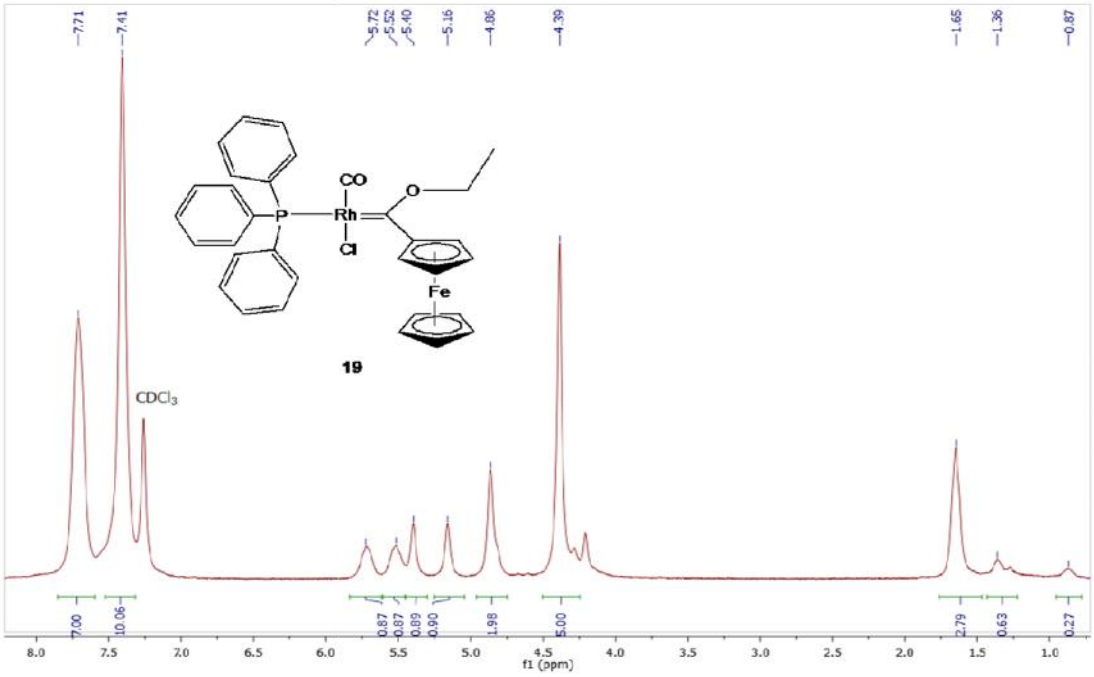

Figure 4.4: ^{1}H NMR spectrum of complex **19** in $CDCl_3$

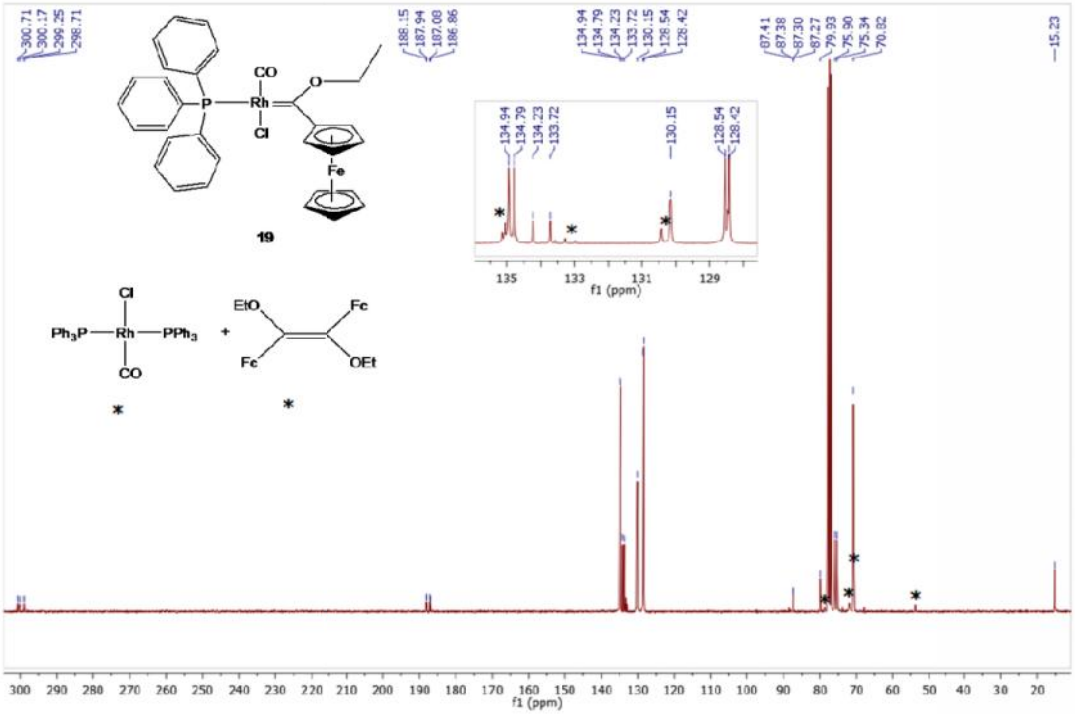

Figure 4.5: ^{13}C NMR spectrum of complex **19** in $CDCl_3$ with decomposition products indicated by *

Single crystals suitable for X-ray diffraction were grown by the slow diffusion of distilled hexanes into a concentrated solution of **19** in chloroform-*d*, and the crystal structure of **19** was determined (Figure 4.6).

Chapter 4: Ligand substitution in the coordination sphere of the Rh(I) carbene complexes

The complex displays a square planar geometry at the rhodium(I) center with the triphenylphosphine ligand in the expected *trans*-position to the carbene ligand as is sterically and electronically favourable. The longer Rh–$C_{carbene}$ bond distance of 2.017(4) Å is indicative of the reduced π-acceptor ability of the triphenylphosphine ligand compared to the carbonyl ligand (compare the Rh-$C_{carbene}$ bond length of the rhodium(I) cyclooctadiene ethoxycarbene complex **15** (1.958(2) Å).

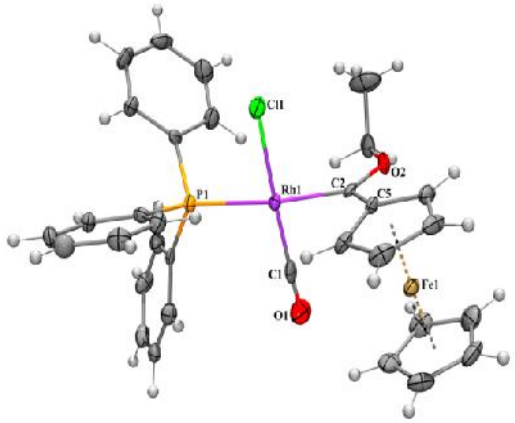

Figure 4.6: Crystal structure of **19**.

4.3.1.2: Carbonylchloridotricyclohexylphosphine{(ferrocenyl)ethoxycarbene}rhodium(I) complex 20

To compare with a more donating phosphine ligand, the reaction was similarly carried out with tricyclohexylphosphine as shown in Scheme 4.1 above and monitored by FT-IR and ^{31}P NMR spectroscopic methods, both of which indicated the formation of the desired product by disappearance of one of the carbonyl peaks (and subsequent shift of the remaining one to 1946 cm^{-1}) and appearance of one phosphorus doublet signal (34.7 ppm) respectively. The use of the tricyclohexylphosphine ligand resulted in a more stable phosphine-substituted carbene complex as evidenced by the ease of isolation of the pure purple-red prism-like crystals (67% yield).

The ^{1}H NMR spectrum (Figure 4.7) shows the earlier-mentioned and thus expected lack of symmetry in the complex with an overlap of signals belonging to the ethoxy-CH_3 and some cyclohexyl protons at 1.62 ppm. There is no evidence of decomposition products (loss of carbene ligand or dimerization of carbene) forming even over a long period of time in solution (^{13}C NMR spectrum in Figure 4.8), which is indicative of the overall increased stability of this complex brought about by the more electron donating tricyclohexylphosphine ligand effected by the less electronegative nature of the cyclohexyl substituent as compared to its phenyl counterpart in complex **19**. The slight downfield shift of the carbene and carbonyl carbon signals from complex **19** ($\delta C_{Carbene}$ = 300 ppm and δC_{CO} = 188 ppm) to **20** ($\delta C_{Carbene}$ = 303 ppm and δC_{CO} = 189 ppm) is however not as significant as expected and thus does not attest to the electron donating strengths of the two complexes relative to each other. The carbonyl stretching frequency (1946 cm^{-1}) is lower than for **19** (1965 cm^{-1}) and for the dicarbonyl complex **17** (2001 cm^{-1}),

Chapter 4: Ligand substitution in the coordination sphere of the Rh(I) carbene complexes

indicative of the decreased π-acidity of phosphine co-ligand in **20**. The inferred greater π-acidity of the phosphine co-ligand in **19** is brought about by the higher electronegativity of the phenyl substituents as compared to the cyclohexyl substituents in **20**.

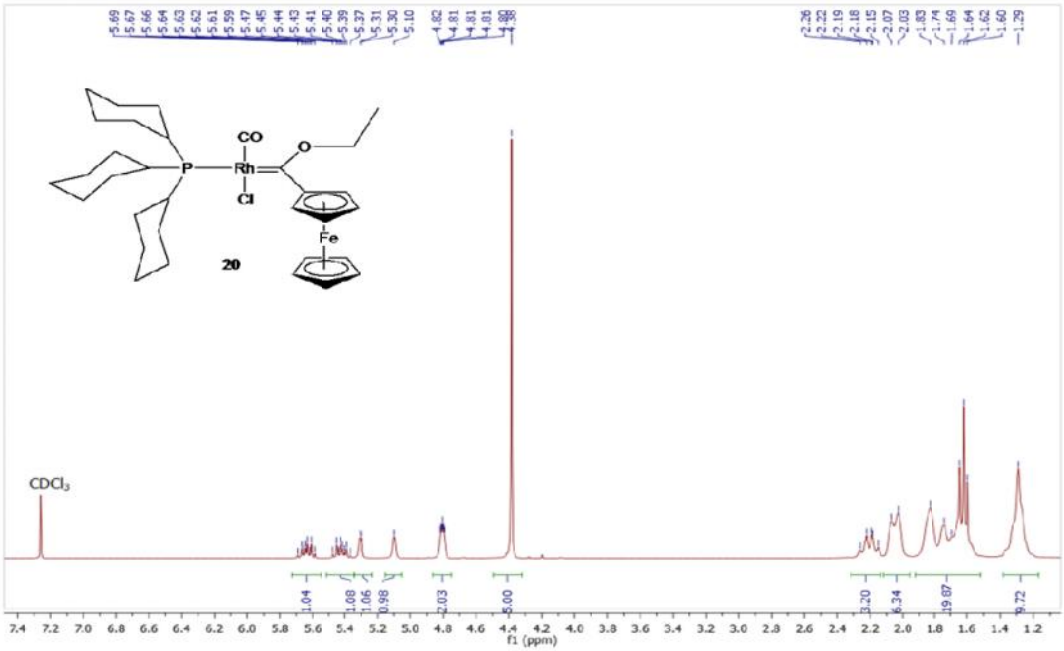

Figure 4.7: ^{1}H NMR spectrum of complex **20** in $CDCl_3$

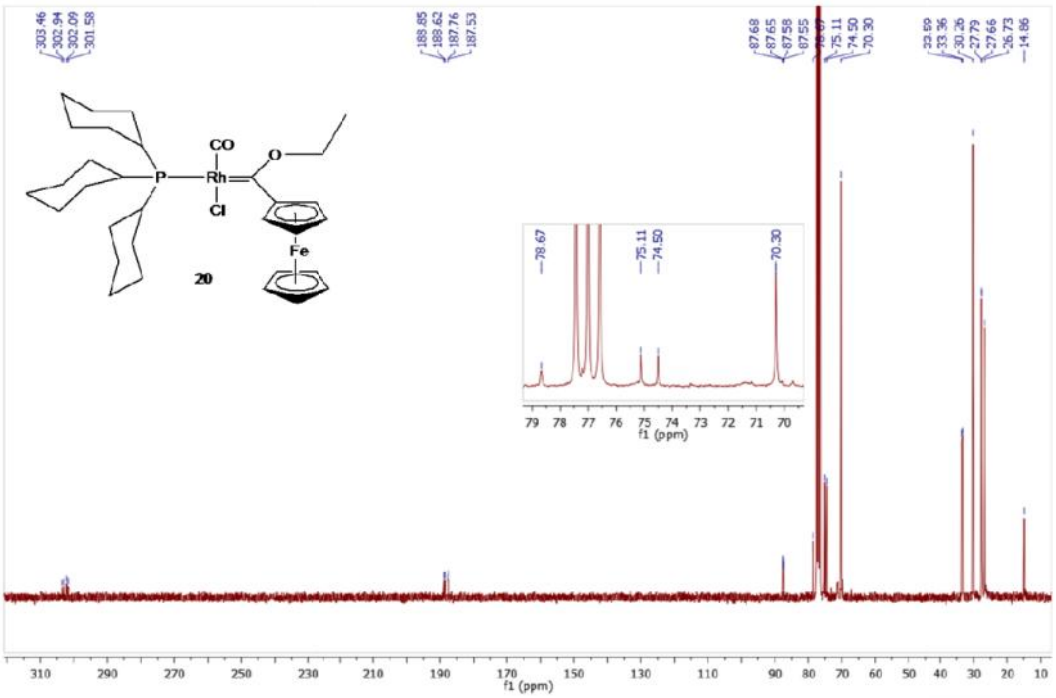

Figure 4.8: ^{13}C NMR spectrum of complex **20** in $CDCl_3$

Chapter 4: Ligand substitution in the coordination sphere of the Rh(I) carbene complexes

Single crystals suitable for X-ray diffraction were grown by the slow diffusion of distilled hexanes into a concentrated solution of **20** in dichloromethane and the crystal structure is shown in Figure 4.9 below. The complex displays a square planar geometry at the rhodium(I) center with the tricyclohexylphosphine ligand in a *trans*-position to the carbene ligand as is sterically and electronically required. As expected, the Rh–$C_{carbene}$ bond distance of 2.027(1) Å is slightly longer than that of complex **19** (2.017(2) Å), attesting to the electron-donor effect of the tricyclohexylphosphine ligand to the rhodium(I) metal and the overall reduced π-back donation required from the metal towards the stabilization of the carbene double bond.

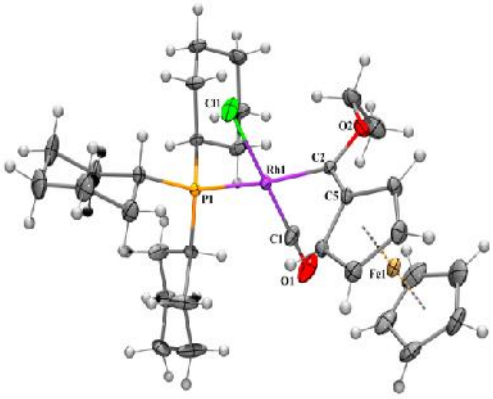

Figure 4.9: Crystal structure of **20**.

4.3.1.3: Carbonylchloridotriphenylphosphite{(ferrocenyl)ethoxycarbene}rhodium(I) complex 21.

The more electron withdrawing triphenylphosphite was employed for the synthesis of complex **21** as depicted in Scheme 4.1. The reaction was similarly monitored by FT-IR (1986 cm^{-1}) and ^{31}P NMR (127 ppm) spectroscopic methods and the product was isolated in high yield (63%).

The reduced stability of complex **21** as compared to complexes **19** and **20** is evidenced by the decomposition product resonances in both the ^{1}H (Figure 4.10) and ^{13}C (Figure 4.11) NMR spectra below. These impurities are due to the earlier-mentioned carbene ligand dissociation, with subsequent dimerization of the carbene ligand and the corresponding co-decompostition product, *trans*-carbonylchorido(*bis*-triphenylphosphite) rhodium(I) complex. This is ascribed to the stronger π-accepting ability of the triphenylphosphite ligand. However, as seen for complexes **19** and **20**, the carbene signal shift (298 ppm) is relatively insensitive to the electronic variations of the coligands. The complex **21** proved to be the least stable of the complexes prepared in this chapter, with carbene ligand dissociation (Scheme 4.3) occurring in solution. The lower carbonyl stretching frequency of **21** (1986 cm^{-1}) compared its dicarbonyl analogue **17** (2001 cm^{-1}) due to the earlier-mentioned relative π-acidity of the phosphine and CO coligands. Additionally, this stretching frequency is significantly higher than for

Chapter 4: Ligand substitution in the coordination sphere of the Rh(I) carbene complexes

complex **19** (1965cm $^{-1}$), thus the phosphite coligand in **21** is more π-acidic than its phosphine analogue in **19**.

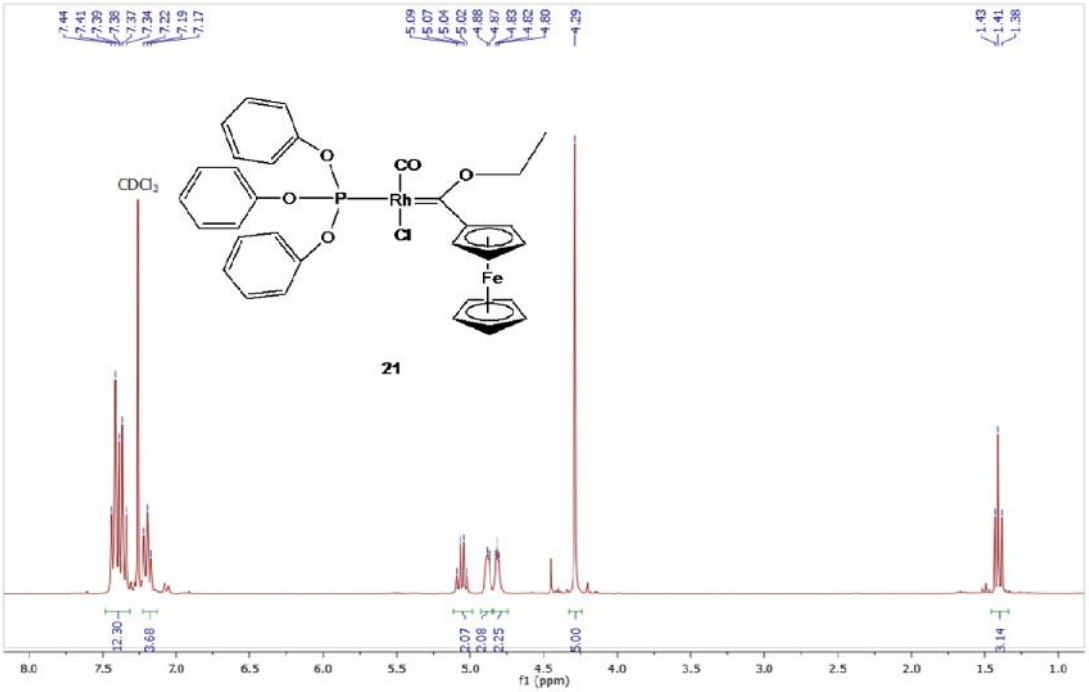

Figure 4.10: ^{1}H NMR spectrum of complex **21** in $CDCl_3$

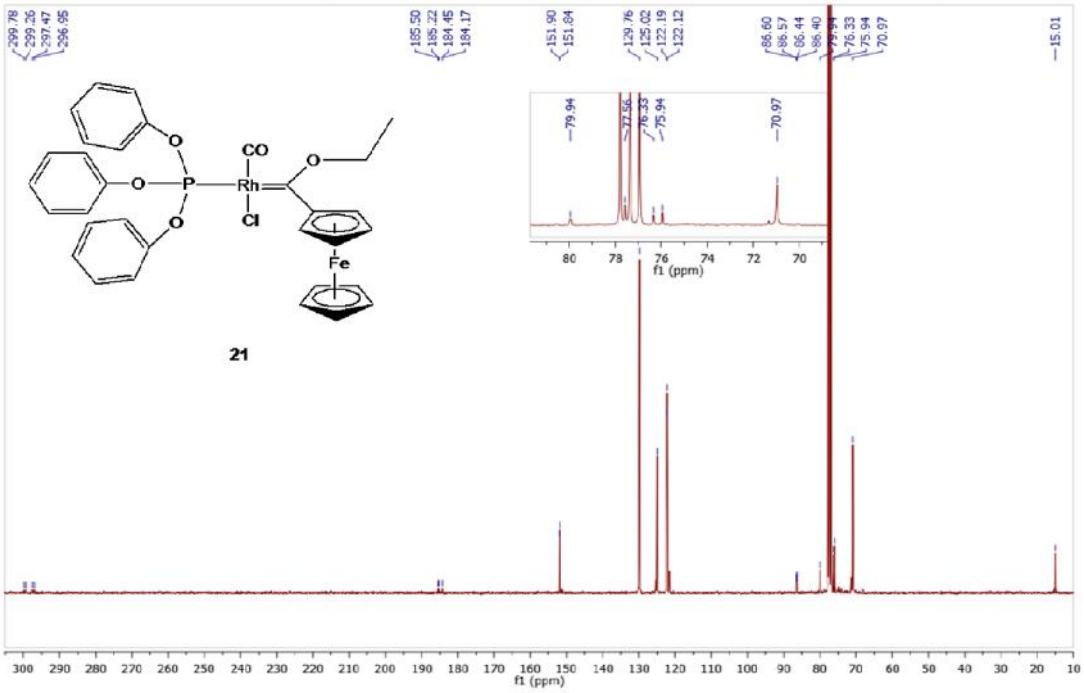

Figure 4.11: ^{13}C NMR spectrum of complex **21** in $CDCl_3$

Chapter 4: Ligand substitution in the coordination sphere of the Rh(I) carbene complexes

4.3.1.4: Carbonylchloridotriphenylarsine{(ferrocenyl)ethoxycarbene}rhodium(I) complex 22

Triphenylarsine was similarly employed as a carbonyl substituting-ligand, and the reaction was monitored by FT-IR spectroscopy (1966 cm^{-1}). The Fischer carbene complex **22** was isolated in good yield (63%).

The ^{1}H (Figure 4.12) and ^{13}C (Figure 4.13) NMR spectra show the formation of small amounts of dimerised products in addition to the desired Fischer carbene complex **22**. As expected, the same dimerization decomposition pathway, as observed for complex **19** (Scheme 4.3) is brought about by the chemical similarities of the triphenylphosphine and triphenylarsine ligands in **19** and **22**, respectively. The carbene and carbonyl carbon ^{13}C NMR (Figure 4.13) chemical shifts of 295 ppm and 189 ppm, respectively are relatively insensitive to the electronic differences introduced by the different phosphine/ arsine coligands. However, it can be concluded that the reactivity and thus stability of the Fischer carbene complex **19** is similar to that of complex **22** as evidenced by their respective slow decomposition in solution, and supported by the near-identical carbonyl stretching frequencies of 1965 cm^{-1} for **19** and 1966 cm^{-1} for **22**, respectively. The carbonyl stretching frequency of **22** is lower than in the dicarbonyl ethoxy (**17**, 2001 cm^{-1}) and amino (**19**, 1995 cm^{-1}) complexes, indicative of the decreased π-acidity of the phosphine co-ligand in complex **22**.

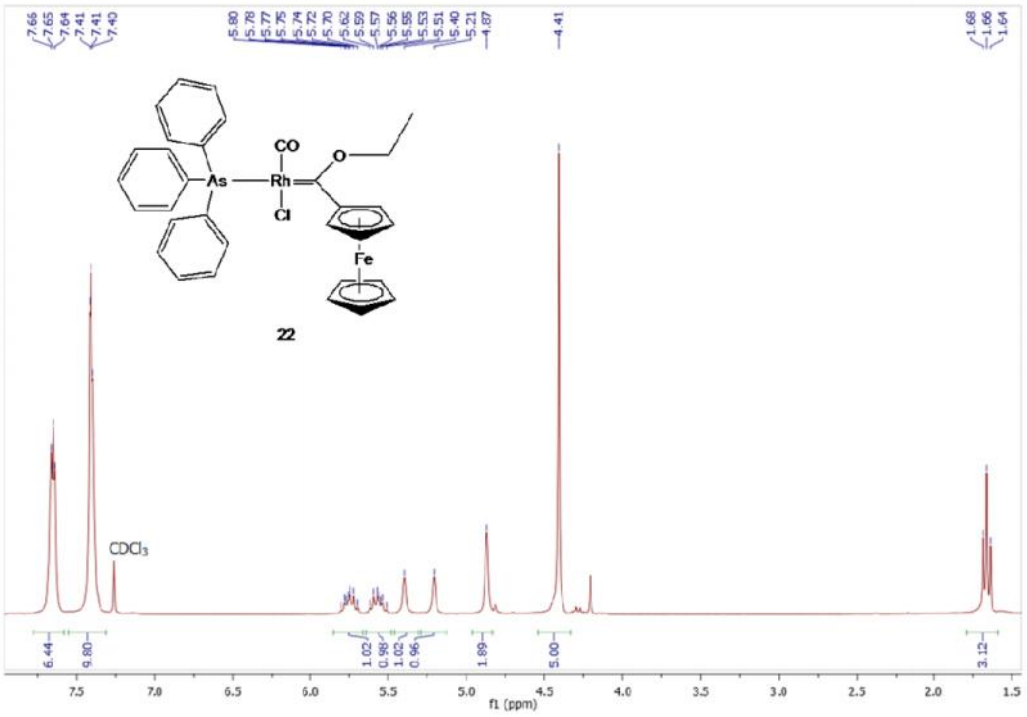

Figure 4.12: ^{1}H NMR spectrum of complex **22** in $CDCl_3$

Chapter 4: Ligand substitution in the coordination sphere of the Rh(I) carbene complexes

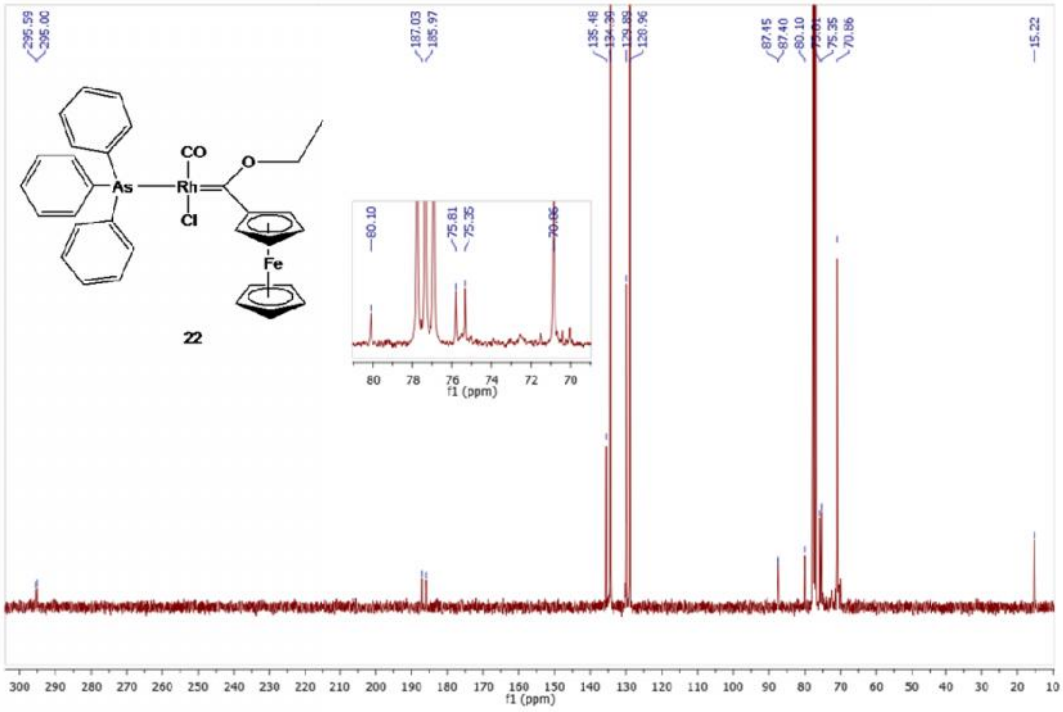

Figure 4.13: ^{13}C NMR spectrum of complex **22** in $CDCl_3$

4.3.1.5: Carbonylchloridotricyclohexylphosphine{(ferrocenyl)*iso*-propylaminocarbene}rhodium(I) complex 23

To investigate the possibility of the formation of the potentially most stable monocarbonyl carbene complex, the aminocarbene complex **16** was reacted in like manner with the most electron donating phosphine ligand in this series, the tricyclohexylphosphine ligand (Scheme 4.2). The reaction was monitored by FT-IR (1939 cm^{-1}) and ^{31}P NMR (37.4 ppm) spectroscopic methods. The product was isolated in high yield (82%) as yellow-orange needle-like crystals. The low carbonyl stretching frequency is indicative of the decreased π-acidity of both the carbene ligand (with stronger donor amino-substituent) and the phosphine coligand, as compared to its ethoxycarbene counterpart in the above discussed Fischer carbene complexes **20** (1946 cm^{-1}) and the dicarbonyl precursor **18** (1995 cm^{-1}), as well as the rest of the analogue complexes in the series (**19** – **22**, 1946 – 1986 cm^{-1})

The ^{1}H NMR spectrum (Figure 4.14) shows only one amino-NH proton at 8.68 ppm, indicating the presence of only the *anti*-isomer. This observation is indicative of the maintained hindered rotation of the amino substituent reported for amino carbene complexes **16** and **17** in Chapter 3. Some of the proton signals are broadened due to the low solubility of the complex in chloroform-*d*, which was employed for comparative sake of **23** to complexes **19** – **22**. The ^{13}C NMR (Figure 4.15) spectrum shows

Chapter 4: Ligand substitution in the coordination sphere of the Rh(I) carbene complexes

the carbene and carbonyl carbon chemical shifts (247 and 189 ppm) exhibiting the same splitting pattern as observed for complexes **19** – **21** as a doublet of doublets for each signal. This high field chemical shift (however, lower chemical shift relative to those of complexes **19** – **21** (295 – 303 ppm)) demonstrates the decreased electrophilic character of the amino-substituted carbene ligand, as previously it has been shown that the effect of the co-ligands on the chemical shift of the carbene carbon atom is negligible. The ferrocenyl *ipso*-carbon signal however only appears as a doublet (86 ppm, 3.5 Hz) which suggests that there is no carbon-phosphorus coupling in this case. However, this might be due to signal broadening due to decreased solubility of the complex in the deuterated solvent.

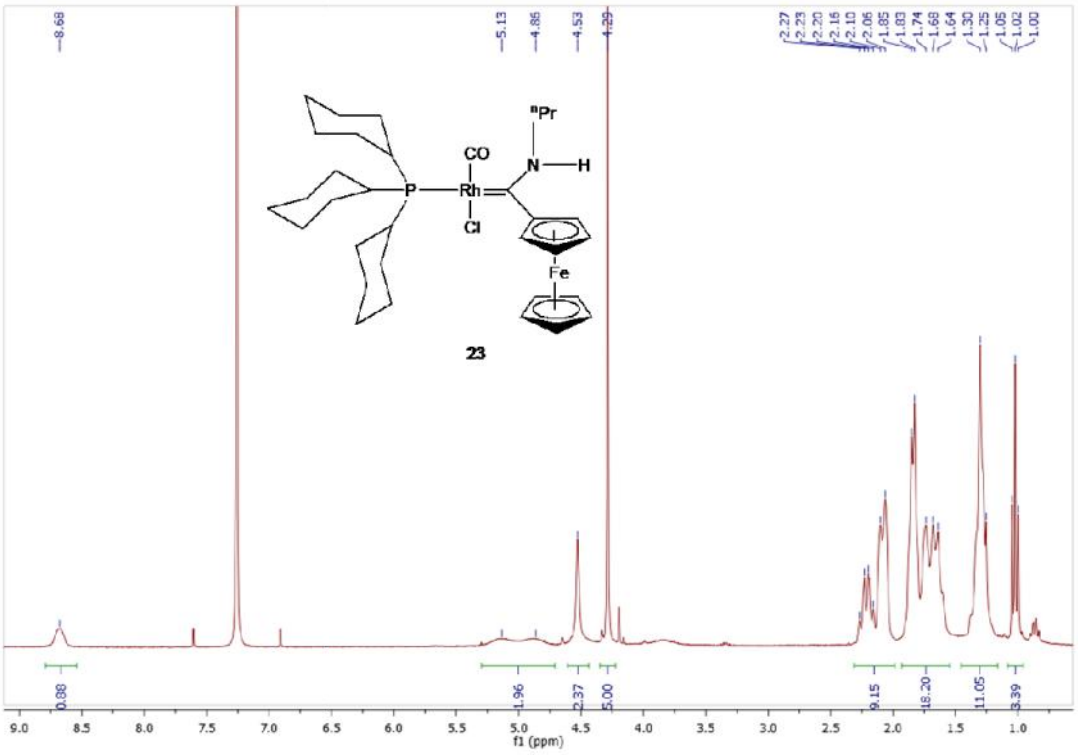

Figure 4.14: ^{1}H NMR spectrum of complex **23** in $CDCl_3$

Chapter 4: Ligand substitution in the coordination sphere of the Rh(I) carbene complexes

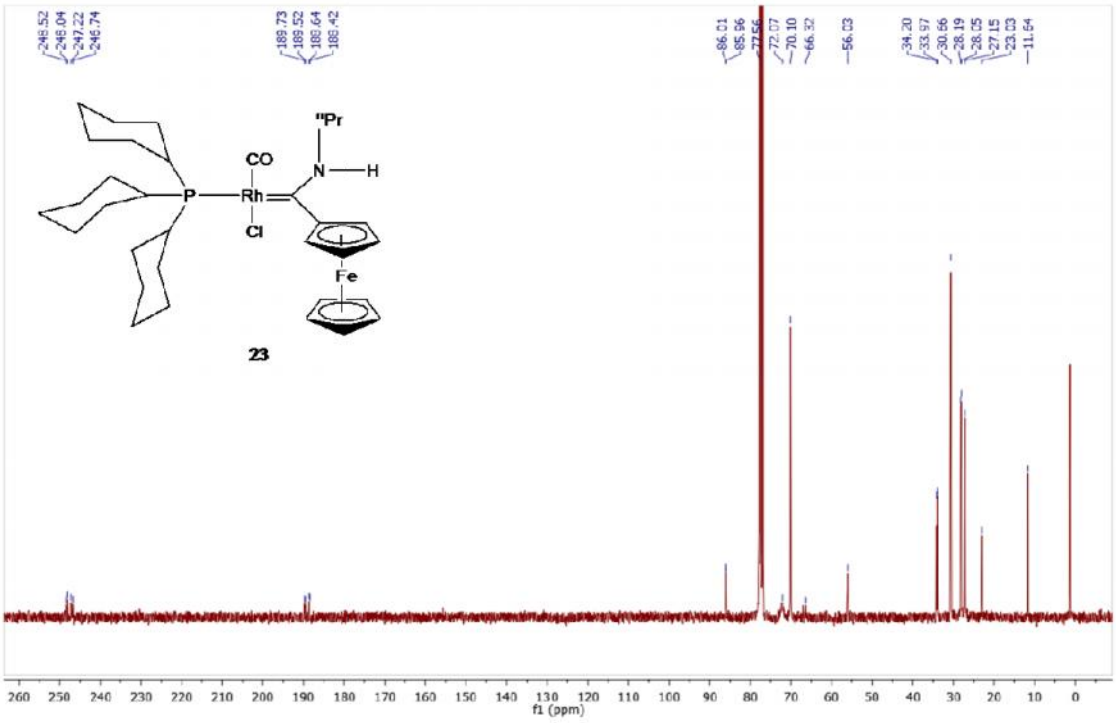

Figure 4.15: ^{13}C NMR spectrum of complex **23** in $CDCl_3$

Single crystals suitable for X-ray diffraction were grown by the slow diffusion of distilled hexanes into a concentrated solution of **23** in dichloromethane and the crystal structure is shown in Figure 4.16 below. The complex displays a square planar geometry at the rhodium(I) center. The structure shows that the *anti*-conformation of the amino substituent is maintained as observed from aminocarbene complexes **16** and **18** The Rh–$C_{carbene}$ bond distance of 2.054(2) Å is slightly longer than those of **19** and **20** (2.027(1) and 2.017(2) Å respectively) as a result of less back donation required from the rhodium(I) metal, effected by the electron donation from the amino substituent to the carbene carbon atom. The $C_{carbene}$-N bond distance of 1.301(2)Å is the same as that of the dicarbonyl amino complex **18** (1.305(2) Å).

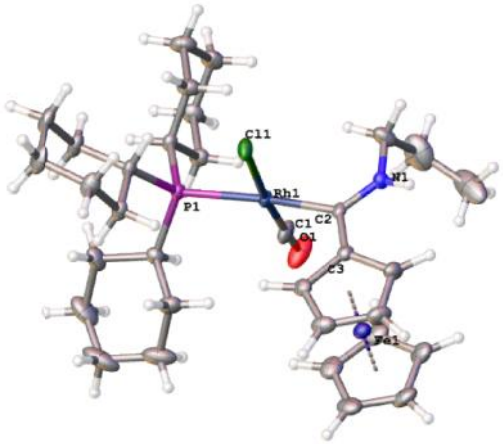

Figure 4.16: Crystal structure of complex **23**.

Chapter 4: Ligand substitution in the coordination sphere of the Rh(I) carbene complexes

4.3.2: A comparative view

4.3.2.1: Spectroscopic data

Table 4.1: Spectroscopic data for complexes **19** - **23**

Com-plex	$^{13}C\delta(C_{carbene})^{a}$, ($^{1}J$(RhC) and ^{2}J(PC) (Hz))	$^{13}C\ \delta(CO)^{a}$, (^{1}J(RhC)and ^{2}J(PC) (Hz))	IR^{b} ν(CO) (cm^{-1})
19	300 (dd, 110, 40)	188 (dd, 81, 16)^{c}	1965^{c}
20	303 (dd, 103, 39)	189 (dd, 83, 17)^{c}	1946^{c}
21	298 (dd, 174, 39)	185 (dd, 79, 21)^{c}	1986^{c}
22	295 (d, 45)	187 (d, 80)^{c}	1966^{c}
23	247(dd, 98, 36)	189 (dd, 82, 16)^{c}	1939^{c}

^{a}Recorded in $CDCl_3$. ^{b}Recorded in CH_2Cl_2. ^{c}CO-ligand trans to Cl.

The carbonyl ^{13}C resonances are relatively insensitive to the changes in the electronic properties of the metal. The infrared carbonyl stretching frequencies of the monocarbonyl carbene complexes **19** – **23** (Table 4.1) give a better reflection of the donating ability of the electronic environment around the Rh(I) centre, and correlate with the expected donor ability of the ligands in the order PCy_3> PPh_3 , $AsPh_3$> $P(OPh)_3$.[2] In the case of the aminocarbene complex **23**, its lowest carbonyl infrared stretching frequency of 1939 cm^{-1} attests to the least Rh-$C_{carbene}$ back donation required in comparison to all the other rhodium(I) carbonyl complexes (**17** – **22**), indicative of collective electron donor effect of the phosphine ligand to the rhodium(I) metal and the amino substituent to the carbene carbon atom .

Table 4.2: Selected bond lengths (Å) and angles (°) for the complexes **19**, **20**, **23**.

Bond lengths	19	20	23
Rh-$C_{carbene}$	2.017(4)	2.027(1)	2.054(2)
$C_{carbene}$-O/N	1.312 (7)	1.312(2)	1.301(2)
$C_{carbene}$-$C_{ipso\text{-}Fc}$	1.448(6)	1.441(2)	1.465(2)
Rh-Cl	2.381(1)	2.374(1)	2.394(9)
Rh-CO	1.832(6)	1.799(2)	1.798(5)
Rh-P	2.329(1)	2.357(1)	2.338(8)
Bond angles			
$C_{carbene}$-Rh-Cl	86.4(1)	86.28(4)	85.11(1)
O/N-$C_{carbene}$-$C_{ipso\text{-}Fc}$	111.5(4)	110.5(1)	115.5(4)

Chapter 4: Ligand substitution in the coordination sphere of the Rh(I) carbene complexes

The increased Rh–$C_{carbene}$ distance of the aminocarbene complex compared to the ethoxy-analogue **23** (2.054(2) Å), is indicative of the greater carbene carbon stabilization from the N-heteroatom compared to the O-carbene substituents in **19** and **20**, and resultant decreased π-back bonding required from the rhodium metal towards the carbene carbon atom. Likewise, shorter $C_{carbene}$–N bond distance of 1.301(2) Å for **23** compared to the $C_{carbene}$–O bond lengths (1.312(7) Å for **19** and 1.312(2) Å for **20**), and less acute N–$C_{carbene}$–C_{Fc} bond angle of 115.5(4)° for **23** compared to the O–$C_{carbene}$–C_{Fc} bond angles (111.5(4) Å for **19** and 110.5(1) Å for **20**), also attest to the increased $C_{carbene}$-N bond order (Table 4.2). Additionally, the effect of the π-acidic carbonyl ligands on the π-back donation of the metal to the carbene carbon in **19, 20** and **23** is evidenced by the Rh–CO bond lengths of the carbonyl ligands *trans* to the chlorido-ligand as they are all significantly shorter (1.798(5) –1.832(6) Å), than those of the Rh–P bond lengths (2.329(1) – 2.338(8) Å). The steric bulk of the coligand *trans* to the carbene influences the rotational freedom of the ferrocenyl moiety.

4.3.2.2: Electrochemical studies of complexes 15 – 22

The cyclic voltammograms (CVs) of **15** – **22** at a glassy carbon electrode in CH_2Cl_2 show irreversible reduction of the carbene at *ca.* -2.3 V, reversible oxidation of the ferrocenyl moiety at *ca.* 0.2 V and ill-defined peaks related to the Rh(I/II) and Rh(II/III) couples at higher potentials, ranging between 0.52 V for **20** and 1.02 V for **15** (*vs.* Ag/Ag^+, $E^{\circ\prime}$= -0.54 V for the couple $[Fe(\eta^5\text{-}C_5Me_5)_2]^{+1/0}$ as an internal standard, referenced to the ferrocene/ferrocenium couple at 0V).

Table 4.3: Potentials (V) for the three redox processes observed for complexes **15**– **22** *vs.* the Ag/Ag^+ couple using the redox couple $[Fe(\eta\text{-}C_5Me_5)_2]^{+1/0}$ as internal standard in the test solutions.

Complex	$E_{p,}^{red}$ (V) [Rh=C/˙Rh-C˙]	Eîà (V) [Fe(II/III)]	E_p^{ox}(V) [Rh(I/II)], [Rh(II/III)]
15	-2.42	0.25	0.80, 1.02
16	-2.60	0.13	0.52, 0.69
17	-1.95	0.36	-[b]
18	-2.30	0.24	0.87[a]
19	-2.30	0.28	0.54, 0.59
20	-2.34	0.28	0.66, 0.79
21	-2.16	0.31	0.92[a]
22	-2.20	0.29	0.61, 0.71

[a]*Overlapping waves of [Rh(I/II)] and [Rh(II/III)].* [b]*Notobserved in the solvent window employed.*

The values obtained for **15 – 22** are summarized in Table 4.3. The CV of **15**, from -1.05 V to 1.3 V, shows three oxidation waves with peak potentials, at $E^{\circ\prime}$ = 0.25 V and, E_p^{ox} = 0.80 and 1.02 V (Figure 4.17a (2)).

Chapter 4: Ligand substitution in the coordination sphere of the Rh(I) carbene complexes

When the scan was curtailed at 0.4 V (Figure 4.17a(1)), the first oxidation wave was reversible. Thus, the one-electron oxidation product of **15**, $[Rh(cod)Cl\{C(OEt)Fc\}]^+$, is stable on the CV timescale.

This result is consistent with that shown for **21** in Figure 4.17c. The CV of **16** from -2.71 to 0.79 V (Figure 4.17b) shows one reduction wave with peak potencial, E_p^{red}= -2.60 V and three oxidation waves with peak potentials at $E^{\circ\prime}$ = 0.13 V, and E_p^{ox} = 0.52 and 0.69 V. The CVs also show no overlap between the wave corresponding to Fe(II/III) and of the redox potentials of the Rh(I/II) and Rh(II/III) processes. The similitude of the Fe(II/III) redox potential values of the ferrocenylcarbene-substituents (the only waves that meet the criteria for a fully reversible system in our series) allow only in certain cases the data to be useful as a comparative tool to discriminate between the overall electronic effect of the more (aminocarbene) or less (ethoxycarbene) donating carbene ligands, and the co-ligands (cod; $(CO)_2$; CO, PR_3 (R = Ph, Cy or OPh) and CO, $AsPh_3$). For example, there is a significant difference of 0.11 V between $E^{\circ\prime}$ observed for the Fe(II/III) redox potential values of **18** and its cod analogue **16** (which can be oxidized at lower potentials because it has a more donating ligand). However, the irreversible nature of the Rh(I/II) and Rh(II/III) processes (tabulated as E_p^{ox} in Table 4.3) means that a correlation between the LEPs and TEPs is not possible.

The irreversible reduction wave at negative potential corresponds to the one-electron reduction of the Rh=C bond to $^{-}$Rh-C$^{\bullet}$, similarly to the reduction of carbene ligands of Group 6 Fischer complexes.[15,16] In this case, a clear qualitative trend of the overall electron withdrawing ability of the carbene ligand and the co-ligands can be established, corresponding to the trend observed for the IR carbonyl stretching frequencies of the complexes **15 – 22**. The reduction potentials can be arranged in order of decreasing negative values for **16** (cod, NH^nPr; -2.60 V) >**15** (cod, OEt; -2.42 V) >**20** (PCy_3, CO, OEt; -2.34 V) >**19** (PPh_3, CO, OEt; -2.30 V); **18** ($(CO)_2$, NH^nPr; -2.30 V) >**22** ($AsPh_3$, CO, OEt; -2.20 V) >**21** ($P(OPh)_3$, CO, OEt; -2.16 V)>**17** ((CO_2), OEt; -1.95 V) where the more electron withdrawing carbene and coligands display greater ease of reduction.

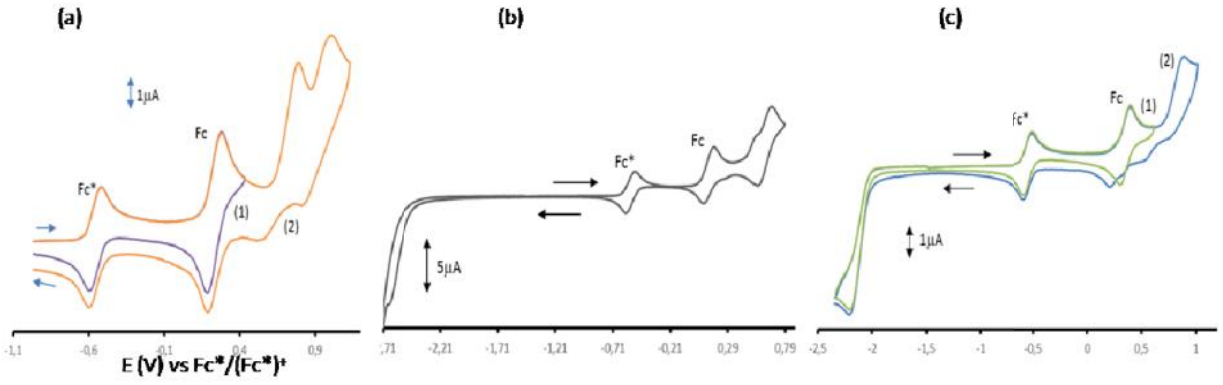

Figure 4.17: The cyclic voltammograms of (a) [Rh(cod)Cl{C(OEt)Fc}] (**15**), (b) [Rh(cod)Cl{C(NH^nPr)Fc}] (**16**) and (c) [Rh(CO){$P(OPh)_3$}Cl{C(OEt)Fc}] (**21**) respectively, at a glassy carbon electrode, scan rate 0.1 V s^{-1} in CH_2Cl_2, with the internal standard used (marked as Fc*).

Chapter 4: Ligand substitution in the coordination sphere of the Rh(I) carbene complexes

4.4: Conclusion

The synthesis and characterization of rhodium(I) ferrocenyl Fischer carbbene complexes **19** – **23** was achieved. The restricted rotation of the ferrocenyl ligand brought about by the steric bulk around the rhodium metal coordination sphere results in the lack of symmetry as observed in the NMR spectra for all complexes is maintained from complexes **15** – **18** synthesized in Chapter 3, as is the formation of only the *anti*-aminocarbene isomer in the case of complex **23** as attested to by both NMR and single crystal X-ray diffraction studies. As expected, this complex is more stable in solution (no dimerization decomposition observed) than the ethoxy analogues, complexes **19** – **22**.The cyclic voltammetric studies done on carbene complexes **15** – **22** showed the general expected trend for the coligands cod > CO, PCy_3> CO, PPh_3> CO, $AsPh_3$ > CO, $P(OPh)_3$> $(CO)_2$ towards decreasing donor-ability. This trend was also confirmed by FT-IR (and to some lesser extent NMR) spectroscopic results.

4.5: Experimental

4.5.1: [Rh(CO)(PPh_3)Cl{C(OEt)Fc}] 19.

Carbon monoxide gas was bubbled for 5 min through a stirred solution of **[Rh(cod)Cl{C(OEt)Fc}] 15** (0.215 g, 0.44 mmol) in CH_2Cl_2(10 mL) in the absence of light at -10 ^oC. The flow of CO was stopped and the solution allowed to reach room temperature. Solid PPh_3 (0.116 g, 0.44 mmol) was then added and the mixture stirred for 5 minutes. Slow concentration of the mixture of the filtrate and *n*-hexane under reduced pressure gave a purple-red solid. Yield = 0.265 g, 90%. Mp: 100–102 ^oC.^{1}H NMR (300 MHz, $CDCl_3$) δ 7.74 – 7.68 (m, 6H, PPh_3), 7.42–7.39 (m, 9H, PPh_3), 5.73 (dq, ^2J(HH) = 10.5 Hz, ^3J(HH) = 7.2 Hz, 1H,O$\underline{CH_2}CH_3$), 5.52 (dq, ^2J(HH) = 10.5 Hz, ^3J(HH) = 7.2 Hz, 1H, O$\underline{CH_2}CH_3$), 5.40 (s, br, 1H, FeCp'), 5.16 (s, br, 1H, FeCp'), 4.87 (dd, ^1J(HH) = 3.9, ^2J(HH) = 2.4 Hz, 2H, FeCp'), 4.39 (s, 5H, FeCp), 1.65 (t, ^3J(HH) = 7.2 Hz, 3H, OCH$_2\underline{CH_3}$). ^{13}C{^{1}H} NMR (75 MHz, $CDCl_3$) δ 299.7 (dd, ^2J(PC) = 110.2 Hz, ^1J(RhC) 40.1 Hz, $C_{carbene}$), 187.5 (dd, ^1J(RhC) = 81.4 Hz, ^2J(PC) = 16.2 Hz, CO), 134.9 (d, ^1J(PC) = 11.9 Hz, PPh_3-C_{ipso}), 134.0 (d, ^2J(PC)= 38.3 Hz, PPh_3), 130.2 (PPh_3), 128.48 (d, ^3J(PC) = 9.7 Hz, PPh_3), 87.3 (dd, ^2J(RhC) = 8.2, ^3J(PC) = 2.3 Hz, FeCp'-C_{ipso}), 79.9 (O$\underline{CH_2}CH_3$), 75.9 (FeCp'), 75.3 (FeCp'), 70.8 (FeCp), 15.23 (OCH$_2\underline{CH_3}$). ^{31}P{^{1}H} NMR (121 MHz, $CDCl_3$) δ 27.4 (d, ^1J(RhP) = 99.9 Hz).(IR, CH_2Cl_2, ν(CO), cm^{-1}): 1965. Anal. Calcd. For $C_{32}H_{29}O_2PClFeRh$: C 57.30, H 4.36. Found: C 56.47, H 4.27. ESI-HRMS (15V, positive mode, *m/z*): calcd. for $[M\text{-}Cl\text{-}PPh_3]^+$ 372.9398; found, 372.9416.

The analogues **[Rh(LL)Cl{C(OEt)Fc}] [LL = (CO, PR_3) (R = Cy or OPh) and (CO, $AsPh_3$)] 20 –22** were prepared similarly as purple-red powders (**20**) or as oily solids (**21** and **22**). In like manner, the complex

Chapter 4: Ligand substitution in the coordination sphere of the Rh(I) carbene complexes

[Rh(CO)(PCy$_3$)Cl{C(NH^{n}Pr)Fc}] 23 was also prepared from the precursor monocarbene complex **[Rh(cod)Cl{C(NH^{n}Pr)Fc}] 16** as yellow-orange crystals.

4.5.2: [Rh(CO)(PCy$_3$)Cl{C(OEt)Fc}] 20.

Yield = 0.102 g, 67%. Mp: 167–169 ºC. ^{1}H NMR (300 MHz, $CDCl_3$) δ 5.64 (dq, ^2J(HH) = 10.5 Hz, ^3J(HH) = 7.2 Hz, 1H, O$\underline{CH_2}CH_3$), 5.42 (dq, ^2J(HH) = 10.6 Hz, ^3J(HH) = 7.2 Hz, 1H, O$\underline{CH_2}CH_3$), 5.31 (s, br, 1H, FeCp'), 5.10 (s, br 1H, FeCp'), 4.81 (dd, ^2J(HH) = 2.6 Hz, ^2J(HH) = 2.6 Hz, 2H, FeCp'), 4.38 (s, 5H, FeCp), 2.26 – 2.16 (m, 3H, PCy_3), 2.07 – 2.03 (m, 6H, PCy_3), 1.83–1.60 (m, 15H, PCy_3), 1.62 (t, ^3J(HH) = 7.2 Hz, 3H, OCH$_2\underline{CH_3}$), 1.29 (s, 9H, PCy_3).^{13}C{^{1}H} NMR (75 MHz, $CDCl_3$) δ 302.5 (dd, ^2J(PC) = 103.2 Hz, ^1J(RhC) = 38.9 Hz. $C_{carbene}$), 188.0 (dd, ^1J(RhC) = 82.3 Hz, ^2J(PC) = 16.7 Hz, CO), 87.6 (dd, ^2J(RhC) = 7.5 Hz, ^3J(PC) = 2.5 Hz, FeCp'-C_{ipso}), 78.7 (O$\underline{CH_2}CH_3$), 75.1 (FeCp'), 74.5 (FeCp'), 70.3 (FeCp), 33.4 (d, ^1J(PC) = 17.7 Hz, PCy_3-C_{ipso}), 30.3 (PCy_3), 27.8 (PCy_3), 27.7 (PCy_3), 26.7 (PCy_3), 14.9 (OCH$_2\underline{CH_3}$). ^{31}P{^{1}H} NMR (121 MHz, $CDCl_3$) δ 34.7 (d, ^1J(RhP) = 98.4 Hz). (IR, CH_2Cl_2, ν(CO), cm^{-1}): 1946. Anal. Calcd. For $C_{32}H_{47}O_2PClFeRh$: C 55.79, H 6.88. Found: C 56.41, H 6.57. ESI-HRMS (15V, positive mode, *m/z*): calcd. for [M-Cl-CO]$^+$ 625.1769; found, 625.1733; calcd. for [M-Cl-PCy_3]$^+$ 372.9398; found, 372.9416.

4.5.3: [Rh(CO)(P(OPh)$_3$)Cl{C(OEt)Fc}] 21.

Yield = 0.163 g, 63%. Mp: 74–76 °C. ^{1}H NMR (300 MHz, $CDCl_3$) δ 7.41 (dd, ^2J(HH) = 7.8 Hz, ^3J(HH) = 7.8 Hz, 6H, OPh_3), 7.37 (dd, ^2J(HH) = 7.9 Hz, ^2J(HH) = 7.9 Hz, 6H, OPh_3), 7.19 (dd, ^2J(HH) = 8.1 Hz, ^3J(HH) = 8.1 Hz, 3H, OPh_3), 5.06 (q, ^3J(HH) = 7.1 Hz, 2H, O$\underline{CH_2}CH_3$), 4.88–4.87 (m, 2H, FeCp'), 4.83 – 4.80 (m, 2H, FeCp'), 4.38 (s, 5H, FeCp), 1.41 (t, ^3J(HH) = 7.2 Hz, 3H, OCH$_2\underline{CH_3}$). ^{13}C{^{1}H} NMR (75 MHz, $CDCl_3$) δ 298.4 (dd, ^2J(PC) = 174.1 Hz, ^1J(RhC) = 38.9 Hz, $C_{carbene}$), 184.8 (dd, ^1J(RhC) = 79.1 Hz, ^2J(PC) = 21.0 Hz, CO), 151.9 (d, ^2J(PC) = 4.8 Hz, OPh_3-C_{ipso}), 129.8 (OPh_3), 125.0 (OPh_3), 122.2 (d, ^3J(PC) = 5.5 Hz, OPh_3), 86.5 (dd, ^2J(RhC) = 12.6 Hz, ^3J(PC) = 2.5 Hz, FeCp'-C_{ipso}), 79.9 (O$\underline{CH_2}CH_3$), 76.3 (FeCp'), 75.9 (FeCp'), 71.0 (FeCp), 15.0 (OCH$_2\underline{CH_3}$). ^{31}P{^{1}H} NMR (121 MHz, $CDCl_3$) δ 127.0 (d, ^1J(RhP) = 177.4 Hz).(IR, CH_2Cl_2, ν(CO), cm^{-1}): 1986. Anal. Calcd. For $C_{32}H_{29}O_5PClFeRh$: C 53.47, H 4.07. Found: C 48.19, H 3.77. ESI-HRMS (15 V, positive mode, *m/z*): calcd. for [M-Cl-CO]$^+$ 655.0208; found, 655.0435; calcd. for [M-Cl-P(OPh)$_3$]$^+$ = 372.9398; found, 372.9282.

4.5.4: [Rh(CO)(AsPh$_3$)Cl{C(OEt)Fc}] 22.

Yield = 0.096 g, 63%. Mp: 98–100 °C. ^{1}H NMR (300 MHz, $CDCl_3$) δ 7.65 (dd, ^3J(HH) = 3.6 Hz, ^3J(HH) = 3.6 Hz, 6H, $AsPh_3$), 7.41 – 7.40 (m, 9H, $AsPh_3$), 5.75 (dq, ^2J(HH) = 10.4 Hz, ^3J(HH) = 7.2 Hz, 1H, O$\underline{CH_2}CH_3$), 5.57 (dq, ^2J(HH) = 10.2 Hz, ^3J(HH) = 7.2 Hz, 1H, O$\underline{CH_2}CH_3$), 5.40 (s, br, 1H, FeCp'), 5.21 (s, br, 1H, FeCp'), 4.87 (s, br, 2H, FeCp'), 4.41 (s, 5H, FeCp), 1.66 (t, ^3J(HH) = 7.1 Hz, 3H, OCH$_2\underline{CH_3}$). ^{13}C{^{1}H} NMR (75 MHz, $CDCl_3$) δ 295.3 (d, ^1J(RhC) = 45.1 Hz, $C_{carbene}$), 186.5 (d, ^1J(RhC) = 80.3 Hz, CO), 135.5 ($AsPh_3$), 134.4 ($AsPh_3$), 129.9($AsPh_3$), 129.0 ($AsPh_3$), 87.4(d, ^2J(RhC) = 3.5 Hz, FeCp'-C_{ipso}), 80.1 (O$\underline{CH_2}CH_3$), 75.8 (FeCp'), 75.4 (FeCp'), 70.9 (FeCp), 15.2 (OCH$_2\underline{CH_3}$). (IR, CH_2Cl_2, ν(CO), cm^{-1}): 1966. Anal. Calcd. For $C_{32}H_{29}O_2AsClFeRh$: C 53.78, H 4.09. Found: C 51.71, H 3.52.ESI-HRMS (15 V, positive mode, *m/z*): calcd. for [M-Cl-AsPh)$_3$]$^+$ = 372.9398; found, 372.9282.

4.5.5: [Rh(CO)(PCy$_3$)Cl{C(NH^{n}Pr)Fc}] 23

Chapter 4: Ligand substitution in the coordination sphere of the Rh(I) carbene complexes

Yield = 0.062 g, 82%. ^{1}H NMR (300 MHz, $CDCl_3$) δ8.68 (s, br, 1H, $\underline{NH}CH_2CH_2CH_3$), 5.13 (s, br, 1H, FeCp'), 4.86 (s, br 1H, FeCp'),), 4.53 (s, br 2H, FeCp'), 4.29 (s, 5H, FeCp), 2.27 – 2.16 (m, 3H, $NH\underline{CH_2}\underline{CH_2}CH_3$(overlap)), 2.27 – 2.06 (m, 5H, PCy_3), 1.85 – 1.64 (m, 18H, PCy_3), 1.30–1.25 (m, 11H, PCy_3), 1.02 (t, ^{3}J(HH) = 7.4 Hz, 3H,$NHCH_2CH_2\underline{CH_3}$).^{13}C{^{1}H} NMR (75 MHz, $CDCl_3$) δ 247.6 (dd, ^{2}J(PC) = 98.1 Hz, ^{1}J(RhC) = 36.1 Hz. $C_{carbene}$), 189.1 (dd, ^{1}J(RhC) = 82.8 Hz, ^{2}J(PC) = 16.3 Hz, CO), 86.0 (d,br,^{2}J(RhC) = 3.5 Hz,FeCp'-C_{ipso}), 77.6 (FeCp'), 72.1 (FeCp'), 70.1 (FeCp), 66.3 (FeCp'), 56.0 ($NH\underline{CH_2}CH_2CH_3$), 34.1 (d, ^{1}J(PC) = 17.9 Hz, PCy_3-C_{ipso}), 30.7 (PCy_3), 28.2 (PCy_3), 28.1 (PCy_3), 27.2 (PCy_3), 23.0 ($NHCH_2\underline{CH_2}CH_3$), 11.6 ($NHCH_2CH_2\underline{CH_3}$). ^{31}P{^{1}H} NMR (121 MHz, $CDCl_3$) δ 37.4 (d, ^{1}J(RhP) = 104.7 Hz). (IR, CH_2Cl_2, ν(CO) and ν(NH), cm^{-1}): 1939, 3315.ESI-HRMS (15V, positive mode, *m/z*): calcd. for $[M\text{-}Cl\text{-}CO]^+$ 638.2085; found, 638.2054; calcd. for $[M\text{-}Cl]^+$ 666.2034; found, 666.2056.

4.6: References

1 W. Gil and A. M. Trzeciak, *Coord. Chem. Rev.*, 2011, **255**, 473–483.

2 C. A. Tolman, *Chem. Rev.*, 1977, **77**, 313–348.

3 L. Perrin, E. Clot, O. Eisenstein, J. Loch and R. H. Crabtree, *Inorg. Chem.*, 2001, **40**, 5806–5811.

4 D. Evans, J. A. Osborn and G. Wilkinson, *J. Chem. Soc. A Inorganic, Phys. Theor.*, 1968, 3133–3142.

5 R. A. Kelly III, H. Clavier, S. Giudice, N. M. Scott, E. D. Stevens, J. Bordner, I. Samardjiev, C. D. Hoff, L. Cavallo and S. P. Nolan, *Organometallics*, 2008, **27**, 202–210.

6 J. Huang, E. D. Stevens and S. P. Nolan, *Organometallics*, 2000, **19**, 1194–1197.

7 S. Gonell, R. G. Alabau, M. Poyatos and E. Peris, *Chem. Commun.*, 2013, **49**, 7126.

8 A. B. P. Lever, *Inorg. Chem.*, 1990, **29**, 1271–1285.

9 L. Mercs, G. Labat, A. Neels, A. Ehlers and M. Albrecht, *Organometallics*, 2006, **25**, 5648–5656.

10 M. S. Collins, E. L. Rosen, V. M. Lynch and C. W. Bielawski, *Organometallics*, 2010, **29**, 3047–3053.

11 S. Wolf and H. Plenio, *J. Organomet. Chem.*, 2009, **694**, 1487–1492.

12 D. Evans, J. A. Osborn, G. Wilkinson, Robert Paine and R. W. Parry, in *Inorganic Syntheses*, ed. W. L. Jolly, John Wiley and Sons, Inc., Hoboken, NJ, 1968, pp. 99–101.

13 B. E. Mann, *J. Chem. Soc. Perkin Trans. 2*, 1972, 30.

14 M. Zeldin, P. Mehta and W. D. Vernon, *Inorg. Chem.*, 1979, **18**, 463–466.

Chapter 4: Ligand substitution in the coordination sphere of the Rh(I) carbene complexes

15 D. I. Bezuidenhout, W. Barnard, B. van der Westhuizen, E. van der Watt and D. C. Liles, *Dalton Trans.*, 2011, **40**, 6711–6721.

16 D. I. Bezuidenhout, I. Fernández, B. Van Der Westhuizen, P. J. Swarts and J. C. Swarts, *Organometallics*, 2013, **32**, 7334–7344.

Chapter 5: Hydroformylation Catalysis

5.1: Overview

The rhodium-catalyzed hydroformylation of terminal alkenes to aldehydes is a well-known process,[1] whereby the most widely known rhodium-based catalyst commonly used included phosphine ligands in the rhodium(I) coordination sphere.[2] The generally accepted mechanism of rhodium-catalyzed alkene hydroformylation,[3] involves a rhodium(I)-hydrido complex as the key catalytic species as outlined in Scheme 5.1 below, thus all non-hydride complexes will henceforth be referred to as catalyst precursors. The modulation of the steric and electronic properties of the commonly-used phosphine ligands has been directed towards the optimization of both the activity and the selectivity of these rhodium-based catalysts. Specifically, an increase in the *n*/*iso* ratio of the aldehydes has been found due to a high steric demand around the rhodium-center when excess phosphines were employed, or when phosphines with stronger π-acceptor properties were used.[4]

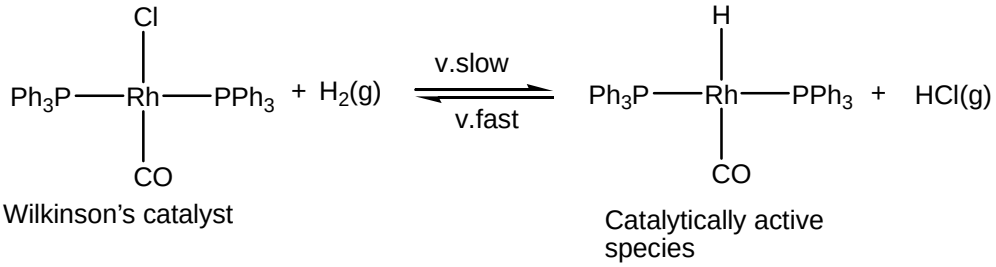

Scheme 5.1: The formation of the rhodium(I)-hydrido active catalyst during the hydroformylation process.[2]

5.1.1: Rhodium(I)-NHC hydroformylation catalysts

The only types of carbene complexes used in hydroformylation reactions to date are rhodium-NHCs,[5–7] mainly due to the fact that N-heterocyclic carbenes are the most stable of all types of carbenes (in addition to their ease of coordination to the metal), thus rendering them more practically applicable. In addition, a water-soluble rhodium-NHC has also been applied in the biphasic hydroformylation of 1-octene and reused over 4 cycles,[8] thus attesting to the truly robust and stabilizing nature of the NHC ligand.[9]

The shape of the NHC ligand differs from that of a phosphine thus the application of the Tolman cone angle[10] cannot be used for the estimation of the steric demand of carbenes. Unlike phosphines (that impart steric parameterization by a cone), NHCs provide an 'umbrella' or 'fan' type of steric crowding around the metal centre. A convenient measure of this steric effect is called the 'buried volume' parameter ($\%V_{bur}$),[11] which measures the volume of the central metal atom 'buried' or occupied by the metal upon ligand coordination. Some reviews suggest that the most promising and selective system for hydroformylation is constituted by a Rh-NHC catalyst precursor, with stoichiometric amounts of electron withdrawing phosphorus ligands added to

Chapter 5: Hydroformylation Catalysis

the catalytic system.[4,5] Studies have found that electron-poor NHC complexes provide for more active catalysts than complexes with electron-rich NHCs coordinated to the rhodium(I) metal. However the selectivity of the products formed does not significantly alter even after the introduction of bulky substituents on the NHCs.[12] This conclusion prompted the investigation into the use of electrophilic Fischer carbene complexes of rhodium(I) as catalyst precursors for the hydroformylation of 1-octene in an attempt to isolate a catalyst precursor with a π-accepting carbene ligand, and coligands of varying π-acceptor ability, for improved regio- or chemoselectivity of product formation during hydroformylation. The approach of including a second metal centre (the redox-active ferrocenylcarbene substituent) also confers possible advantages such as increased stability of the carbene ligand and improved activity of the catalyst precursor and increased reaction rates, specifically involving examples where one metal acts as the main catalytic center whereas the other metal serves as an electron reservoir.[13–16]

5.2: Aim

In this chapter, the aim was to apply the rhodium(I) Fischer carbene complexes **15** – **22** as catalyst precursors for the hydroformylation of 1-octene.

5.2.1: Catalytic method

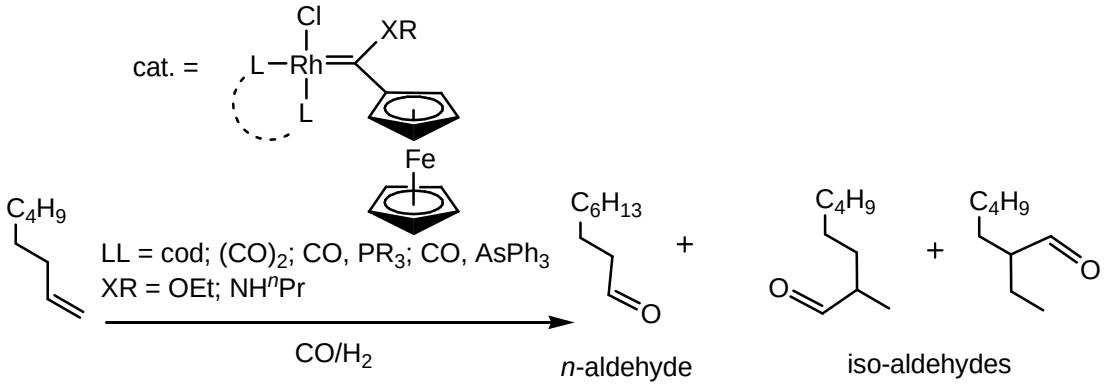

Scheme 5.2: The conversion of 1-octene to aldehydes *via* the use of complexes **15** – **22** as catalyst precursors.

Hydroformylation reactions were conducted (in triplicate to confirm reproducibility of the results) in a 90 mL stainless steel pipe reactor. Under ideal conditions, the terminal alkene is completely converted into aldehydes as outlined in Scheme 5.2. In each experiment, the catalyst precursor (**15** – **22**) (0.0039 mmol), substrate 1-octene (721.0 mg, 6.37 mmol), and the internal standard, *n*-decane (180.0 mg, 1.26 mmol), were dissolved in toluene (5.0 mL) and transferred into a stainless steel pipe reactor (90 mL). The air-tight reactor was then deaerated by flushing three times with N_2 gas, twice with syn-gas, then pressurized with syn-gas (1:1, CO:H_2 ratio) and heated to the desired temperature and pressure. After the reaction time, the reactor was

depressurized and the reaction mixture transferred to a glass vial for cooling. The samples were analyzed by gas chromatography and the products were confirmed in relation to authentic *iso*-octenes and aldehydes.

5.3: Results and Discussion

Complexes **15** – **22** were evaluated as catalyst precursors in the hydroformylation of 1-octene. The reaction conditions for **15** were optimized by variation of the syn-gas pressure (20 – 40 bar), temperature (70 – 90 °C) and reaction time (4 – 8hrs). Under the optimized conditions of 40 bar and 80 °C, the catalyst precursors displayed excellent conversion (>99%) of 1-octene after 4 hours, as well as good chemoselectivity (85–100%) towards aldehydes (Table 5.1). Only moderate regioselectivity was observed with *n/iso*-aldehyde ratios ranging from 0.79 - 1.33, generally favoring the formation of linear aldehydes. A mercury drop-test was performed on catalyst **15** with no resulting significant change in either the conversion or chemo/ regioselectivity of the catalyst, thereby indicating that a heterogeneous catalytic mode of action can be excluded.[17,18]

Chapter 5: Hydroformylation Catalysis

Table 5.1: Hydroformylation of 1-octene with catalyst precursors **15** – **22**. Reactions[a] were carried out with (CO:H2) (1:1) at 40 bar, 80 °C in toluene (5 mL) with 6.37 mmol of 1-octene and 0.0039 mmol Rh catalyst. After 4 hours, the GC conversions were obtained using *n*-decane as an internal standard in relation to authentic standard internal octenes and aldehydes.

Catalyst	% Conversion	% Total Aldehydes	% Internal Octenes	% *n*-Aldehydes	n/isoratio	TOF[b]
15	100	100	0	44 (4.0)	0.79 (0.130)	418 (14.2)
15[c]	91 (1.0)	63 (11.1)	37 (11.1)	62 (0.1)	1.63 (0.01)	256 (51.7)
15[d]	98 (0.6)	58 (7.9)	42 (7.9)	70 (2.1)	2.37 ((0.240)	233 (29.0)
15[e]	90 (10.1)	55 (4.0)	45 (4.0)	62 (8.7)	1.69 (0.610)	204 (40.0)
16	100	90 (2.3)	10 (2.3)	55 (3.0)	1.25 (0.160)	366 (9.0)
17	100	100	0	50 (1.2)	0.98 (0.047)	379 (14.1)
18	99 (0.1)	85 (0.5)	15 (0.5)	57 (3.8)	1.33 (0.210)	343 (8.3)
19	100	100	0	49 (2.7)	0.98 (0.100)	407 (0.9)
20	100	94 (1.2)	6 (1.2)	55 (1.1)	1.20 (0.050)	380 (3.9)
21	100	100	0	51 (0.5)	1.06 (0.020)	409 (27.2)
22	100	85 (2.4)	15 (2.4)	57 (2.7)	1.32 (0.140)	346 (10.0)

[a]Reactions were performed in triplicate, and the standard deviations given in brackets for all results. [b]TOF = (mol aldehydes/mol cat.)h^{-1}. [c]Reaction conditions 40 bar, 70 °C, 4hrs. [d]Reaction conditions 30 bar, 80 °C, 4 hrs. [e]Reaction conditions 20 bar, 80 °C, 4 hrs.

The TOF (turnover frequency)-values ranged from 343–418 h^{-1}, where the ethoxycarbene complexes consistently display higher activities than the analogous aminocarbene complexes **16** and **18.** The effect of the donating capacity of the coligands also result in the general trend for activity (TOF) of the ferrocenylcarbene complexes, arranged in order of decreasing activity: $(CO)_2$< CO, L (PR_3, $AsPh_3$) < cod. In contrast, the *n/iso*-selectivity (regioselectivity) displays the reversed trend, with *n/iso* (aminocarbene **16**, **18**) >*n/iso* (ethoxycarbene **15**, **17**), contrary to the expected improved selectivity for more electron-withdrawing carbene ligands. Again this trend is also reflected by the results obtained for complexes **19** – **22**, where the most donating phosphine coligand (PCy_3, **20**) displays a higher *n/iso* ratio than for example **19** (PPh_3) or **21** ($P(OPh)_3$). However this observation should take into account the overall chemoselectivity, as the

Chapter 5: Hydroformylation Catalysis

n/iso-ratio generally decreases as the total percentage of aldehyde formation increases. The steric properties of the ligands "L" were not investigated in this study.

Examples of very active [Rh(cod)X(NHC)] complexes as 1-octene hydroformylation catalyst precursors, with TOFs ranging from 480–3540 h^{-1}, were reported by Weberskirch and co-workers,[19] however the selectivity decreased to *n/iso*-ratios of less than 0.50 close to full conversion due to olefin isomerization. In contrast, Trzeciak *et al.* reported excellent selectivities with *n/iso*-ratios in the range of 16 – 27 with the addition of phosphorous ligands to the [Rh(cod)Cl(NHC)] catalysts, but this occurred at the expense of low aldehyde yields of 18–26%.[6] Examples of dinuclear Rh-NHC complexes featuring a bridging bisNHC-pyridyl ligand showed full conversion to aldehydes, but mostly branched aldehydes (86 – 100%) were obtained with TOF-values ranging between 3.2–15.7 h^{-1}.[20]

To address the issue of the Rh-$C_{carbene}$ bond stability, a reaction similar to those proposed to test Rh-NHC bond stability was performed.[17,18,21] A high pressure NMR-tube was charged with **15** (0.03 g, 0.06 mmol) and substrate 1-hexene (0.50 mmol, 0.6 mL) dissolved in C_6D_6 (0.70 mL). The reaction vessel was sequentially pressurized with CO (g) and H_2(g), and heated at 80°C for 8 hours. The immediate formation of **17** from **15** was observed (see Figure 5.1a, $^{13}C\{^1H\}$ NMR δ 290.8 (d, *J* = 39.0 Hz, Rh-$C_{carbene}$), 188.2 (d, *J*= 49.8 Hz, Rh-CO) and 184.0 (d, *J* = 75.7 Hz, Rh-CO)). After 8 hours of heating, a new carbene chemical shift, and a new broadened carbonyl ligand resonance were observed (Figure 5.1b, ^{13}C NMR δ 285.3 (d, *J* = 48.7 Hz, Rh-$C_{carbene}$), 185.2 (d, *J* = 92.2 Hz, Rh-CO). This result clearly evidences the retention of the Rh-$C_{carbene}$ bond, albeit a modified Rh-carbene carbonyl complex. Presumably, a dimeric Rh-carbene carbonyl complex[22] is formed as only one new carbonyl and carbene carbon doublet is observed (Scheme 5.3 and Figure 5.1a and b). The coupling constant of the carbonyl resonance (J_{Rh-C} = 92.2 Hz) demonstrates the presence of the bridging chloride ligand *trans* to the remaining carbonyl ligand.

Chapter 5: Hydroformylation Catalysis

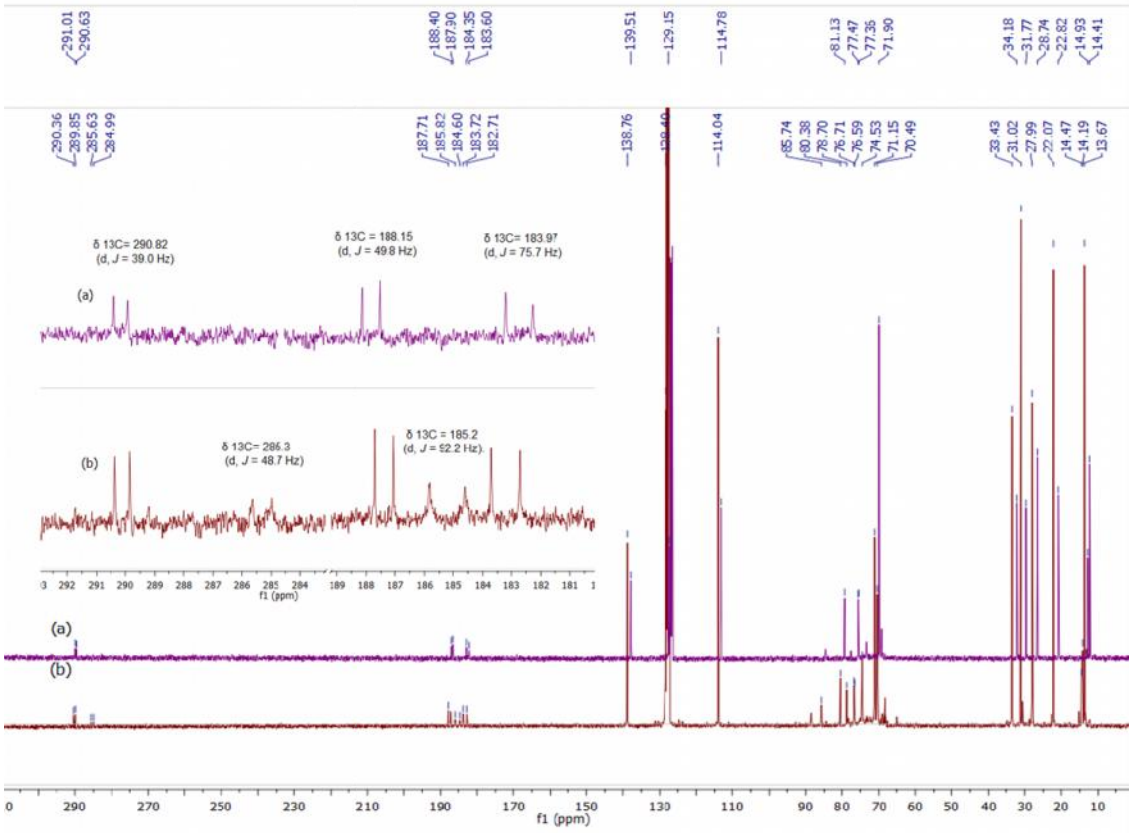

Figure 5.1: ^{13}C NMR spectrum of the Rh-$C_{carbene}$ bond stability test reaction in C_6D_6.

No upfield hydride resonance (up to -20 ppm) was observed in the ^{1}H NMR spectrum (Figure 5.1a) to support the formation of a catalytically active Rh(carbene)-hydrido species **25** (analogous to the Wilkinson catalyst),[23] according to the underlying mechanism of hydroformylation.[3,12,24] The dimeric rhodium-carbene (**24**) is formed as outlined in Scheme 5.3 below, which can be attested to by the earlier-outlined Scheme 5.1. This postulated dimer most probably forms due to the insufficient hydrogen gas pressure required for the formation and stabilization of the rhodium-hydrido complex.[4] This observation was also reported by Wilkinson and co-workers whereby the rhodium-hydrido complex reacted with carbon monoxide to form a dimer by loss of a gaseous hydrogen molecule.[25]

Chapter 5: Hydroformylation Catalysis

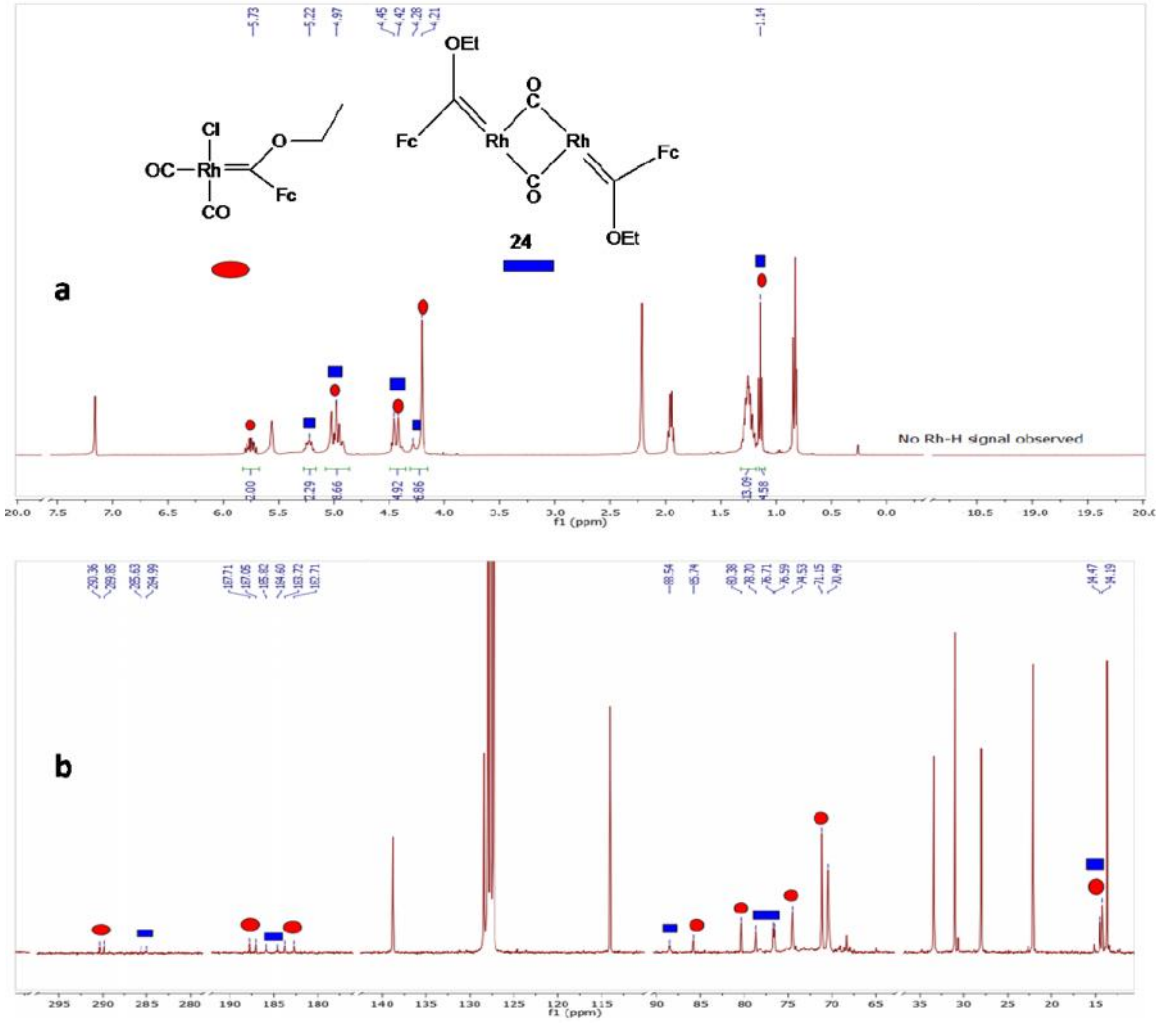

Figure 5.2: (a) ^{1}H NMR and (b) ^{13}C NMR spectrum of the formed dimeric complex from **17**

Chapter 5: Hydroformylation Catalysis

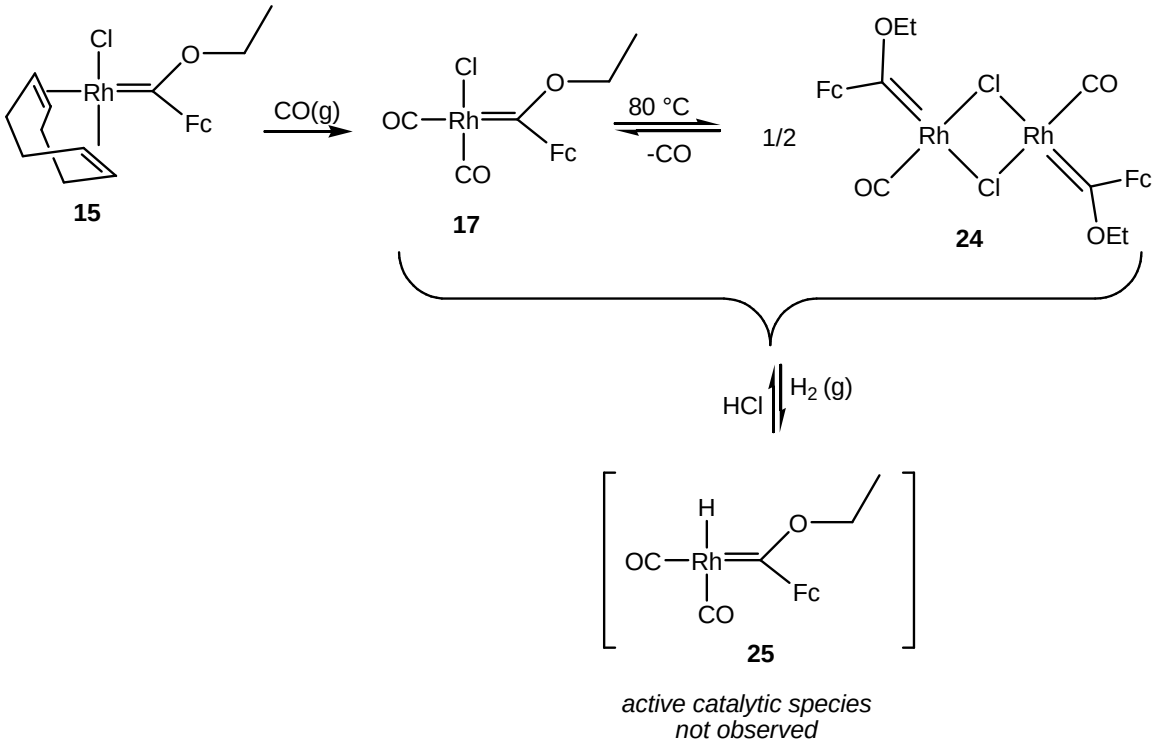

Scheme 5.3: Formation of observed dimeric carbene carbonyl rhodium(I) complex **24**.

5.4: Conclusion

The complexes **15** – **22** were screened as catalyst precursors for the hydroformylation of 1-octene. Excellent conversion of the substrate olefins were observed, with turnover frequencies and chemo- and regioselectivity towards the linear aldehydes, comparable to results reported for rhodium NHC-complexes. Although the ferrocenyl substituent results in Fischer carbene ligands with electron donating abilities similar to NHCs, the Fischer carbene ligand is dissymmetric in contrast to typical NHCs and phosphines. Undoubtedly this steric effect also plays a role with regards to the selectivity of the precursor catalysts. Finally, the retention of the rhodium-carbene bond under hydroformylation conditions was confirmed in a $^{13}C\{^{1}H\}$ NMR spectroscopic study, which also showed the formation of a new dimeric Fischer carbene complex due to the unstable nature of the rhodium(I) hydridocarbene complex, the presumed catalytically active species.

Chapter 5: Hydroformylation Catalysis

5.5: References

1 B. R. James, P. W. N. M. Van Leeuwen, S. D. Ittel, A. Nakamura, R. L. Richards and A. Yamamoto, *Rhodium Catalyzed Hydroformylation*, Kluwer Academic Publishers, Dordrecht, 2000.

2 D. Evans, J. A. Osborn and G. Wilkinson, *J. Chem. Soc. A Inorganic, Phys. Theor.*, 1968, 3133–3142.

3 A. J. Pardey and C. Longo, *Coord. Chem. Rev.*, 2010, **254**, 254–272.

4 A. Van Rooy, P. C. J. Kamer, P. W. N. M. Van Leeuwen, K. Goubitz, J. Fraanje, N. Veldman and A. L. Spek, *Organometallics*, 1996, **15**, 835.

5 W. Gil and A. M. Trzeciak, *Coord. Chem. Rev.*, 2011, **255**, 473–483.

6 W. Gil, A. M. Trzeciak and J. J. Ziółkowski, *Organometallics*, 2008, **27**, 4131–4138.

7 A. C. Chen, L. Ren, A. Decken and C. M. Crudden, *Organometallics Commun.,* 2000, **19**, 18–20.

8 M. T. Zarka, M. Bortenschlager, K. Wurst, O. Nuyken and R. Weberskirch, *Organometallics*, 2004, **23**, 4817–4820.

9 J. W. Herndon, *Coord. Chem. Rev.*, 2014, **272**, 48–144.

10 C. A. Tolman, *Chem. Rev.*, 1977, **77**, 313–348.

11 M. N. Hopkinson, C. Richter, M. Schedler and F. Glorius, *Nature*, 2014, **510**, 485–496.

12 M. Bortenschlager, J. Schütz, D. von Preysing, O. Nuyken, W. A. Herrmann and R. Weberskirch, *J. Organomet. Chem.*, 2005, **690**, 6233–6237.

13 D. G. H. Hetterscheid, S. H. Chikkali, B. deBruin and J. N. H. Reek, *Chem. Cat. Chem.*, 2013, **5**, 2785–2793.

14 J. I. van der Vlugt, *Eur. J. Inorg. Chem.*, 2012, **2012**, 363–375.

15 S. Liu, A. Motta, M. Delferro and T. J. Marks, *J. Am. Chem. Soc.*, 2013, **135**, 8830–8833.

16 S. Siangwata, N. Baartzes, B. C. E. Makhubela and G. S. Smith, *J. Organomet. Chem.*, 2015, **796**, 26–32.

17 D. R. Anton and R. H. Crabtree, *Organometallics*, 1983, **2**, 855–859.

18 J. A. Widegren and R. G. Finke, *J. Mol. Catal. A Chem.*, 2003, **198**, 317–341.

Chapter 5: Hydroformylation Catalysis

19 M. Bortenschlager, J. Schutz, D. von Preysing, O. Nuyken, W. A. Herrmann and R. Weberskirch, *J. Organomet. Chem.*, 2005, **690**, 6233−6237.

20 M. Poyatos, P. Uriz, J. A. Mata, C. Claver, E. Fernandez and E. Peris, *Organometallics*, 2003, **22**, 440–444.

21 J. M. Praetorius and C. M. Crudden, *Dalton Trans.*, 2008, **9226**, 4079–4094.

22 J. Barluenga, R. Vicente, L. A. López and M. Tomás, *J. Organomet. Chem.*, 2006, **691**, 5654–5659.

23 D. Cauzzi, M. Costa, L. Gonsalvi, M. A. Pellinghelli, G. Predieri, A. Tiripicchio and R. Zanoni, *J. Organomet. Chem.*, 1997, **541**, 377–389.

24 S. A. Decker and T. R. Cundari, *Organometallics*, 2001, **20**, 2827–2841.

25 D. Evans, G. Yagupsky and G. Wilkinson, *J. Chem. Soc. A Inorganic, Phys. Theor.*, 1968, 2660–2665.

Chapter 6: Conclusions and Future Work

Prior to this study, Fischer carbene complexes have mainly been applied as stoichiometric reagents in template organic synthesis reactions wherein the carbene ligand is transferred, and is thus incorporated in the formed reaction products. NHC metal complexes are the only types of carbene complexes used for hydroformylation catalysis to date due to their robust nature, even though reports suggested that the strongly donating, negligible π-accepting nature of these types of carbene ligands have had limited success in mediating the selective hydroformylation of alkenes for linear aldehydes. For this reason, the use of the more π-acidic Fischer carbene ligands was envisaged to provide increased selectivity for rhodium(I) hydroformylation (pre)catalysts. However, it has been shown that the electrophilic Fischer carbene rhodium(I) complexes decomposed by a ligand dissociation and dimerization route. In order for these Fischer carbene complexes to be useful as catalysts, the complexes need to be stable enough to isolate yet not so robust as to prevent alkene coordination to the metal center. During this study, the synthesis, isolation and application of rhodium(I) Fischer carbene complexes as hydroformylation catalyst precursors were investigated.

Utilization of heteroaryl (2-thienyl or 2-furyl) substituted Fischer carbene complexes of tungsten(0) or chromium(0) pentacarbonyl as precursor complexes for rhodium(I) carbene complex synthesis, proved unsuccessful. A novel rhodium(I)carbene complex [Rh(cod)Cl{C(OEt)(Fc)}] (**15**) was isolated *via* transmetallation facilitated by employing a more electron-donating ferrocenylcarbene substituent to prevent self-dimerization of the carbene ligand of the precursor complex [$Cr(CO)_5${C(OEt)Fc)}] (**10**). A series of modified rhodium(I) Fischer carbene complexes **16** – **23** were subsequently synthesized by performing ligand modifications on complex **15**. All complexes were successfully characterized by NMR spectroscopy, and the carbonyl carbene complexes **17** – **23** were additionally characterized by FT-IR spectroscopy. The IR-active carbonyl stretching frequencies allowed for the first time, the calculation of TEPs of Fischer carbene ligands for complexes **17** and **18**, thus enabling better comparison of the electronic (and steric) characteristics of Fischer carbenes with NHCs. Surprisingly, the calculated TEPs for the ferrocenylcarbene ligands were found to be of very similar magnitude as commonly reported NHCs, demonstrating the effective electron donation of the ferrocenyl group. The carbonyl stretching frequencies of complexes **19** – **23** also confirmed the π-acceptor ability trend of the coligands PCy_3>PPh_3, $AsPh_3$>$P(OPh)_3$.

Single crystal XRD analyses of complexes **15**, **16**, **18** – **20** and **23** were done and the complexes displayed a square planar (**18** – **20** and **23**) or pseudo-square planar (**15** and **16**) geometry around the rhodium(I) coordination sphere. In addition, only the *anti*-isomer of the aminocarbene complexes **16** and **18** was observed to have formed due to restricted rotation of the ferrocenyl substituent brought about by the steric bulk around the rhodium(I) metal center. The longer Rh-$C_{carbene}$ bond distances for the aminocarbene complexes **16** and **23** (compared to their ethoxy analogues **15** and **20**) demonstrated the lesser requirement for π-back donation from the rhodium metal center to the carbene carbon atom, effected by the increased electron-donor ability of the aminocarbene substituent.

The preliminary screening of complexes **15** – **22** as (pre)catalysts for the hydroformylation of 1-octene showed excellent conversion of the substrate olefins, with (TOF) turnover frequencies and chemo- and regioselectivity towards the linear aldehydes, comparable to results reported for rhodium *N*-Heterocyclic

Chapter 6: Conclusions and Future Work

carbene complexes. The TOF-values ranged from 343 – 418 h^{-1}, where the ethoxycarbene complexes consistently display higher activities than the analogous aminocarbene complexes **16** and **18**, with the general conversion of the 1-octene to both linear and branched aldehydes (*n*/*iso* ratios = 0.79 – 1.33) and low to no isomerisation (% internal octenes = 0 – 15%). The Rh-$C_{carbene}$ bond was also proven to be stable under hydroformylation conditions, albeit a modified Rh-carbene carbonyl complex, possibly a dimeric Rh-carbene carbonyl complex as evidenced by ^{13}C NMR spectroscopy and supported by previous literature studies.

The syntheses of multimetal Fischer carbene complexes may in the future be explored, to exploit the interplay between the electron donating ability of the carbene substituent against the stabilization of the rhodium(I)-$C_{carbene}$ bond, whilst introducing more electron-withdrawing coligands for increased selectivities during hydroformylation. Trimetallic Fischer multicarbene complexes will similarly be explored in the near future through the isolation of dirhodium biscarbene complexes with bridging ferrocendiyl moieties for improved catalytic activities, whereby the number of active sites in the catalytic species can be increased.

The presence of the ferrocenyl moiety in the prepared complexes allows for electrochemical measurements of the electronic effect of not only the ethoxy- *vs* aminocarbene substituents, but could also be used as a probe for the overall electronic environment as effected by the different co-ligands. Thus the use of other redox-active metals in multimetal Fischer carbene complexes should in future work afford the same opportunity for electrochemical evaluation of metal substituent effects. In light of the reversibility of the ferrocene/ferrocenium couple in the studied complexes, it is hoped that the redox active ferrocenylcarbenerhodium(I) complexes may be chemically oxidized in an effort to prepare Fischer carbene complexes of rhodium with very electron withdrawing carbene ligands for increased *n*/*iso*-aldehyde product ratios in the hydroformylation reaction.

.

Chapter 7: Experimental

7.1: Standard Operating Procedures

The preparation, purification and reactions of the complexes described were carried out under an atmosphere of dry, oxygen-free dinitrogen or argon, using standard Schlenk techniques. All reaction mixtures were mechanically stirred and, where appropriate, the progress of a reaction was monitored by IR spectroscopy. The precursor $[Rh(cod)Cl]_2$[1] and reagent Et_3OBF_4[2] were prepared according to literature procedures. Silica gel 60 (particle size 0.0063-0.200 mm) was used as resin for all separation in column chromatography. Anhydrous tetrahydrofuran, diethyl ether and *n*-hexane were distilled over sodium metal and dichloromethane over CaH_2. All other reagents are commercially available and were used as received. NMR samples that require strictly inert environments were prepared in the glove box.

7.2: Characterization Techniques

7.2.1: Nuclear Magnetic Resonance Spectroscopy

Nuclear magnetic resonance (NMR) spectra were recorded on Bruker Ultrashield Plus 400 AVANCE 3 and Bruker Ultrashield 300 AVANCE 3 spectrometers using $CDCl_3$ and C_6D_6 as solvents at 25°C. The NMR spectra were recorded for ^{1}H at 300.13 MHz, ^{13}C at 100.163 and 75.468 MHz and ^{31}P at 161.976 and 121.495 MHz. The chemicals shifts were recorded as δ (in ppm), using deuterated solvent signals for internal references. For $CDCl_3$ an C_6D_6 respectively, δH at 7.2600 and 7.1500 ppm, and δC at 77.360 and 128.000 ppm, and the $^{31}P\{^{1}H\}$ NMR spectra were referenced to the deuterated lock solvent which had been referenced to 85% H_3PO_4.

7.2.2: Infrared Spectroscopy

Infrared spectroscopy was performed on a Perkin Elmer Spectrum RXI FT-IR spectrophotometer over the range 3400 to 1600 cm^{-1}. Solution IR spectra were recorded in hexane (complexes **1** – **11**) and in CH_2Cl_2 (complexes **12**, **13**, **16** – **23**) using a NaCl cell with a cell width of 1.0 mm.

7.2.3: Mass Spectrometry

Chemicals and reagents: MS-grade acetonitrile was purchased from Romil. Acetonotrile with 0.1% formic acid was purchased from Fluka.

Flow Injection Analysis (FIA)-Electronspray ionization (ESI)-Mass spectrometry: ESI mass spectra were acquired by Dr. D. Koot and Ms. M. Wooding, in positive ionization mode using a Waters, Synapt G2 mass spectrometer (Milford, MA, USA). Prior to analysis, a 5mM sodium formate solution was used to calibrate the instrument in resolution mode achieving a mass accuracy of less than 0.5mDa over a mass range of 100 – 1200 Da using the IntelliStart function of Masslynx software. During the analyses of samples, the instrument was operated under the following conditions: capillary voltage 2.8 kV; sampling

Chapter 7: Experimental

cone (ramped from 20 – 40 V), extraction cone 4 V, source temperature 100 °C, desolvation temperature 200 °C, cone gas 100 L/h, desolvation gas 500 L/h, MS gas: nitrogen.

Samples were made up in 100% acetonitrile to an approximate concentration of 10 µg/mL. Flow injection using acetonitrile (0.1% formic acid) as mobile phase (with the aid of an Acquity autosampler injecting 5 µL of sample) was used to introduce the compounds to the ionization source such that a minimum of 10 scans with a scan time of 0.5 seconds in continuum format could be combined across a bolus peak. A 2 ng/µL solution of Leucine enkephalin was constantly infused *via* a syringe through a separate ESI probe with an angle perpendicular to the sample spray at a flow rate of 3 µL/min and was sampled every 10 seconds to compensate for possible experimental drift. The mass spectra resolution attained was typically > 15000 (FWHM definition) as calculated using ResCalc (verison 2.2.3). Quality control samples consisted of sodium formate clusters that were likewise analysed and used to confirm that the method was working. The attained spectrum list was saved as a txt file and further processed using mMass.

7.2.4: X-Ray Crystallography

X-ray single crystal intensity data for **15**, **16**, **19**, **20** and **23** were collected at 120 K (**15**) or 150 K (**16**, **19**, **20** and **23**) on a Bruker D8 Venture diffractometer with a kappa geometry goniometer and a photon 100 CMOS detector and were refined using *SAINT*[3] by Mr. David C. Liles, at the University of Pretoria. Data for **18** were collected at 173 K on a Nonius diffractometer with a kappa geometry goniometer and CCD detector, and were scaled and reduced using *DENZO-SMN*[4] by Dr. Hong Su, at the University of Cape Town. Absorption corrections were performed using SADABS.[3] The structures were solved by a novel duel-space algorithm using SHELXT[5] (**15**, **16**, **19**, **20** and **23**) or by direct methods (**18**) and were refined by full-matrix least-squares methods based on F^2 using SHELXL version 2014/7.[6] All non-hydrogen atoms were refined anisotropically. All hydrogen atoms except amine-H atoms were placed in idealized positions and refined using riding models. The amine-H atom positions in **16**, **18** and **23** were located and were refined. The N-H bond distance in **18** was constrained to 0.970(5)Å. In **20**, the chlorine and *trans* carbonyl ligands are disordered with the chlorine and carbonyl position interchanged. The site occupation factors refined to 0.8077(15) for the main orientation and 0.1923(15) for the flipped orientation.

The data tables for the complexes analysed by X-ray diffraction analysis are attached as appendices 1 – 7 at the end of this chapter.

7.2.5: Cyclic Voltammetry

Electrochemical studies were carried out using Metrohm µAutolab type III potentiostat linked to a computer using GPES Electrochemistry software, in conjunction with a three-electrode cell. The working electrode was a glassy carbon disc (3.0 mm diameter) and the counter electrode was a platinum wire. The reference was a non-aqueous Ag/Ag^+electrode separated from the test solution by a fine porosity

Chapter 7: Experimental

frit. Solutions in CH_2Cl_2 were 1.0×10^{-3} mol dm^{-3} in the test compound and 0.1 mol dm^{-3} in $[N^nBu_4][PF_6]$ as the supporting electrolyte. Under these conditions, E°′ for the redox couple $[Fe(\eta\text{-}C_5Me_5)_2]^{0/1+}$, added to the test solutions as internal standard, is -0.54 V. All E_p^{ox}, E_p^{red} and E°′values are at scan rates of 100 mVs^{-1}.

7.2.6: Melting Point Determination

Melting points were measured with a Stuart SMP10 melting point apparatus.

7.2.7: Elemental Analysis

Elemental analyses were carried out using a Thermo Flash 1112 Series CHNS-O Analyzer. Following extensive drying, analyses of complexes **16**, **19** and **21** – **22** are outside acceptable limits and are ascribed to the presence of solvent molecules. To attest to purity, full ^1H, ^{13}C (and where applicable, ^{31}P) NMR spectra are therefore included in appropriate sections of this dissertation.

7.3: General Procedure for the Hydroformylation Experiments

Hydroformylation reactions were conducted (in triplicate) in a 90 mL stainless steel pipe reactor. In a typical experiment, the catalyst precursor (**15** – **22**) (0.0039 mmol), substrate 1-octene (721.0 mg, 6.37 mmol), and the internal standard, *n*-decane (180.0 mg, 1.26 mmol), were dissolved in toluene (5.0 mL) and transferred into a stainless steel pipe reactor (90 mL). The airtight reactor was then deaerated by flushing three times with N_2 gas and twice with syngas, then pressurized with syngas (1:1, CO/H_2 ratio) and heated to the desired temperature and pressure. After the reaction time, the reactor was depressurized and the reaction mixture transferred for cooling. The samples were analyzed by gas chromatography, and the products were confirmed in relation to authentic internal-octenes and aldehydes.

7.4: References

1 D. E. Giordano, G.; Crabtree, R. H.; Heintz, R.M.; Forster, D.; Morris, in *Inorganic Syntheses*, ed. R. J. Angelici, Wiley & Sons, Inc., New york, 28th edn., 1991, pp. 88 – 89.

2 H. Meerwein, *Org. Synth.*, 1966, **46**, 113.

3 APEX2 (including SAINT and SADABS); Bruker AXS Inc.: Madison, WI, 2015.

4 Z. Otwinowski and W. Minor, *Macromolecular Crystallography Part A*, ed. B. T.-M. in Enzymology, Academic Press, 1997, vol. Volume 276, pp. 307–326.

5 G. M. Sheldrick, *Acta Cryst. Sect. A Crystallogr.*, 2015, **A71**, 3–8.

6 G. M. Sheldrick, *Acta Cryst. Sect. C Struct. Chem.*, 2015, **C71**, 3–8.

Appendix 1: Summarized crystal data collection and refinement for complexes 15, 16, 18 – 20 and 23

Table 1: Crystal data and summary of data collection and refinement for complexes **15, 16, 18 – 20** and **23.**

Crystal data for:	**15**	**16**	**18**	**19**	**20**	**23**
Chemical formula	$C_{21}H_{26}ClFeORh$	$C_{22}H_{29}ClFeNRh$	$C_{16}H_{17}ClFeNO_2Rh$	$C_{32}H_{29}ClFeO_2PRh\cdot 2(CH_2Cl_2)$	$C_{32}H_{47}ClFeO_2PRh$	$C_{33}H_{50}ClFeNOPRh$
M_r	488.63	501.67	449.51	840.58	688.87	701.92
Crystal system	Orthorhombic	Triclinic	Monoclinic	Triclinic	Monoclinic	Triclinic
Space group	$P2_12_12_1$	*P*-1	$P2_1/n$	*P*-1	$P2_1/c$	*P*-1
Temperature (K)	120	150	173	150	150	150
a (Å)	7.1117 (3)	7.6240 (4)	9.2379 (5)	10.1692 (6)	11.3093 (10)	10.0664(4)
b(Å)	15.6717 (7)	10.9419 (6)	11.6398 (4)	13.2020 (8)	25.726 (2)	13.6643(5)
c (Å)	17.0417 (8)	12.8133 (7)	15.4055 (9)	13.6942 (8)	10.9898 (10)	14.7237(6)
α (°)	90	110.510 (2)	90	83.776 (3)	90	74.3270(16)
β (°)	90	92.852 (2)	93.669 (2)	88.267 (3)	101.349 (3)	83.1727(7)
γ (°)	90	94.140 (2)	90	71.216 (2)	90	69.3136(16)
V (Å^3)	1899.34 (15)	995.30 (9)	1653.12 (14)	1730.30 (18)	3134.9 (5)	1823.61(13)
Z	4	2	4	2	4	2
Radiation type	Mo *K*α	Mo *K*α	Mo *K*α	Mo *K*α	Mo *K*α	Mo *K*α
μ (mm^{-1})	1.78	1.70	2.04	1.36	1.15	0.990
Crystal size (mm)	0.31 × 0.17 × 0.12	0.29 × 0.20 × 0.15	0.20 × 0.18 × 0.13	0.42 × 0.38 × 0.06	0.46 × 0.46 × 0.44	0.280 × 0.245 × 0.174
Data collection						
Absorption correction			Multi-scan*SADABS* (Bruker, 2014)			
T_{min}, T_{max}	0.605, 0.748	0.663, 0.802	0.893, 1.000	0.303, 0.746	0.481, 0.568	
No. of						

reflections						
measured	120529	65516	54063	7590	196951	74252
independent	12080	9779	3758	7590	15325	10307
observed [$I > 2\sigma(I)$]	10819	8131	3366	6226	12385	
R_{int}	0.061	0.052	0.052	0.080	0.070	0.0514
$(\sin \theta/\lambda)_{max}$ ($Å^{-1}$)	0.913	0.840	0.649	0.641	0.837	
Refinement						
$R[F^2 > 2\sigma(F^2)]$	0.034	0.030	0.024	0.067	0.036	0.0283
$wR(F^2)$	0.070	0.059	0.061	0.202	0.071	0.095
S	1.07	1.01	1.16	1.05	1.10	1.01
No. of reflections	12080	9779	3758	7590	15325	10307
No. of parameters	227	239	204	398	354	
No. of restraints	0	0	1	0	0	0
H-atom treatment	constrained	mixed	mixed	constrained	constrained	
$\Delta\rho_{max}$, $\Delta\rho_{min}$ (e $Å^{-3}$)	1.32, −0.57	1.16, −0.81	0.58, −0.55	1.36, −1.43	0.68, −0.72	0.40, -0.46
Absolute structureNo. of quotients (q)	4470					
Absolute structure parameter (x)	0.502 (5)					

Appendix 2: Crystal data tables for complex 15

Table 1: Fractional Atomic Coordinates (×10^4) and Equivalent Isotropic Displacement Parameters (Å^2×10^3). U_{eq} is defined as 1/3 of the trace of the orthogonalised U_{IJ} tensor.

Atom	*x*	*y*	*z*	U(eq)
Rh1	4181.3(2)	3868.6(2)	3601.1(2)	10.37(3)
Cl1	5410.6(9)	5103.6(4)	2977.1(4)	21.39(12)
C1	6317(4)	3065.0(17)	2954.7(15)	18.6(4)
C2	4755(4)	3102.8(16)	2487.3(14)	18.1(4)
C3	3332(4)	2392.0(17)	2413.7(15)	20.4(4)
C4	1659(4)	2512.3(16)	2973.3(16)	18.9(4)
C5	2178(3)	2889.6(14)	3758.5(14)	14.2(4)
C6	3788(3)	2684.4(14)	4204.1(14)	14.5(4)
C7	5193(4)	1998.0(16)	3979.2(15)	18.8(4)
C8	6840(4)	2338.5(18)	3491.3(17)	22.7(5)
C9	2987(3)	4495.9(13)	4460.7(13)	12.1(3)
O1	1286(3)	4835.5(12)	4452.4(11)	18.3(3)
C10	289(4)	4927.6(17)	3713.2(15)	21.2(5)
C11	559(4)	5820.2(18)	3408.6(17)	25.0(5)
Fe1	5158.4(6)	5640.6(2)	5553.0(2)	15.55(6)
C12	3765(3)	4564.0(14)	5243.4(13)	14.7(4)
C13	5663(4)	4364.0(15)	5466.1(15)	19.7(4)
C14	5914(5)	4636.0(16)	6257.6(15)	26.5(6)
C15	4193(6)	4997.6(17)	6525.3(13)	26.7(5)
C16	2865(4)	4963.6(17)	5911.3(14)	20.8(5)
C17	4828(5)	6561.0(19)	4708.4(19)	28.9(6)
C18	6658(6)	6268(2)	4718(2)	37.1(8)
C19	7405(7)	6434(3)	5488(4)	60.2(16)
C20	5963(10)	6823(2)	5924(2)	57.3(16)
C21	4407(7)	6894(2)	5447(2)	45.2(11)

Table 2: Anisotropic Displacement Parameters (Å^2×10^3) . The Anisotropic displacement factor exponent takes the form: $-2\pi^2[h^2a^{*2}U_{11}+2hka^*b^*U_{12}+\ldots]$.

Atom	U_{11}	U_{22}	U_{33}	U_{23}	U_{13}	U_{12}
Rh1	11.54(5)	9.26(5)	10.32(5)	0.12(5)	0.55(5)	-0.74(5)
Cl1	24.4(3)	15.1(2)	24.6(3)	5.5(2)	5.0(2)	-4.03(19)
C1	15.4(9)	20.1(10)	20.2(10)	-1.9(8)	6.5(8)	1.4(8)
C2	22.4(10)	18.1(10)	13.7(9)	-1.3(7)	3.6(8)	1.7(8)
C3	24.0(11)	20.0(11)	17.3(10)	-6.4(8)	-1.9(8)	1.5(9)

C4	16.7(10)	15.4(10)	24.7(11)	-4.4(8)	-3.7(8)	-1.5(8)
C5	13.1(8)	10.3(8)	19(1)	-0.3(7)	2.0(7)	-1.0(6)
C6	17.2(9)	12.3(8)	14.1(8)	1.1(7)	2.0(7)	0.4(7)
C7	19.7(10)	14.2(9)	22.5(10)	1.8(8)	-2.1(8)	3.8(8)
C8	16(1)	22.9(11)	29.1(14)	-0.1(10)	1.1(9)	5.6(8)
C9	15.0(8)	8.5(8)	13.0(8)	0.8(6)	0.7(7)	-0.8(6)
O1	17.3(7)	20.1(8)	17.5(7)	-4.0(6)	-0.8(6)	6.3(6)
C10	21.4(10)	20.5(10)	21.7(11)	-4.7(8)	-7.9(8)	7.2(8)
C11	30.6(15)	21.7(11)	22.7(11)	-1.5(9)	-3.2(10)	8.8(10)
Fe1	24.12(16)	9.63(12)	12.89(13)	-0.69(10)	-4.10(11)	0.02(12)
C12	21(1)	10.7(8)	12.3(8)	-0.5(6)	-0.9(7)	-0.4(7)
C13	26.2(12)	11.8(8)	21.1(10)	-0.3(7)	-7.8(9)	2.6(9)
C14	43.3(16)	16(1)	20.3(11)	1.5(8)	-16.0(11)	0.9(11)
C15	48.9(17)	19.5(10)	11.6(9)	0.9(7)	-3.8(11)	-2.4(12)
C16	30.3(13)	18.6(10)	13.5(9)	-1.1(8)	3.4(8)	-2.4(9)
C17	39.6(16)	20.4(12)	26.9(13)	10.8(10)	-7.2(12)	-8.0(12)
C18	48(2)	16.6(13)	46.9(19)	-1.0(12)	24.5(16)	-6.5(12)
C19	45(2)	34.9(19)	100(4)	33(2)	-41(3)	-24.9(18)
C20	129(5)	18.5(13)	24.8(14)	-0.8(11)	-17(2)	-25(2)
C21	73(3)	14.8(11)	48(2)	8.0(12)	27(2)	11.0(15)

Table 3: Bond Lengths

Atom	Atom	Length/Å	Atom	Atom	Length/Å
Rh1	C9	1.958(2)	Fe1	C19	2.027(4)
Rh1	C5	2.111(2)	Fe1	C18	2.033(3)
Rh1	C6	2.140(2)	Fe1	C13	2.038(2)
Rh1	C1	2.260(2)	Fe1	C16	2.040(3)
Rh1	C2	2.283(2)	Fe1	C20	2.040(3)
Rh1	Cl1	2.3751(6)	Fe1	C21	2.044(3)
C1	C2	1.368(4)	Fe1	C17	2.051(3)
C1	C8	1.507(4)	Fe1	C14	2.052(3)
C2	C3	1.510(4)	Fe1	C15	2.057(3)
C3	C4	1.536(4)	C12	C13	1.437(4)
C4	C5	1.509(3)	C12	C16	1.449(3)
C5	C6	1.411(3)	C13	C14	1.426(3)
C6	C7	1.518(3)	C14	C15	1.424(5)
C7	C8	1.533(4)	C15	C16	1.411(4)
C9	O1	1.322(3)	C17	C18	1.380(5)
C9	C12	1.448(3)	C17	C21	1.395(5)
O1	C10	1.453(3)	C18	C19	1.439(7)

C10	C11	1.504(4)	C19	C20	1.406(8)
Fe1	C12	2.027(2)	C20	C21	1.378(8)

Table 4: Bond Angles.

Atom	Atom	Atom	Angle/°	Atom	Atom	Atom	Angle/°
C9	Rh1	C5	88.69(9)	C12	Fe1	C17	110.28(11)
C9	Rh1	C6	91.11(9)	C19	Fe1	C17	67.71(15)
C5	Rh1	C6	38.77(9)	C18	Fe1	C17	39.50(16)
C9	Rh1	C1	159.40(10)	C13	Fe1	C17	131.26(12)
C5	Rh1	C1	96.35(9)	C16	Fe1	C17	118.96(13)
C6	Rh1	C1	80.72(9)	C20	Fe1	C17	67.10(14)
C9	Rh1	C2	164.53(10)	C21	Fe1	C17	39.82(15)
C5	Rh1	C2	81.04(9)	C12	Fe1	C14	69.00(10)
C6	Rh1	C2	88.09(9)	C19	Fe1	C14	107.23(15)
C1	Rh1	C2	35.05(10)	C18	Fe1	C14	130.08(17)
C9	Rh1	Cl1	94.90(6)	C13	Fe1	C14	40.81(10)
C5	Rh1	Cl1	153.84(7)	C16	Fe1	C14	68.60(14)
C6	Rh1	Cl1	165.92(6)	C20	Fe1	C14	116.24(14)
C1	Rh1	Cl1	89.34(7)	C21	Fe1	C14	149.08(14)
C2	Rh1	Cl1	89.45(7)	C17	Fe1	C14	168.61(15)
C2	C1	C8	125.9(2)	C12	Fe1	C15	68.82(10)
C2	C1	Rh1	73.39(14)	C19	Fe1	C15	127.42(18)
C8	C1	Rh1	106.94(16)	C18	Fe1	C15	167.49(17)
C1	C2	C3	124.1(2)	C13	Fe1	C15	68.68(11)
C1	C2	Rh1	71.56(14)	C16	Fe1	C15	40.28(12)
C3	C2	Rh1	109.69(16)	C20	Fe1	C15	106.79(14)
C2	C3	C4	112.2(2)	C21	Fe1	C15	117.06(14)
C5	C4	C3	114.1(2)	C17	Fe1	C15	150.61(15)
C6	C5	C4	125.9(2)	C14	Fe1	C15	40.56(14)
C6	C5	Rh1	71.72(13)	C13	C12	C9	125.9(2)
C4	C5	Rh1	109.71(16)	C13	C12	C16	107.6(2)
C5	C6	C7	124.1(2)	C9	C12	C16	125.9(2)
C5	C6	Rh1	69.52(13)	C13	C12	Fe1	69.73(14)
C7	C6	Rh1	114.04(16)	C9	C12	Fe1	119.21(16)
C6	C7	C8	113.2(2)	C16	C12	Fe1	69.61(14)
C1	C8	C7	113.8(2)	C14	C13	C12	107.6(3)
O1	C9	C12	109.3(2)	C14	C13	Fe1	70.12(14)
O1	C9	Rh1	126.23(17)	C12	C13	Fe1	68.88(13)
C12	C9	Rh1	124.09(17)	C15	C14	C13	108.3(3)
C9	O1	C10	119.7(2)	C15	C14	Fe1	69.93(15)
O1	C10	C11	109.2(2)	C13	C14	Fe1	69.08(14)
C12	Fe1	C19	151.8(2)	C16	C15	C14	108.8(2)
C12	Fe1	C18	118.49(13)	C16	C15	Fe1	69.18(15)

C19	Fe1	C18	41.5(2)	C14	C15	Fe1	69.51(16)
C12	Fe1	C13	41.40(10)	C15	C16	C12	107.6(3)
C19	Fe1	C13	117.32(18)	C15	C16	Fe1	70.54(18)
C18	Fe1	C13	109.38(12)	C12	C16	Fe1	68.65(14)
C12	Fe1	C16	41.74(10)	C18	C17	C21	108.4(4)
C19	Fe1	C16	165.0(2)	C18	C17	Fe1	69.53(19)
C18	Fe1	C16	151.77(15)	C21	C17	Fe1	69.79(18)
C13	Fe1	C16	69.63(12)	C17	C18	C19	107.4(4)
C12	Fe1	C20	167.0(2)	C17	C18	Fe1	70.98(18)
C19	Fe1	C20	40.5(2)	C19	C18	Fe1	69.0(2)
C18	Fe1	C20	68.30(17)	C20	C19	C18	106.9(4)
C13	Fe1	C20	149.9(2)	C20	C19	Fe1	70.3(2)
C16	Fe1	C20	127.2(2)	C18	C19	Fe1	69.45(19)
C12	Fe1	C21	130.49(17)	C21	C20	C19	107.9(3)
C19	Fe1	C21	67.2(2)	C21	C20	Fe1	70.4(2)
C18	Fe1	C21	67.04(15)	C19	C20	Fe1	69.3(2)
C13	Fe1	C21	169.46(16)	C20	C21	C17	109.3(4)
C16	Fe1	C21	108.51(16)	C20	C21	Fe1	70.2(2)
C20	Fe1	C21	39.4(2)	C17	C21	Fe1	70.39(18)

Table 5: Torsion Angles

A	B	C	D	Angle/°	A	B	C	D	Angle/°
C8	C1	C2	C3	-2.6(4)	C12	C13	C14	C15	0.2(3)
Rh1	C1	C2	C3	-101.7(2)	Fe1	C13	C14	C15	59.10(19)
C8	C1	C2	Rh1	99.2(2)	C12	C13	C14	Fe1	-58.88(17)
C1	C2	C3	C4	94.6(3)	C13	C14	C15	C16	-0.5(3)
Rh1	C2	C3	C4	14.0(3)	Fe1	C14	C15	C16	58.10(19)
C2	C3	C4	C5	-36.3(3)	C13	C14	C15	Fe1	-58.57(19)
C3	C4	C5	C6	-40.5(3)	C14	C15	C16	C12	0.5(3)
C3	C4	C5	Rh1	40.8(2)	Fe1	C15	C16	C12	58.83(17)
C4	C5	C6	C7	-4.3(4)	C14	C15	C16	Fe1	-58.3(2)
Rh1	C5	C6	C7	-105.8(2)	C13	C12	C16	C15	-0.4(3)
C4	C5	C6	Rh1	101.5(2)	C9	C12	C16	C15	-172.0(2)
C5	C6	C7	C8	92.2(3)	Fe1	C12	C16	C15	-60.02(19)
Rh1	C6	C7	C8	11.4(3)	C13	C12	C16	Fe1	59.63(17)
C2	C1	C8	C7	-44.8(4)	C9	C12	C16	Fe1	-111.9(2)
Rh1	C1	C8	C7	36.7(3)	C21	C17	C18	C19	-0.6(3)
C6	C7	C8	C1	-33.2(3)	Fe1	C17	C18	C19	-59.7(2)
C12	C9	O1	C10	173.4(2)	C21	C17	C18	Fe1	59.1(2)
Rh1	C9	O1	C10	-13.7(3)	C17	C18	C19	C20	0.3(4)
C9	O1	C10	C11	-96.9(3)	Fe1	C18	C19	C20	-60.6(3)

O1	C9	C12	C13	-171.9(2)	C17	C18	C19	Fe1	60.9(2)
Rh1	C9	C12	C13	15.0(3)	C18	C19	C20	C21	0.0(4)
O1	C9	C12	C16	-1.8(3)	Fe1	C19	C20	C21	-60.0(3)
Rh1	C9	C12	C16	-174.89(19)	C18	C19	C20	Fe1	60.1(2)
O1	C9	C12	Fe1	-86.8(2)	C19	C20	C21	C17	-0.4(4)
Rh1	C9	C12	Fe1	100.15(19)	Fe1	C20	C21	C17	-59.7(2)
C9	C12	C13	C14	171.7(2)	C19	C20	C21	Fe1	59.3(2)
C16	C12	C13	C14	0.1(3)	C18	C17	C21	C20	0.6(4)
Fe1	C12	C13	C14	59.66(18)	Fe1	C17	C21	C20	59.6(2)
C9	C12	C13	Fe1	112.0(2)	C18	C17	C21	Fe1	-59.0(2)
C16	C12	C13	Fe1	-59.56(17)					

Table 6: Hydrogen Atom Coordinates (Å×10^4) and Isotropic Displacement Parameters (Å^2×10^3)

Atom	*x*	*y*	*z*	U(eq)
H1	7147	3540	2940	22
H2	4554	3608	2190	22
H3A	3952	1841	2529	25
H3B	2864	2370	1867	25
H4A	723	2889	2718	23
H4B	1054	1951	3061	23
H5	1345	3303	3972	17
H6	4005	2995	4674	17
H7A	4536	1549	3676	23
H7B	5692	1732	4463	23
H8A	7845	2533	3852	27
H8B	7357	1866	3171	27
H10A	-1067	4814	3792	25
H10B	778	4511	3327	25
H11A	-325	5926	2978	37
H11B	1850	5887	3217	37
H11C	327	6230	3832	37
H13	6584	4099	5144	24
H14	7038	4585	6555	32
H15	3975	5225	7034	32
H16	1607	5166	5932	25

H17	3995	6539	4273	35
H18	7305	6006	4294	44
H19	8637	6304	5667	72
H20	6047	7006	6455	69
H21	3232	7132	5597	54

Appendix 3: Crystal data tables for complex 16

Table 1: Fractional Atomic Coordinates (×10^4) and Equivalent Isotropic Displacement Parameters (Å^2×10^3). U_{eq} is defined as 1/3 of of the trace of the orthogonalised U_{IJ} tensor.

Atom	*x*	*y*	*z*	U(eq)
Rh1	5117.9(2)	3393.1(2)	6820.0(2)	12.10(3)
Cl1	2576.5(5)	1985.8(3)	5813.3(3)	22.02(7)
N1	6934.7(17)	1120.7(12)	5612.7(10)	17.4(2)
C1	6371.8(17)	1766.1(13)	6583.5(11)	13.7(2)
C2	6798(2)	1519.2(16)	4636.7(12)	20.0(3)
C3	8524(2)	1505.0(16)	4104.5(13)	22.2(3)
C4	8283(2)	1781.9(18)	3019.6(15)	27.0(3)
C5	3414.3(18)	5000.4(13)	7472.7(12)	17.0(2)
C6	4128.9(19)	5120.1(14)	6544.1(12)	18.2(3)
C7	5642(2)	6111.8(16)	6572.5(14)	24.2(3)
C8	7458(2)	5568.0(18)	6553.4(15)	26.2(3)
C9	7541.2(18)	4548.0(14)	7097.7(12)	17.5(2)
C10	6891.3(18)	4671.7(14)	8135.3(11)	15.9(2)
C11	6096(2)	5887.9(14)	8866.2(12)	20.2(3)
C12	4073(2)	5761.2(15)	8671.0(12)	20.7(3)
Fe1	8462.7(2)	1444.1(2)	8677.3(2)	11.88(4)
C13	6502.2(17)	1134.5(13)	7419.2(11)	13.3(2)
C14	7247.6(19)	-70.7(13)	7336.4(12)	17.1(2)
C15	6986(2)	-308.9(14)	8339.3(13)	20.5(3)
C16	6109.7(19)	740.0(15)	9058.4(13)	19.8(3)
C17	5813.4(18)	1628.2(14)	8495.9(11)	15.7(2)
C18	10399.6(18)	2856.0(14)	8665.8(13)	18.3(3)
C19	11110.6(19)	1631.2(15)	8436.9(13)	19.9(3)
C20	10854.3(19)	1218.3(15)	9359.3(13)	19.9(3)
C21	9983.5(19)	2193.4(15)	10161.3(12)	19.0(3)
C22	9706.6(18)	3208.2(14)	9730.4(12)	17.6(2)

Table 2: Anisotropic Displacement Parameters (Å^2×10^3). The Anisotropic displacement factor exponent takes the form: $-2\pi^2[h^2a^{*2}U_{11}+2hka^*b^*U_{12}+\ldots]$.

Atom	U_{11}	U_{22}	U_{33}	U_{23}	U_{13}	U_{12}

Rh1	12.52(4)	11.29(4)	11.29(4)	2.50(3)	-1.96(3)	3.31(3)
Cl1	17.45(15)	16.43(15)	24.80(16)	-0.81(12)	-7.00(12)	2.25(12)
N1	21.6(6)	16.6(5)	14.2(5)	4.5(4)	0.7(4)	8.7(4)
C1	13.6(5)	14.1(5)	12.2(5)	3.3(4)	-2.5(4)	2.3(4)
C2	19.7(6)	26.7(7)	14.5(6)	7.2(5)	0.0(5)	8.3(5)
C3	18.2(6)	26.2(7)	24.5(7)	11.6(6)	1.2(5)	4.6(5)
C4	28.3(8)	31.6(8)	28.7(8)	18.1(7)	9.7(6)	9.1(7)
C5	14.4(6)	14.0(6)	20.6(6)	3.0(5)	-0.7(5)	5.7(4)
C6	20.3(6)	16.7(6)	18.3(6)	6.7(5)	-3.3(5)	7.6(5)
C7	29.4(8)	22.8(7)	26.2(7)	15.4(6)	2.9(6)	5.6(6)
C8	23.0(7)	32.0(8)	31.4(8)	20.8(7)	4.7(6)	1.6(6)
C9	13.3(6)	19.7(6)	21.2(6)	9.6(5)	-1.0(5)	1.6(5)
C10	14.2(5)	16.8(6)	15.4(6)	5.2(5)	-4.4(4)	-0.5(4)
C11	24.1(7)	16.5(6)	15.5(6)	1.0(5)	-4.4(5)	0.8(5)
C12	21.9(7)	19.5(6)	18.0(6)	2.7(5)	2.8(5)	4.5(5)
Fe1	12.20(8)	11.37(8)	12.09(8)	4.96(6)	-2.23(6)	-0.67(6)
C13	13.0(5)	12.2(5)	13.3(5)	3.2(4)	-2.9(4)	0.6(4)
C14	19.1(6)	12.1(5)	17.5(6)	2.9(5)	-5.1(5)	1.2(5)
C15	24.4(7)	13.4(6)	23.8(7)	9.1(5)	-7.2(5)	-4.2(5)
C16	18.3(6)	22.2(7)	20.0(6)	11.2(5)	-1.4(5)	-7.0(5)
C17	12.9(5)	17.5(6)	15.7(6)	5.2(5)	-0.3(4)	-1.1(4)
C18	14.2(6)	19.5(6)	23.3(7)	11.7(5)	-1.8(5)	-3.7(5)
C19	14.3(6)	22.9(7)	21.2(6)	6.4(5)	0.1(5)	1.2(5)
C20	17.0(6)	19.5(6)	23.3(7)	9.0(5)	-6.4(5)	1.1(5)
C21	18.7(6)	21.6(7)	15.4(6)	7.0(5)	-5.9(5)	-4.0(5)
C22	15.3(6)	14.9(6)	19.4(6)	3.3(5)	-2.6(5)	-2.4(5)

Table 3: Bond Lengths

Atom	Atom	Length/Å	Atom	Atom	Length/Å
Rh1	C1	2.0178(13)	Fe1	C21	2.0453(14)
Rh1	C9	2.1022(14)	Fe1	C15	2.0473(14)
Rh1	C10	2.1151(13)	Fe1	C16	2.0497(14)
Rh1	C5	2.2106(13)	Fe1	C20	2.0511(14)
Rh1	C6	2.2163(13)	Fe1	C17	2.0540(14)
Rh1	Cl1	2.3911(4)	Fe1	C22	2.0565(14)
N1	C1	1.3083(18)	Fe1	C13	2.0620(13)
N1	C2	1.4630(19)	Fe1	C18	2.0631(14)
C1	C13	1.4669(18)	Fe1	C19	2.0637(15)

C2	C3	1.511(2)	C13	C17	1.4358(19)
C3	C4	1.528(2)	C13	C14	1.4455(19)
C5	C6	1.376(2)	C14	C15	1.418(2)
C5	C12	1.507(2)	C15	C16	1.430(2)
C6	C7	1.515(2)	C16	C17	1.422(2)
C7	C8	1.544(2)	C18	C22	1.422(2)
C8	C9	1.512(2)	C18	C19	1.422(2)
C9	C10	1.407(2)	C19	C20	1.423(2)
C10	C11	1.522(2)	C20	C21	1.427(2)
C11	C12	1.538(2)	C21	C22	1.426(2)
Fe1	C14	2.0449(14)			

Table 4: Bond Angles

Atom	Atom	Atom	Angle/˚	Atom	Atom	Atom	Angle/˚
C1	Rh1	C9	91.00(5)	C14	Fe1	C13	41.21(5)
C1	Rh1	C10	96.61(5)	C21	Fe1	C13	163.14(6)
C9	Rh1	C10	38.99(5)	C15	Fe1	C13	68.63(5)
C1	Rh1	C5	162.98(6)	C16	Fe1	C13	68.58(6)
C9	Rh1	C5	97.90(6)	C20	Fe1	C13	155.77(6)
C10	Rh1	C5	81.66(5)	C17	Fe1	C13	40.83(5)
C1	Rh1	C6	160.66(5)	C22	Fe1	C13	127.62(6)
C9	Rh1	C6	81.95(5)	C14	Fe1	C18	127.64(6)
C10	Rh1	C6	89.21(5)	C21	Fe1	C18	68.15(6)
C5	Rh1	C6	36.22(5)	C15	Fe1	C18	162.74(7)
C1	Rh1	Cl1	87.61(4)	C16	Fe1	C18	156.22(6)
C9	Rh1	Cl1	158.80(4)	C20	Fe1	C18	68.02(6)
C10	Rh1	Cl1	162.04(4)	C17	Fe1	C18	123.22(6)
C5	Rh1	Cl1	89.19(4)	C22	Fe1	C18	40.38(6)
C6	Rh1	Cl1	92.51(4)	C13	Fe1	C18	110.87(6)
C1	N1	C2	124.54(12)	C14	Fe1	C19	108.26(6)
N1	C1	C13	115.56(12)	C21	Fe1	C19	68.23(6)
N1	C1	Rh1	121.08(10)	C15	Fe1	C19	124.37(6)
C13	C1	Rh1	122.87(10)	C16	Fe1	C19	160.43(6)
N1	C2	C3	112.43(12)	C20	Fe1	C19	40.45(6)
C2	C3	C4	110.86(13)	C17	Fe1	C19	158.12(6)
C6	C5	C12	125.95(13)	C22	Fe1	C19	68.01(6)
C6	C5	Rh1	72.12(8)	C13	Fe1	C19	122.73(6)
C12	C5	Rh1	107.45(9)	C18	Fe1	C19	40.30(6)
C5	C6	C7	124.86(13)	C17	C13	C14	107.19(12)

C5	C6	Rh1	71.67(8)	C17	C13	C1	123.88(12)
C7	C6	Rh1	110.97(9)	C14	C13	C1	128.89(12)
C6	C7	C8	112.81(13)	C17	C13	Fe1	69.29(7)
C9	C8	C7	113.67(13)	C14	C13	Fe1	68.76(7)
C10	C9	C8	124.44(14)	C1	C13	Fe1	128.63(9)
C10	C9	Rh1	71.00(8)	C15	C14	C13	107.97(13)
C8	C9	Rh1	110.94(10)	C15	C14	Fe1	69.81(8)
C9	C10	C11	123.38(13)	C13	C14	Fe1	70.03(7)
C9	C10	Rh1	70.01(8)	C14	C15	C16	108.44(12)
C11	C10	Rh1	113.71(9)	C14	C15	Fe1	69.64(8)
C10	C11	C12	112.22(11)	C16	C15	Fe1	69.67(8)
C5	C12	C11	112.97(12)	C17	C16	C15	108.06(13)
C14	Fe1	C21	152.86(6)	C17	C16	Fe1	69.89(8)
C14	Fe1	C15	40.55(6)	C15	C16	Fe1	69.48(8)
C21	Fe1	C15	117.61(6)	C16	C17	C13	108.33(13)
C14	Fe1	C16	68.70(6)	C16	C17	Fe1	69.57(8)
C21	Fe1	C16	105.18(6)	C13	C17	Fe1	69.88(7)
C15	Fe1	C16	40.85(6)	C22	C18	C19	108.26(13)
C14	Fe1	C20	118.86(6)	C22	C18	Fe1	69.56(8)
C21	Fe1	C20	40.78(6)	C19	C18	Fe1	69.87(8)
C15	Fe1	C20	104.99(6)	C18	C19	C20	108.02(13)
C16	Fe1	C20	122.72(6)	C18	C19	Fe1	69.83(8)
C14	Fe1	C17	68.91(6)	C20	C19	Fe1	69.30(8)
C21	Fe1	C17	124.49(6)	C19	C20	C21	107.94(13)
C15	Fe1	C17	68.48(6)	C19	C20	Fe1	70.25(8)
C16	Fe1	C17	40.54(6)	C21	C20	Fe1	69.39(8)
C20	Fe1	C17	160.49(6)	C22	C21	C20	107.92(13)
C14	Fe1	C22	165.15(6)	C22	C21	Fe1	70.08(8)
C21	Fe1	C22	40.69(6)	C20	C21	Fe1	69.83(8)
C15	Fe1	C22	153.58(6)	C18	C22	C21	107.86(13)
C16	Fe1	C22	119.81(6)	C18	C22	Fe1	70.06(8)
C20	Fe1	C22	68.35(6)	C21	C22	Fe1	69.23(8)
C17	Fe1	C22	108.84(6)				

Table 5: Torsion Angles

A	B	C	D	Angle/°	A	B	C	D	Angle/°
C2	N1	C1	C13	174.96(13)	C1	C13	C14	Fe1	123.17(14)
C2	N1	C1	Rh1	2.79(19)	C13	C14	C15	C16	-0.83(16)
C1	N1	C2	C3	130.87(15)	Fe1	C14	C15	C16	59.04(10)

N1	C2	C3	C4	173.89(13)	C13	C14	C15	Fe1	-59.87(9)
C12	C5	C6	C7	-4.3(2)	C14	C15	C16	C17	0.44(16)
Rh1	C5	C6	C7	-103.21(13)	Fe1	C15	C16	C17	59.46(10)
C12	C5	C6	Rh1	98.93(14)	C14	C15	C16	Fe1	-59.02(10)
C5	C6	C7	C8	92.88(18)	C15	C16	C17	C13	0.13(15)
Rh1	C6	C7	C8	11.14(16)	Fe1	C16	C17	C13	59.33(9)
C6	C7	C8	C9	-30.2(2)	C15	C16	C17	Fe1	-59.21(10)
C7	C8	C9	C10	-45.9(2)	C14	C13	C17	C16	-0.63(15)
C7	C8	C9	Rh1	34.84(18)	C1	C13	C17	C16	177.49(12)
C8	C9	C10	C11	-3.0(2)	Fe1	C13	C17	C16	-59.14(9)
Rh1	C9	C10	C11	-105.83(13)	C14	C13	C17	Fe1	58.50(9)
C8	C9	C10	Rh1	102.84(14)	C1	C13	C17	Fe1	-123.37(12)
C9	C10	C11	C12	94.97(16)	C22	C18	C19	C20	0.19(16)
Rh1	C10	C11	C12	14.04(16)	Fe1	C18	C19	C20	-58.97(10)
C6	C5	C12	C11	-42.8(2)	C22	C18	C19	Fe1	59.17(9)
Rh1	C5	C12	C11	37.38(15)	C18	C19	C20	C21	-0.08(16)
C10	C11	C12	C5	-34.96(18)	Fe1	C19	C20	C21	-59.38(10)
N1	C1	C13	C17	-174.27(13)	C18	C19	C20	Fe1	59.30(10)
Rh1	C1	C13	C17	-2.26(18)	C19	C20	C21	C22	-0.07(16)
N1	C1	C13	C14	3.4(2)	Fe1	C20	C21	C22	-59.98(9)
Rh1	C1	C13	C14	175.44(11)	C19	C20	C21	Fe1	59.92(10)
N1	C1	C13	Fe1	96.23(14)	C19	C18	C22	C21	-0.24(16)
Rh1	C1	C13	Fe1	-91.76(13)	Fe1	C18	C22	C21	59.12(9)
C17	C13	C14	C15	0.90(15)	C19	C18	C22	Fe1	-59.36(10)
C1	C13	C14	C15	-177.10(13)	C20	C21	C22	C18	0.19(16)
Fe1	C13	C14	C15	59.74(10)	Fe1	C21	C22	C18	-59.64(10)
C17	C13	C14	Fe1	-58.84(9)	C20	C21	C22	Fe1	59.83(10)

Table 6: Hydrogen Atom Coordinates (Å×10^4) and Isotropic Displacement Parameters (Å^2×10^3)

Atom	*x*	*y*	*z*	U(eq)
H1	7290(30)	350(20)	5476(16)	21
H2A	6412	2414	4866	24
H2B	5888	920	4078	24
H3A	8979	638	3944	27
H3B	9403	2177	4631	27
H4A	7319	1180	2533	40
H4B	9377	1656	2640	40
H4C	8000	2688	3191	40
H5	2123	4709	7360	20

H6	3260	4893	5878	22
H7A	5632	6896	7257	29
H7B	5463	6389	5921	29
H8A	7747	5176	5767	31
H8B	8366	6304	6942	31
H9	8589	4033	6927	21
H10	7557	4222	8564	19
H11A	6593	6658	8705	24
H11B	6426	6039	9662	24
H12A	3553	5320	9154	25
H12B	3665	6649	8894	25
H14	7837	-639	6685	21
H15	7368	-1074	8518	25
H16	5770	835	9825	24
H17	5235	2459	8801	19
H18	10380	3376	8162	22
H19	11680	1141	7745	24
H20	11222	392	9434	24
H21	9638	2173	10898	23
H22	9125	4022	10109	21

Appendix 4: Crystal data tables for complex 18

Table 1: Fractional Atomic Coordinates (×10^4) and Equivalent Isotropic Displacement Parameters (Å^2×10^3. U_{eq} is defined as 1/3 of of the trace of the orthogonalised U_{IJ} tensor.

Atom	*x*	*y*	*z*	U(eq)
Rh1	8404.5(2)	1591.5(2)	1603.3(2)	24.45(7)
Fe1	7143.9(3)	2760.8(3)	-950.9(2)	23.54(9)
Cl1	7955.1(6)	-414.6(5)	1518.9(4)	31.14(13)
O1	9184(2)	4069.2(16)	1667.1(13)	44.1(5)
O2	6982(3)	1632.6(18)	3340.6(13)	52.7(6)
N1	10563(2)	1452.0(16)	222.2(13)	25.2(4)
C1	8857(3)	3118(2)	1645.1(15)	31.3(5)
C2	7520(3)	1626(2)	2705.9(16)	31.4(5)
C3	9195(2)	1494.7(17)	384.7(14)	22.0(4)
C4	8150(2)	1378.4(18)	-370.6(15)	23.1(4)
C5	6604(2)	1297(2)	-306.4(16)	27.2(5)
C6	5932(3)	1275(2)	-1158.3(16)	30.0(5)
C7	7034(3)	1349(2)	-1762.7(16)	27.9(5)
C8	8406(3)	1415.0(18)	-1287.8(15)	25.0(5)
C9	6915(3)	4163(2)	-169.5(18)	39.2(6)
C10	5787(3)	4140(2)	-842.2(18)	38.9(6)
C11	6426(3)	4180(2)	-1650.9(17)	37.8(6)
C12	7958(3)	4223(2)	-1483.4(19)	40.2(6)
C13	8248(3)	4211(2)	-565.6(19)	40.4(6)
C14	11784(3)	1566(2)	872.6(16)	28.1(5)
C15	12805(3)	2519(3)	663(2)	44.4(7)
C16	14099(3)	2567(3)	1331.6(19)	45.9(7)

Table 2: Anisotropic Displacement Parameters (Å^2×10^3). The Anisotropic displacement factor exponent takes the form: $-2\pi^2[h^2a^{*2}U_{11}+2hka^*b^*U_{12}+\ldots]$.

Atom	U_{11}	U_{22}	U_{33}	U_{23}	U_{13}	U_{12}
Rh1	24.66(11)	25.07(11)	23.62(10)	-1.78(7)	1.58(7)	-0.93(7)
Fe1	22.71(17)	20.51(16)	27.18(17)	-2.21(12)	-0.20(13)	1.15(12)
Cl1	31.5(3)	25.6(3)	37.3(3)	0.5(2)	10.4(2)	-1.2(2)
O1	56.4(13)	31(1)	44.7(11)	-5.8(8)	2.9(9)	-10.2(9)
O2	74.7(15)	46.1(12)	40.0(12)	-7.0(9)	26.0(11)	-6.3(10)
N1	24.2(10)	24.3(9)	27.1(10)	0.4(8)	0.8(8)	-0.8(7)

C1	31.8(13)	38.1(14)	24.2(12)	-3.8(10)	2.4(9)	0.8(11)
C2	37.9(14)	25.9(12)	30.6(13)	-3(1)	3.1(11)	-1.6(10)
C3	24.3(11)	15.5(10)	26.2(11)	1.2(8)	2.0(9)	-0.6(8)
C4	24.2(11)	18.4(10)	26.7(11)	-1.8(8)	1.6(9)	-0.2(8)
C5	25.0(12)	24.7(11)	32.2(12)	0.2(9)	3.3(9)	-3.4(9)
C6	23.6(12)	27.5(12)	38.0(13)	-0.9(10)	-4.2(10)	-4.4(9)
C7	31.1(12)	24.2(11)	28.0(12)	-5.3(9)	-2.2(10)	0.9(9)
C8	25.4(11)	21.3(11)	28.3(11)	-4.2(9)	2.2(9)	1.7(9)
C9	55.5(17)	26.6(12)	35.0(14)	-8.5(11)	-2.0(12)	8.6(12)
C10	39.9(15)	30.8(13)	45.5(15)	-5.5(11)	-0.6(12)	12.5(11)
C11	47.3(16)	27.0(12)	37.9(14)	1.4(10)	-6.5(12)	9.2(11)
C12	46.7(16)	23.0(12)	51.8(17)	5.9(11)	9.1(13)	-1.5(11)
C13	43.7(15)	20.9(12)	54.6(17)	-3.9(11)	-11.8(13)	-2.6(11)
C14	22.8(11)	26.9(12)	33.9(12)	2.3(9)	-3.9(9)	-0.1(9)
C15	42.3(16)	43.8(15)	45.7(16)	7.7(13)	-8.5(13)	-17.7(13)
C16	33.9(15)	60.0(19)	43.3(16)	-8.8(14)	-0.3(12)	-17.1(13)

Table 3: Bond Lengths

Atom	Atom	Length/Å	Atom	Atom	Length/Å
Rh1	C1	1.826(3)	N1	C3	1.305(3)
Rh1	C2	1.932(3)	N1	C14	1.466(3)
Rh1	C3	2.061(2)	C3	C4	1.470(3)
Rh1	Cl1	2.3738(6)	C4	C5	1.440(3)
Fe1	C4	2.036(2)	C4	C8	1.448(3)
Fe1	C8	2.039(2)	C5	C6	1.416(3)
Fe1	C13	2.041(2)	C6	C7	1.425(4)
Fe1	C9	2.047(2)	C7	C8	1.424(3)
Fe1	C5	2.049(2)	C9	C13	1.410(4)
Fe1	C10	2.050(3)	C9	C10	1.422(4)
Fe1	C12	2.053(3)	C10	C11	1.413(4)
Fe1	C11	2.059(3)	C11	C12	1.424(4)
Fe1	C7	2.064(2)	C12	C13	1.422(4)
Fe1	C6	2.074(2)	C14	C15	1.504(3)
O1	C1	1.148(3)	C15	C16	1.528(4)
O2	C2	1.125(3)			

Table 4: Bond Angles

Atom	Atom	Atom	Angle/°	Atom	Atom	Atom	Angle/°
C1	Rh1	C2	93.32(10)	C5	Fe1	C6	40.16(9)
C1	Rh1	C3	89.51(9)	C10	Fe1	C6	109.80(11)
C2	Rh1	C3	175.35(10)	C12	Fe1	C6	146.91(11)
C1	Rh1	Cl1	176.57(8)	C11	Fe1	C6	115.84(10)
C2	Rh1	Cl1	89.21(7)	C7	Fe1	C6	40.29(10)
C3	Rh1	Cl1	88.12(6)	C3	N1	C14	125.3(2)
C4	Fe1	C8	41.63(9)	O1	C1	Rh1	177.9(2)
C4	Fe1	C13	108.69(10)	O2	C2	Rh1	178.6(2)
C8	Fe1	C13	115.22(11)	N1	C3	C4	116.1(2)
C4	Fe1	C9	115.67(10)	N1	C3	Rh1	125.52(17)
C8	Fe1	C9	147.59(10)	C4	C3	Rh1	118.21(16)
C13	Fe1	C9	40.36(12)	C5	C4	C8	107.06(19)
C4	Fe1	C5	41.28(9)	C5	C4	C3	123.8(2)
C8	Fe1	C5	69.23(9)	C8	C4	C3	129.0(2)
C13	Fe1	C5	132.78(11)	C5	C4	Fe1	69.86(13)
C9	Fe1	C5	109.90(11)	C8	C4	Fe1	69.31(12)
C4	Fe1	C10	147.90(10)	C3	C4	Fe1	122.21(15)
C8	Fe1	C10	169.93(10)	C6	C5	C4	108.4(2)
C13	Fe1	C10	68.01(11)	C6	C5	Fe1	70.86(14)
C9	Fe1	C10	40.63(11)	C4	C5	Fe1	68.86(13)
C5	Fe1	C10	116.25(11)	C5	C6	C7	108.4(2)
C4	Fe1	C12	131.45(10)	C5	C6	Fe1	68.99(13)
C8	Fe1	C12	107.75(10)	C7	C6	Fe1	69.48(13)
C13	Fe1	C12	40.66(12)	C8	C7	C6	108.5(2)
C9	Fe1	C12	68.19(12)	C8	C7	Fe1	68.77(13)
C5	Fe1	C12	171.67(11)	C6	C7	Fe1	70.23(13)
C10	Fe1	C12	68.00(12)	C7	C8	C4	107.7(2)
C4	Fe1	C11	170.62(10)	C7	C8	Fe1	70.62(13)
C8	Fe1	C11	130.78(10)	C4	C8	Fe1	69.06(12)
C13	Fe1	C11	68.10(11)	C13	C9	C10	107.8(2)
C9	Fe1	C11	68.06(11)	C13	C9	Fe1	69.60(15)
C5	Fe1	C11	147.18(10)	C10	C9	Fe1	69.79(14)
C10	Fe1	C11	40.22(11)	C11	C10	C9	108.3(3)
C12	Fe1	C11	40.52(11)	C11	C10	Fe1	70.24(15)
C4	Fe1	C7	68.90(9)	C9	C10	Fe1	69.58(14)
C8	Fe1	C7	40.61(9)	C10	C11	C12	107.9(2)

C13	Fe1	C7	147.06(11)	C10	C11	Fe1	69.53(14)
C9	Fe1	C7	171.26(11)	C12	C11	Fe1	69.50(14)
C5	Fe1	C7	68.13(10)	C13	C12	C11	107.6(3)
C10	Fe1	C7	131.79(10)	C13	C12	Fe1	69.24(15)
C12	Fe1	C7	115.03(11)	C11	C12	Fe1	69.99(15)
C11	Fe1	C7	108.66(10)	C9	C13	C12	108.4(2)
C4	Fe1	C6	68.59(9)	C9	C13	Fe1	70.04(15)
C8	Fe1	C6	68.39(9)	C12	C13	Fe1	70.11(15)
C13	Fe1	C6	171.68(11)	N1	C14	C15	112.7(2)
C9	Fe1	C6	132.89(11)	C14	C15	C16	110.9(2)

Table 5: Torsion Angles

A	B	C	D	Angle/°	A	B	C	D	Angle/°
C14	N1	C3	C4	179.01(19)	C5	C4	C8	C7	-0.4(2)
C14	N1	C3	Rh1	-5.7(3)	C3	C4	C8	C7	-175.6(2)
N1	C3	C4	C5	174.0(2)	Fe1	C4	C8	C7	-60.32(15)
Rh1	C3	C4	C5	-1.7(3)	C5	C4	C8	Fe1	59.94(15)
N1	C3	C4	C8	-11.5(3)	C3	C4	C8	Fe1	-115.3(2)
Rh1	C3	C4	C8	172.79(17)	C13	C9	C10	C11	-0.3(3)
N1	C3	C4	Fe1	-100.0(2)	Fe1	C9	C10	C11	-59.80(18)
Rh1	C3	C4	Fe1	84.34(19)	C13	C9	C10	Fe1	59.47(17)
C8	C4	C5	C6	0.5(3)	C9	C10	C11	C12	0.3(3)
C3	C4	C5	C6	176.0(2)	Fe1	C10	C11	C12	-59.08(18)
Fe1	C4	C5	C6	60.07(17)	C9	C10	C11	Fe1	59.39(18)
C8	C4	C5	Fe1	-59.59(15)	C10	C11	C12	C13	-0.2(3)
C3	C4	C5	Fe1	116.0(2)	Fe1	C11	C12	C13	-59.27(17)
C4	C5	C6	C7	-0.4(3)	C10	C11	C12	Fe1	59.10(18)
Fe1	C5	C6	C7	58.44(16)	C10	C9	C13	C12	0.2(3)
C4	C5	C6	Fe1	-58.83(16)	Fe1	C9	C13	C12	59.82(17)
C5	C6	C7	C8	0.1(3)	C10	C9	C13	Fe1	-59.60(18)
Fe1	C6	C7	C8	58.28(16)	C11	C12	C13	C9	0.0(3)
C5	C6	C7	Fe1	-58.14(16)	Fe1	C12	C13	C9	-59.78(18)
C6	C7	C8	C4	0.2(3)	C11	C12	C13	Fe1	59.75(18)
Fe1	C7	C8	C4	59.34(15)	C3	N1	C14	C15	-123.8(3)
C6	C7	C8	Fe1	-59.19(16)	N1	C14	C15	C16	-177.1(2)

Table 6: Hydrogen Atom Coordinates (Å×10^4) and Isotropic Displacement Parameters (Å^2×10^3)

Atom	*x*	*y*	*z*	U(eq)
H1	10830(30)	1290(20)	-360(8)	39(8)
H5	6119	1264	218	33
H6	4919	1220	-1303	36
H7	6879	1353	-2378	34
H8	9324	1473	-1529	30
H9	6792	4149	438	47
H10	4777	4103	-762	47
H11	5921	4179	-2208	45
H12	8660	4253	-1908	48
H13	9182	4233	-269	48
H14A	12326	833	910	34
H14B	11403	1716	1448	34
H15A	12282	3262	658	53
H15B	13156	2393	77	53
H16A	13756	2736	1907	69
H16B	14768	3172	1169	69
H16C	14601	1825	1348	69

Appendix 5: Crystal data tables for complex 19

Table 1: Fractional Atomic Coordinates (×10^4) and Equivalent Isotropic Displacement Parameters (Å^2×10^3). U_{eq} is defined as 1/3 of of the trace of the orthogonalised U_{IJ} tensor.

Atom	*x*	*y*	*z*	U(eq)
Rh1	4011.6(3)	6558.6(3)	3021.8(2)	13.59(15)
Cl1	2095.3(13)	6945.5(10)	1928.9(9)	25.6(3)
C1	5536(6)	6223(4)	3822(4)	21.4(10)
O1	6461(4)	6006(3)	4295(3)	36.2(10)
C2	4928(4)	5279(4)	2276(3)	15.9(9)
O2	4808(4)	4319(3)	2485(3)	21.7(7)
C3	4052(5)	4120(4)	3369(4)	23.8(11)
C4	2709(7)	4002(6)	3045(5)	48.2(17)
Fe1	7765.0(7)	4958.8(5)	1361.4(5)	18.1(2)
C5	5666(5)	5353(4)	1364(3)	16.5(9)
C6	6065(5)	6271(4)	1003(4)	21.8(10)
C7	6880(6)	6006(5)	151(4)	27.7(12)
C8	6995(5)	4950(5)	-8(4)	27.9(12)
C9	6268(5)	4527(4)	731(4)	23.4(11)
C10	8549(6)	4258(4)	2724(4)	30.5(12)
C11	8863(6)	5210(5)	2487(4)	30.3(12)
C12	9656(6)	5114(5)	1610(4)	31.6(13)
C13	9817(6)	4105(5)	1304(4)	35.4(14)
C14	9137(6)	3569(5)	1989(5)	37.6(14)
P1	2708.9(12)	8051.6(9)	3788.2(8)	14.9(3)
C15	3314(5)	8304(3)	4956(3)	15.6(9)
C16	4523(5)	8596(4)	4948(4)	22.6(11)
C17	5012(5)	8810(4)	5806(4)	23.8(11)
C18	4323(6)	8723(4)	6689(4)	26.7(12)
C19	3149(6)	8429(4)	6699(4)	29.2(12)
C20	2633(6)	8226(4)	5851(4)	23.0(11)
C21	2474(5)	9345(4)	3071(3)	17.0(9)
C22	3078(5)	9359(4)	2143(4)	22.8(10)
C23	3039(6)	10334(4)	1621(4)	27.0(11)
C24	2385(6)	11285(4)	2005(4)	29.4(12)
C25	1771(6)	11284(4)	2921(4)	26.0(11)
C26	1825(5)	10327(4)	3459(4)	21.5(10)
C27	992(5)	7951(4)	4092(3)	17.3(9)

C28	-244(5)	8793(4)	3959(4)	23.7(11)
C29	-1495(6)	8619(4)	4214(4)	30.1(12)
C30	-1519(6)	7610(5)	4591(4)	31.8(13)
C31	-294(6)	6771(5)	4723(4)	32.6(13)
C32	962(6)	6927(4)	4474(4)	27.0(11)
C33	8416(7)	8195(6)	1801(5)	44.8(16)
Cl2	6661.3(19)	8587.5(19)	2100.9(16)	67.6(6)
Cl3	8698.3(19)	8124.1(14)	530.3(11)	46.9(4)
C34	1905(7)	8833(6)	9823(5)	51.2(19)
Cl4	3637.8(18)	8536.6(15)	9469.6(13)	51.6(5)
Cl5	755.8(17)	9249.4(13)	8812.7(11)	40.5(4)

Table 2: Anisotropic Displacement Parameters ($Å^2 \times 10^3$). The Anisotropic displacement factor exponent takes the form: $-2\pi^2[h^2a^{*2}U_{11}+2hka^*b^*U_{12}+\ldots]$.

Atom	U_{11}	U_{22}	U_{33}	U_{23}	U_{13}	U_{12}
Rh1	13.1(2)	12.7(2)	13.7(2)	-3.39(14)	1.73(14)	-1.77(15)
Cl1	22.7(6)	25.0(6)	25.0(6)	-6.9(5)	-3.3(5)	-0.5(5)
C1	25(3)	17(2)	20(2)	-9.8(19)	10(2)	-3(2)
O1	33(2)	43(2)	30(2)	-10.5(18)	0.3(19)	-7.0(19)
C2	7(2)	18(2)	20(2)	-3.5(18)	-3.1(17)	2.2(17)
O2	25.5(19)	11.6(15)	27.8(19)	-6.3(13)	7.0(15)	-4.9(14)
C3	29(3)	12(2)	29(3)	0.3(19)	6(2)	-6(2)
C4	32(4)	60(4)	58(4)	14(3)	-4(3)	-29(3)
Fe1	13.1(4)	21.2(4)	18.3(4)	-5.1(3)	1.2(3)	-2.2(3)
C5	11(2)	17(2)	20(2)	-6.0(18)	1.0(17)	-0.7(18)
C6	14(2)	23(2)	23(3)	0.2(19)	-0.2(19)	1.4(19)
C7	21(3)	39(3)	20(3)	5(2)	-1(2)	-8(2)
C8	16(3)	49(3)	18(3)	-15(2)	0.8(19)	-7(2)
C9	16(2)	31(3)	24(3)	-14(2)	2.4(19)	-4(2)
C10	30(3)	34(3)	22(3)	7(2)	-5(2)	-5(2)
C11	26(3)	41(3)	26(3)	-9(2)	-8(2)	-10(2)
C12	22(3)	46(3)	30(3)	-1(2)	-3(2)	-16(3)
C13	15(3)	47(3)	35(3)	-12(3)	-2(2)	5(2)
C14	28(3)	25(3)	51(4)	-1(3)	-11(3)	4(2)
P1	15.0(6)	12.5(6)	15.9(6)	-3.2(4)	2.2(4)	-2.3(5)
C15	14(2)	9(2)	20(2)	-3.2(17)	1.7(17)	1.3(17)
C16	25(3)	22(2)	20(2)	-2.4(19)	5.1(19)	-5(2)
C17	23(3)	13(2)	32(3)	-2.4(19)	-6(2)	-1.2(19)
C18	31(3)	21(2)	21(3)	-6(2)	-8(2)	3(2)

C19	23(3)	37(3)	22(3)	-6(2)	6(2)	-1(2)
C20	25(3)	21(2)	23(3)	-5.7(19)	5(2)	-7(2)
C21	17(2)	17(2)	19(2)	-0.7(18)	-1.0(18)	-7.9(19)
C22	21(3)	21(2)	22(3)	-2.5(19)	-1.8(19)	-1(2)
C23	29(3)	32(3)	21(3)	0(2)	-2(2)	-12(2)
C24	38(3)	19(2)	33(3)	6(2)	-13(2)	-14(2)
C25	30(3)	14(2)	31(3)	-7(2)	-10(2)	-1(2)
C26	19(3)	16(2)	27(3)	-5.6(19)	-1.5(19)	-1.6(19)
C27	15(2)	19(2)	19(2)	-11.9(18)	4.9(18)	-6.1(19)
C28	18(3)	22(2)	29(3)	-6(2)	1(2)	-1(2)
C29	16(3)	30(3)	37(3)	-9(2)	5(2)	3(2)
C30	18(3)	51(4)	33(3)	-18(3)	6(2)	-16(3)
C31	34(3)	28(3)	39(3)	-6(2)	11(2)	-14(2)
C32	23(3)	21(3)	35(3)	-5(2)	6(2)	-4(2)
C33	40(4)	54(4)	34(3)	6(3)	2(3)	-9(3)
Cl2	34.8(10)	92.6(16)	82.7(15)	-53.2(13)	4.1(9)	-16.6(10)
Cl3	61.1(11)	52.7(10)	30.4(8)	1.4(7)	-7.1(7)	-24.3(8)
C34	42(4)	71(5)	27(3)	5(3)	2(3)	-2(4)
Cl4	37.0(9)	65.9(11)	42.7(9)	-11.4(8)	0.0(7)	-2.0(8)
Cl5	37.3(8)	52.0(9)	31.1(8)	-11.3(7)	4.2(6)	-10.9(7)

Table 3: Bond Lengths

Atom	Atom	Length/Å	Atom	Atom	Length/Å
Rh1	C1	1.832(6)	C12	C13	1.398(9)
Rh1	C2	2.018(4)	C13	C14	1.411(9)
Rh1	P1	2.3291(12)	P1	C21	1.824(5)
Rh1	Cl1	2.3807(13)	P1	C27	1.825(5)
C1	O1	1.100(7)	P1	C15	1.832(5)
C2	O2	1.312(6)	C15	C20	1.400(6)
C2	C5	1.447(6)	C15	C16	1.401(7)
O2	C3	1.460(6)	C16	C17	1.380(7)
C3	C4	1.508(8)	C17	C18	1.392(8)
Fe1	C5	2.028(5)	C18	C19	1.369(8)
Fe1	C13	2.031(5)	C19	C20	1.375(7)
Fe1	C9	2.033(5)	C21	C22	1.395(7)
Fe1	C14	2.033(5)	C21	C26	1.405(6)
Fe1	C12	2.040(6)	C22	C23	1.393(7)
Fe1	C6	2.042(5)	C23	C24	1.371(7)
Fe1	C11	2.046(5)	C24	C25	1.384(8)

Fe1	C10	2.053(5)	C25	C26	1.378(7)
Fe1	C8	2.057(5)	C27	C28	1.385(7)
Fe1	C7	2.064(5)	C27	C32	1.406(7)
C5	C6	1.433(7)	C28	C29	1.392(7)
C5	C9	1.434(6)	C29	C30	1.383(8)
C6	C7	1.419(7)	C30	C31	1.376(8)
C7	C8	1.402(8)	C31	C32	1.384(8)
C8	C9	1.407(7)	C33	Cl2	1.740(7)
C10	C11	1.395(8)	C33	Cl3	1.763(6)
C10	C14	1.417(8)	C34	Cl4	1.743(7)
C11	C12	1.420(8)	C34	Cl5	1.761(7)

Table 4: Bond Angles

Atom	Atom	Atom	Angle/°	Atom	Atom	Atom	Angle/°
C1	Rh1	C2	91.11(19)	C9	C5	Fe1	69.5(3)
C1	Rh1	P1	95.57(14)	C2	C5	Fe1	120.4(3)
C2	Rh1	P1	173.16(13)	C7	C6	C5	107.3(4)
C1	Rh1	Cl1	177.39(14)	C7	C6	Fe1	70.6(3)
C2	Rh1	Cl1	86.43(13)	C5	C6	Fe1	68.8(3)
P1	Rh1	Cl1	86.91(4)	C8	C7	C6	108.4(5)
O1	C1	Rh1	178.8(5)	C8	C7	Fe1	69.9(3)
O2	C2	C5	111.6(4)	C6	C7	Fe1	69.0(3)
O2	C2	Rh1	125.0(3)	C7	C8	C9	109.2(4)
C5	C2	Rh1	123.0(3)	C7	C8	Fe1	70.4(3)
C2	O2	C3	118.5(4)	C9	C8	Fe1	68.9(3)
O2	C3	C4	107.4(5)	C8	C9	C5	107.4(5)
C5	Fe1	C13	162.0(2)	C8	C9	Fe1	70.8(3)
C5	Fe1	C9	41.36(18)	C5	C9	Fe1	69.1(3)
C13	Fe1	C9	122.8(2)	C11	C10	C14	107.6(5)
C5	Fe1	C14	126.3(2)	C11	C10	Fe1	69.8(3)
C13	Fe1	C14	40.6(3)	C14	C10	Fe1	68.9(3)
C9	Fe1	C14	105.9(2)	C10	C11	C12	108.3(5)
C5	Fe1	C12	157.3(2)	C10	C11	Fe1	70.3(3)
C13	Fe1	C12	40.2(2)	C12	C11	Fe1	69.4(3)
C9	Fe1	C12	160.0(2)	C13	C12	C11	108.0(5)
C14	Fe1	C12	67.7(3)	C13	C12	Fe1	69.6(3)
C5	Fe1	C6	41.23(19)	C11	C12	Fe1	69.9(3)
C13	Fe1	C6	153.5(2)	C12	C13	C14	107.9(5)
C9	Fe1	C6	69.2(2)	C12	C13	Fe1	70.3(3)

C14	Fe1	C6	165.5(2)	C14	C13	Fe1	69.7(3)
C12	Fe1	C6	121.4(2)	C13	C14	C10	108.2(5)
C5	Fe1	C11	123.0(2)	C13	C14	Fe1	69.6(3)
C13	Fe1	C11	68.0(2)	C10	C14	Fe1	70.5(3)
C9	Fe1	C11	156.5(2)	C21	P1	C27	108.0(2)
C14	Fe1	C11	67.6(2)	C21	P1	C15	100.4(2)
C12	Fe1	C11	40.7(2)	C27	P1	C15	103.0(2)
C6	Fe1	C11	111.0(2)	C21	P1	Rh1	114.87(15)
C5	Fe1	C10	110.0(2)	C27	P1	Rh1	109.78(15)
C13	Fe1	C10	68.2(2)	C15	P1	Rh1	119.56(14)
C9	Fe1	C10	120.6(2)	C20	C15	C16	118.4(4)
C14	Fe1	C10	40.6(2)	C20	C15	P1	123.6(4)
C12	Fe1	C10	67.8(2)	C16	C15	P1	117.9(3)
C6	Fe1	C10	129.2(2)	C17	C16	C15	120.2(5)
C11	Fe1	C10	39.8(2)	C16	C17	C18	120.4(5)
C5	Fe1	C8	68.18(19)	C19	C18	C17	119.4(5)
C13	Fe1	C8	105.1(2)	C18	C19	C20	121.1(5)
C9	Fe1	C8	40.2(2)	C19	C20	C15	120.4(5)
C14	Fe1	C8	117.8(2)	C22	C21	C26	118.9(4)
C12	Fe1	C8	124.3(2)	C22	C21	P1	118.7(4)
C6	Fe1	C8	67.9(2)	C26	C21	P1	122.1(4)
C11	Fe1	C8	163.1(2)	C21	C22	C23	120.0(5)
C10	Fe1	C8	153.7(2)	C24	C23	C22	120.4(5)
C5	Fe1	C7	68.3(2)	C23	C24	C25	120.3(5)
C13	Fe1	C7	117.9(2)	C26	C25	C24	120.3(5)
C9	Fe1	C7	68.0(2)	C25	C26	C21	120.2(5)
C14	Fe1	C7	151.8(2)	C28	C27	C32	119.3(5)
C12	Fe1	C7	108.1(2)	C28	C27	P1	124.9(4)
C6	Fe1	C7	40.44(19)	C32	C27	P1	115.8(4)
C11	Fe1	C7	128.5(2)	C27	C28	C29	119.8(5)
C10	Fe1	C7	166.0(2)	C30	C29	C28	120.7(5)
C8	Fe1	C7	39.8(2)	C31	C30	C29	119.7(5)
C6	C5	C9	107.6(4)	C30	C31	C32	120.6(5)
C6	C5	C2	123.7(4)	C31	C32	C27	119.9(5)
C9	C5	C2	128.3(4)	Cl2	C33	Cl3	112.6(4)
C6	C5	Fe1	69.9(3)	Cl4	C34	Cl5	112.4(3)

Table 5: Torsion Angles

A	B	C	D	Angle/˚	A	B	C	D	Angle/˚

C5	C2	O2	C3	-178.2(4)		C21	P1	C15	C20	121.2(4)
Rh1	C2	O2	C3	-5.3(6)		C27	P1	C15	C20	9.8(4)
C2	O2	C3	C4	109.8(5)		Rh1	P1	C15	C20	-112.2(4)
O2	C2	C5	C6	-173.8(4)		C21	P1	C15	C16	-58.5(4)
Rh1	C2	C5	C6	13.1(6)		C27	P1	C15	C16	-169.9(4)
O2	C2	C5	C9	-1.9(7)		Rh1	P1	C15	C16	68.0(4)
Rh1	C2	C5	C9	-174.9(4)		C20	C15	C16	C17	-0.7(7)
O2	C2	C5	Fe1	-88.8(4)		P1	C15	C16	C17	179.1(4)
Rh1	C2	C5	Fe1	98.1(4)		C15	C16	C17	C18	1.0(7)
C9	C5	C6	C7	0.9(5)		C16	C17	C18	C19	-0.4(7)
C2	C5	C6	C7	174.3(4)		C17	C18	C19	C20	-0.5(8)
Fe1	C5	C6	C7	60.4(3)		C18	C19	C20	C15	0.8(8)
C9	C5	C6	Fe1	-59.5(3)		C16	C15	C20	C19	-0.2(7)
C2	C5	C6	Fe1	113.9(4)		P1	C15	C20	C19	-180.0(4)
C5	C6	C7	C8	-0.4(6)		C27	P1	C21	C22	-123.3(4)
Fe1	C6	C7	C8	58.9(4)		C15	P1	C21	C22	129.2(4)
C5	C6	C7	Fe1	-59.3(3)		Rh1	P1	C21	C22	-0.4(5)
C6	C7	C8	C9	-0.2(6)		C27	P1	C21	C26	63.0(4)
Fe1	C7	C8	C9	58.1(4)		C15	P1	C21	C26	-44.5(4)
C6	C7	C8	Fe1	-58.3(4)		Rh1	P1	C21	C26	-174.1(3)
C7	C8	C9	C5	0.8(6)		C26	C21	C22	C23	0.5(7)
Fe1	C8	C9	C5	59.7(3)		P1	C21	C22	C23	-173.4(4)
C7	C8	C9	Fe1	-59.0(4)		C21	C22	C23	C24	-1.4(8)
C6	C5	C9	C8	-1.0(5)		C22	C23	C24	C25	0.8(8)
C2	C5	C9	C8	-174.0(5)		C23	C24	C25	C26	0.7(8)
Fe1	C5	C9	C8	-60.8(3)		C24	C25	C26	C21	-1.6(8)
C6	C5	C9	Fe1	59.8(3)		C22	C21	C26	C25	1.0(7)
C2	C5	C9	Fe1	-113.2(5)		P1	C21	C26	C25	174.6(4)
C14	C10	C11	C12	-0.5(6)		C21	P1	C27	C28	-11.1(5)
Fe1	C10	C11	C12	-59.3(4)		C15	P1	C27	C28	94.5(4)
C14	C10	C11	Fe1	58.8(4)		Rh1	P1	C27	C28	-137.1(4)
C10	C11	C12	C13	0.5(6)		C21	P1	C27	C32	167.9(4)
Fe1	C11	C12	C13	-59.3(4)		C15	P1	C27	C32	-86.5(4)
C10	C11	C12	Fe1	59.9(4)		Rh1	P1	C27	C32	41.9(4)
C11	C12	C13	C14	-0.3(6)		C32	C27	C28	C29	0.8(8)
Fe1	C12	C13	C14	-59.9(4)		P1	C27	C28	C29	179.7(4)
C11	C12	C13	Fe1	59.5(4)		C27	C28	C29	C30	-0.7(8)
C12	C13	C14	C10	0.0(7)		C28	C29	C30	C31	0.5(9)

Fe1	C13	C14	C10	-60.2(4)	C29	C30	C31	C32	-0.5(9)
C12	C13	C14	Fe1	60.2(4)	C30	C31	C32	C27	0.6(8)
C11	C10	C14	C13	0.3(6)	C28	C27	C32	C31	-0.7(8)
Fe1	C10	C14	C13	59.6(4)	P1	C27	C32	C31	-179.8(4)
C11	C10	C14	Fe1	-59.4(4)					

Table 6: Hydrogen Atom Coordinates (Å×10^4) and Isotropic Displacement Parameters (Å^2×10^3)

Atom	*x*	*y*	*z*	U(eq)
H3A	3860	4728	3775	29
H3B	4608	3455	3766	29
H4A	2150	4676	2680	72
H4B	2194	3836	3623	72
H4C	2912	3418	2622	72
H6	5827	6935	1282	26
H7	7281	6466	-244	33
H8	7486	4578	-533	33
H9	6190	3825	798	28
H10	8035	4101	3277	37
H11	8592	5817	2851	36
H12	10013	5643	1288	38
H13	10300	3829	736	43
H14	9082	2868	1962	45
H16	5008	8647	4350	27
H17	5824	9019	5794	29
H18	4665	8866	7279	32
H19	2683	8363	7303	35
H20	1810	8032	5872	28
H22	3515	8703	1867	27
H23	3469	10341	995	32
H24	2353	11948	1641	35
H25	1310	11946	3180	31
H26	1422	10330	4094	26
H28	-238	9487	3694	28
H29	-2341	9199	4129	36
H30	-2378	7497	4759	38
H31	-310	6079	4987	39
H32	1802	6342	4561	32
H33A	8891	7481	2157	54
H33B	8832	8715	2022	54

H34A	1679	9410	10266	61
H34B	1772	8187	10194	61

Appendix 6: Crystal data tables for complex 20

Table 1: Fractional Atomic Coordinates (×10^4) and Equivalent Isotropic Displacement Parameters (Å^2×10^3). U_{eq} is defined as 1/3 of of the trace of the orthogonalised U_{IJ} tensor.

Atom	*x*	*y*	*z*	U(eq)
Rh1	2469.5(2)	4014.5(2)	7135.3(2)	12.48(2)
Cl1	3223.9(6)	3416.9(2)	8747.2(5)	31.11(13)
C1	1919(2)	4488.4(8)	5956(2)	23.9(4)
O1	1576(2)	4787.3(8)	5190.7(17)	44.3(5)
Cl1A	1594(3)	4611.8(12)	5551(3)	31.11(13)
O1A	3686(10)	3344(3)	9111(7)	44.3(5)
C1A	3206(8)	3599(4)	8341(8)	23.9(4)
C2	1733.3(12)	4399.1(5)	8414.1(12)	14.5(2)
O2	687.3(9)	4291.5(4)	8699.3(10)	21.5(2)
C3	-83.8(15)	3903.4(7)	7969.2(17)	28.0(3)
C4	-929.7(17)	4161.1(9)	6903.1(19)	37.1(4)
Fe1	2063.1(2)	5562.1(2)	8762.8(2)	16.65(4)
C5	2343.0(12)	4800.3(5)	9215.5(12)	14.5(2)
C6	3451.7(12)	5043.0(5)	9057.2(13)	16.3(2)
C7	3708.6(13)	5453.2(6)	9925.1(13)	19.8(3)
C8	2772.0(14)	5472.7(6)	10624.3(13)	21.1(3)
C9	1919.2(13)	5078.1(6)	10191.0(13)	19.2(2)
C10	700.4(18)	5640.6(7)	7234.7(19)	37.7(4)
C11	1798.4(19)	5814.1(7)	6955.7(16)	33.9(4)
C12	2234.7(18)	6223.3(6)	7783.4(17)	31.8(4)
C13	1414.0(18)	6301.7(7)	8577.9(18)	34.0(4)
C14	455.5(17)	5943.1(8)	8241(2)	38.7(4)
P1	3198.9(3)	3494.2(2)	5678.9(3)	11.48(6)
C15	881.3(13)	3229.8(6)	4478.9(16)	23.9(3)
C16	-60.1(15)	2821.2(7)	3972.3(17)	29.2(4)
C17	-238.1(14)	2437.7(7)	4969.5(16)	26.7(3)
C18	950.2(14)	2188.6(6)	5581.9(15)	24.2(3)
C19	1896.8(14)	2599.1(6)	6096.7(14)	21.5(3)
C20	2086.5(11)	2981.8(5)	5084.9(12)	14.1(2)
C21	4579.1(12)	3127.1(5)	6326.5(12)	15.8(2)
C22	5615.4(13)	3471.1(6)	6999.9(16)	24.7(3)
C23	6613.6(15)	3131.4(7)	7734.1(17)	32.0(4)
C24	7065.1(16)	2734.0(8)	6898.9(19)	37.6(4)

C25	6031.2(17)	2403.7(8)	6212.1(18)	36.3(4)
C26	5039.4(15)	2744.1(7)	5463.3(15)	28.4(3)
C27	3367.1(12)	3839.7(5)	4245.4(12)	14.4(2)
C28	3463.8(19)	3515.7(6)	3105.7(14)	29.6(4)
C29	3354.2(17)	3863.1(7)	1966.7(14)	29.4(3)
C30	4294.1(15)	4290.9(7)	2162.7(15)	26.8(3)
C31	4236(2)	4604.6(7)	3310.6(16)	40.9(5)
C32	4345.2(18)	4256.0(7)	4458.6(15)	32.8(4)

Table 2: Anisotropic Displacement Parameters ($Å^2×10^3$). The Anisotropic displacement factor exponent takes the form: $-2π^2[h^2a^{*2}U_{11}+2hka^*b^*U_{12}+…]$.

Atom	U_{11}	U_{22}	U_{33}	U_{23}	U_{13}	U_{12}
Rh1	15.57(4)	11.71(4)	10.70(4)	-0.17(3)	3.92(3)	2.01(3)
Cl1	49.8(3)	31.3(3)	13.9(2)	7.99(18)	10.3(2)	20.3(2)
C1	38.6(10)	19.9(8)	14.2(8)	-0.1(7)	7.9(7)	9.0(8)
O1	78.8(14)	33.5(9)	20.2(8)	8.0(7)	8.8(8)	27.0(9)
Cl1A	49.8(3)	31.3(3)	13.9(2)	7.99(18)	10.3(2)	20.3(2)
O1A	78.8(14)	33.5(9)	20.2(8)	8.0(7)	8.8(8)	27.0(9)
C1A	38.6(10)	19.9(8)	14.2(8)	-0.1(7)	7.9(7)	9.0(8)
C2	16.9(5)	13.2(5)	14.4(5)	1.9(4)	5.5(4)	2.6(4)
O2	19.2(5)	23.1(5)	24.9(5)	-5.4(4)	11.2(4)	-4.4(4)
C3	23.6(7)	27.2(8)	34.8(9)	-6.9(6)	9.5(6)	-9.2(6)
C4	27.7(8)	48.8(11)	35.0(9)	-2.9(8)	6.3(7)	-9.4(8)
Fe1	17.72(9)	13.24(8)	17.97(9)	-1.16(7)	1.03(7)	3.68(7)
C5	16.4(5)	14.0(5)	13.7(5)	-0.1(4)	4.6(4)	3.3(4)
C6	15.2(5)	16.7(6)	17.2(6)	1.3(4)	4.0(4)	3.2(4)
C7	17.5(6)	20.0(6)	20.2(6)	-1.0(5)	-0.7(5)	0.2(5)
C8	25.3(7)	20.9(6)	16.7(6)	-5.6(5)	2.9(5)	1.6(5)
C9	20.7(6)	21.9(6)	16.7(6)	-3.2(5)	8.1(5)	1.6(5)
C10	38.4(10)	24.3(8)	39.4(10)	4.3(7)	-18.8(8)	4.6(7)
C11	53.1(11)	22.1(7)	23.6(8)	5.5(6)	0.4(7)	9.7(7)
C12	41.0(9)	15.7(7)	37.0(9)	7.1(6)	3.4(7)	3.4(6)
C13	42.8(10)	18.4(7)	37.9(9)	-2.7(6)	0.9(8)	13.6(7)
C14	24.6(8)	35.8(10)	53.0(12)	9.4(8)	0.9(8)	15.6(7)
P1	13.08(13)	11.33(13)	10.20(13)	-0.77(10)	2.7(1)	-0.05(10)
C15	18.1(6)	18.3(6)	31.1(8)	7.9(6)	-5.3(5)	-3.1(5)
C16	22.7(7)	27.1(8)	32.3(8)	9.2(6)	-8.3(6)	-9.7(6)
C17	18.8(7)	27.0(8)	33.4(8)	5.1(6)	2.6(6)	-7.7(6)
C18	24.0(7)	17.9(6)	29.2(7)	7.7(5)	1.4(6)	-6.2(5)

C19	22.0(6)	20.1(6)	20.7(6)	7.8(5)	-0.2(5)	-5.7(5)
C20	15.4(5)	12.6(5)	13.8(5)	0.8(4)	1.9(4)	-2.0(4)
C21	14.9(5)	17.0(6)	15.0(5)	-1.6(4)	1.8(4)	1.8(4)
C22	16.5(6)	23.0(7)	31.7(8)	-2.3(6)	-2.3(5)	-0.2(5)
C23	21.7(7)	35.5(9)	33.2(9)	-1.8(7)	-8.0(6)	3.6(6)
C24	22.8(8)	47.4(11)	39.9(10)	4.0(8)	-0.4(7)	17.7(8)
C25	36.0(9)	34.0(9)	35.1(9)	-7.8(7)	-2.0(7)	21.7(7)
C26	27.3(8)	32.2(8)	23.4(7)	-8.9(6)	-0.8(6)	14.6(6)
C27	17.4(6)	14.8(5)	11.7(5)	-1.7(4)	4.3(4)	-3.6(4)
C28	56.4(11)	20.0(7)	16.1(6)	-3.2(5)	16.5(7)	-4.9(7)
C29	44.6(10)	32.2(8)	12.8(6)	-1.6(6)	8.9(6)	-9.8(7)
C30	24.5(7)	37.2(9)	19.9(7)	9.5(6)	7.2(6)	-3.9(6)
C31	70.7(14)	28.6(9)	23.5(8)	2.7(7)	9.7(8)	-26.9(9)
C32	45.9(10)	35.7(9)	15.6(6)	0.8(6)	3.0(6)	-26.0(8)

Table 3: Bond Lengths

Atom	Atom	Length/Å	Atom	Atom	Length/Å
Rh1	C1A	1.777(10)	C10	C11	1.409(3)
Rh1	C1	1.799(2)	C10	C14	1.423(3)
Rh1	C2	2.0267(13)	C11	C12	1.415(3)
Rh1	P1	2.3566(4)	C12	C13	1.408(3)
Rh1	Cl1	2.3738(6)	C13	C14	1.416(3)
Rh1	Cl1A	2.386(3)	P1	C21	1.8432(13)
C1	O1	1.150(3)	P1	C20	1.8502(13)
O1A	C1A	1.122(12)	P1	C27	1.8510(13)
C2	O2	1.3116(16)	C15	C16	1.522(2)
C2	C5	1.4413(19)	C15	C20	1.5333(19)
O2	C3	1.4580(19)	C16	C17	1.517(2)
C3	C4	1.512(3)	C17	C18	1.521(2)
Fe1	C5	2.0314(13)	C18	C19	1.531(2)
Fe1	C9	2.0349(15)	C19	C20	1.5316(19)
Fe1	C13	2.0353(16)	C21	C26	1.528(2)
Fe1	C6	2.0380(13)	C21	C22	1.537(2)
Fe1	C12	2.0425(17)	C22	C23	1.527(2)
Fe1	C14	2.0456(17)	C23	C24	1.527(3)
Fe1	C10	2.0536(17)	C24	C25	1.520(3)
Fe1	C11	2.0542(17)	C25	C26	1.529(2)
Fe1	C8	2.0580(15)	C27	C32	1.524(2)

Fe1	C7	2.0585(14)	C27	C28	1.5263(19)
C5	C6	1.4416(19)	C28	C29	1.523(2)
C5	C9	1.4465(18)	C29	C30	1.516(2)
C6	C7	1.414(2)	C30	C31	1.510(3)
C7	C8	1.427(2)	C31	C32	1.533(2)
C8	C9	1.417(2)			

Table 4: Bond Angles

Atom	Atom	Atom	Angle/°	Atom	Atom	Atom	Angle/°
C1A	Rh1	C2	88.4(3)	C2	C5	C6	124.01(12)
C1	Rh1	C2	92.15(7)	C2	C5	C9	128.19(12)
C1A	Rh1	P1	89.4(3)	C6	C5	C9	107.35(12)
C1	Rh1	P1	90.77(6)	C2	C5	Fe1	120.56(9)
C2	Rh1	P1	174.09(4)	C6	C5	Fe1	69.50(7)
C1	Rh1	Cl1	177.70(7)	C9	C5	Fe1	69.29(8)
C2	Rh1	Cl1	86.27(4)	C7	C6	C5	108.07(12)
P1	Rh1	Cl1	90.946(16)	C7	C6	Fe1	70.60(8)
C1A	Rh1	Cl1A	176.1(3)	C5	C6	Fe1	69.01(7)
C2	Rh1	Cl1A	91.34(7)	C6	C7	C8	108.29(13)
P1	Rh1	Cl1A	91.19(6)	C6	C7	Fe1	69.04(8)
O1	C1	Rh1	178.98(19)	C8	C7	Fe1	69.70(8)
O1A	C1A	Rh1	178.7(10)	C9	C8	C7	108.80(12)
O2	C2	C5	110.52(11)	C9	C8	Fe1	68.88(8)
O2	C2	Rh1	125.15(10)	C7	C8	Fe1	69.75(8)
C5	C2	Rh1	124.11(9)	C8	C9	C5	107.47(12)
C2	O2	C3	118.88(12)	C8	C9	Fe1	70.63(9)
O2	C3	C4	110.18(14)	C5	C9	Fe1	69.03(8)
C5	Fe1	C9	41.67(5)	C11	C10	C14	108.10(17)
C5	Fe1	C13	164.19(7)	C11	C10	Fe1	69.97(10)
C9	Fe1	C13	124.54(7)	C14	C10	Fe1	69.38(10)
C5	Fe1	C6	41.49(5)	C10	C11	C12	107.85(18)
C9	Fe1	C6	69.68(6)	C10	C11	Fe1	69.92(10)
C13	Fe1	C6	151.63(7)	C12	C11	Fe1	69.35(10)
C5	Fe1	C12	154.98(7)	C13	C12	C11	108.43(18)
C9	Fe1	C12	161.14(7)	C13	C12	Fe1	69.52(10)
C13	Fe1	C12	40.41(8)	C11	C12	Fe1	70.24(10)
C6	Fe1	C12	118.63(7)	C12	C13	C14	107.98(17)
C5	Fe1	C14	128.16(7)	C12	C13	Fe1	70.07(9)

C9	Fe1	C14	107.92(8)	C14	C13	Fe1	70.09(10)
C13	Fe1	C14	40.61(8)	C13	C14	C10	107.64(18)
C6	Fe1	C14	166.65(7)	C13	C14	Fe1	69.30(10)
C12	Fe1	C14	67.96(8)	C10	C14	Fe1	69.98(10)
C5	Fe1	C10	110.54(6)	C21	P1	C20	103.68(6)
C9	Fe1	C10	122.00(8)	C21	P1	C27	110.71(6)
C13	Fe1	C10	68.19(8)	C20	P1	C27	102.62(6)
C6	Fe1	C10	128.69(7)	C21	P1	Rh1	114.32(4)
C12	Fe1	C10	67.72(8)	C20	P1	Rh1	109.86(4)
C14	Fe1	C10	40.64(9)	C27	P1	Rh1	114.43(4)
C5	Fe1	C11	121.83(6)	C16	C15	C20	111.69(12)
C9	Fe1	C11	156.96(7)	C17	C16	C15	111.58(13)
C13	Fe1	C11	68.12(8)	C16	C17	C18	111.24(13)
C6	Fe1	C11	108.75(7)	C17	C18	C19	111.45(13)
C12	Fe1	C11	40.41(7)	C18	C19	C20	111.28(12)
C14	Fe1	C11	68.01(9)	C19	C20	C15	110.07(11)
C10	Fe1	C11	40.12(9)	C19	C20	P1	112.61(9)
C5	Fe1	C8	68.73(6)	C15	C20	P1	109.96(9)
C9	Fe1	C8	40.49(6)	C26	C21	C22	110.45(12)
C13	Fe1	C8	105.43(7)	C26	C21	P1	117.17(10)
C6	Fe1	C8	68.39(6)	C22	C21	P1	113.48(10)
C12	Fe1	C8	123.92(7)	C23	C22	C21	109.84(13)
C14	Fe1	C8	118.88(8)	C22	C23	C24	111.43(14)
C10	Fe1	C8	155.06(8)	C25	C24	C23	110.92(15)
C11	Fe1	C8	161.88(7)	C24	C25	C26	110.98(16)
C5	Fe1	C7	68.80(6)	C21	C26	C25	109.79(13)
C9	Fe1	C7	68.77(6)	C32	C27	C28	110.05(13)
C13	Fe1	C7	116.97(7)	C32	C27	P1	113.55(9)
C6	Fe1	C7	40.37(6)	C28	C27	P1	118.17(10)
C12	Fe1	C7	105.80(7)	C29	C28	C27	110.27(13)
C14	Fe1	C7	152.15(8)	C30	C29	C28	111.59(14)
C10	Fe1	C7	164.17(8)	C31	C30	C29	111.22(14)
C11	Fe1	C7	125.79(8)	C30	C31	C32	111.42(16)
C8	Fe1	C7	40.55(6)	C27	C32	C31	110.23(13)

Table 5: Torsion Angles

A	B	C	D	Angle/˚	A	B	C	D	Angle/˚
C5	C2	O2	C3	178.37(12)	C20	C15	C16	C17	55.7(2)

Rh1	C2	O2	C3	-6.79(18)	C15	C16	C17	C18	-55.0(2)
C2	O2	C3	C4	-91.29(17)	C16	C17	C18	C19	55.07(19)
O2	C2	C5	C6	-173.25(12)	C17	C18	C19	C20	-55.85(18)
Rh1	C2	C5	C6	11.85(18)	C18	C19	C20	C15	55.53(17)
O2	C2	C5	C9	-1.86(19)	C18	C19	C20	P1	178.62(11)
Rh1	C2	C5	C9	-176.77(11)	C16	C15	C20	C19	-55.59(17)
O2	C2	C5	Fe1	-88.54(13)	C16	C15	C20	P1	179.78(12)
Rh1	C2	C5	Fe1	96.56(11)	C21	P1	C20	C19	58.28(11)
C2	C5	C6	C7	173.77(12)	C27	P1	C20	C19	173.58(10)
C9	C5	C6	C7	0.85(15)	Rh1	P1	C20	C19	-64.31(10)
Fe1	C5	C6	C7	60.03(9)	C21	P1	C20	C15	-178.57(10)
C2	C5	C6	Fe1	113.74(13)	C27	P1	C20	C15	-63.27(11)
C9	C5	C6	Fe1	-59.18(9)	Rh1	P1	C20	C15	58.84(10)
C5	C6	C7	C8	-0.23(16)	C20	P1	C21	C26	55.04(13)
Fe1	C6	C7	C8	58.81(10)	C27	P1	C21	C26	-54.38(13)
C5	C6	C7	Fe1	-59.04(9)	Rh1	P1	C21	C26	174.62(11)
C6	C7	C8	C9	-0.50(17)	C20	P1	C21	C22	-174.33(11)
Fe1	C7	C8	C9	57.90(10)	C27	P1	C21	C22	76.26(12)
C6	C7	C8	Fe1	-58.40(10)	Rh1	P1	C21	C22	-54.75(11)
C7	C8	C9	C5	1.02(16)	C26	C21	C22	C23	-58.06(18)
Fe1	C8	C9	C5	59.45(9)	P1	C21	C22	C23	168.05(12)
C7	C8	C9	Fe1	-58.43(10)	C21	C22	C23	C24	56.3(2)
C2	C5	C9	C8	-173.68(13)	C22	C23	C24	C25	-55.7(2)
C6	C5	C9	C8	-1.15(15)	C23	C24	C25	C26	56.3(2)
Fe1	C5	C9	C8	-60.46(10)	C22	C21	C26	C25	58.80(19)
C2	C5	C9	Fe1	-113.22(14)	P1	C21	C26	C25	-169.18(13)
C6	C5	C9	Fe1	59.31(9)	C24	C25	C26	C21	-57.9(2)
C14	C10	C11	C12	-0.09(19)	C21	P1	C27	C32	-64.11(13)
Fe1	C10	C11	C12	-59.19(12)	C20	P1	C27	C32	-174.21(12)
C14	C10	C11	Fe1	59.10(12)	Rh1	P1	C27	C32	66.84(13)
C10	C11	C12	C13	0.32(19)	C21	P1	C27	C28	67.02(13)
Fe1	C11	C12	C13	-59.23(12)	C20	P1	C27	C28	-43.09(13)
C10	C11	C12	Fe1	59.55(12)	Rh1	P1	C27	C28	-162.04(11)
C11	C12	C13	C14	-0.4(2)	C32	C27	C28	C29	-58.12(19)
Fe1	C12	C13	C14	-60.10(12)	P1	C27	C28	C29	169.20(12)
C11	C12	C13	Fe1	59.68(12)	C27	C28	C29	C30	56.7(2)
C12	C13	C14	C10	0.4(2)	C28	C29	C30	C31	-55.1(2)
Fe1	C13	C14	C10	-59.72(12)	C29	C30	C31	C32	54.9(2)

C12	C13	C14	Fe1	60.09(12)	
C11	C10	C14	C13	-0.17(19)	
Fe1	C10	C14	C13	59.30(12)	
C11	C10	C14	Fe1	-59.47(12)	
C28	C27	C32	C31	58.0(2)	
P1	C27	C32	C31	-166.99(14)	
C30	C31	C32	C27	-56.6(2)	

Table 6: Hydrogen Atom Coordinates (Å×10^4) and Isotropic Displacement Parameters (Å^2×10^3)

Atom	*x*	*y*	*z*	U(eq)
H3A	-557	3719	8504	34
H3B	421	3644	7642	34
H4A	-462	4312	6328	56
H4B	-1382	4437	7225	56
H4C	-1493	3902	6465	56
H6	3927	4945	8472	20
H7	4388	5677	10026	24
H8	2728	5711	11274	25
H9	1200	5009	10487	23
H10	209	5369	6823	45
H11	2178	5680	6324	41
H12	2958	6413	7800	38
H13	1490	6551	9226	41
H14	-228	5910	8619	46
H15A	581	3446	5099	29
H15B	1008	3460	3794	29
H16A	-836	2995	3634	35
H16B	197	2631	3285	35
H17A	-810	2164	4595	32
H17B	-592	2620	5606	32
H18A	1254	1971	4967	29
H18B	815	1960	6266	29
H19A	2670	2425	6445	26
H19B	1633	2792	6776	26
H20	2396	2782	4432	17
H21	4353	2906	6993	19
H22A	5941	3681	6386	30
H22B	5310	3712	7570	30
H23A	6304	2947	8398	38
H23B	7294	3355	8132	38
H24A	7456	2917	6291	45

H24B	7675	2507	7409	45
H25A	5692	2194	6817	44
H25B	6338	2162	5646	44
H26A	5362	2937	4821	34
H26B	4366	2523	5042	34
H27	2597	4038	3994	17
H28A	4249	3333	3250	36
H28B	2816	3251	2963	36
H29A	3452	3650	1243	35
H29B	2540	4020	1782	35
H30A	5107	4135	2245	32
H30B	4160	4523	1430	32
H31A	3461	4795	3185	49
H31B	4897	4863	3448	49
H32A	5149	4089	4633	39
H32B	4266	4470	5187	39

Table 7: Atomic Occupancy

Atom	***Occupancy***	**Atom**	***Occupancy***	**Atom**	***Occupancy***
Cl1	0.8077(15)	C1	0.8077(15)	O1	0.8077(15)
Cl1A	0.1923(15)	O1A	0.1923(15)	C1A	0.1923(15)

Appendix 7: Crystal data tables for complex 23

Table 1: Fractional Atomic Coordinates (×10^4) and Equivalent Isotropic Displacement Parameters (Å^2×10^3). U_{eq} is defined as 1/3 of of the trace of the orthogonalised U_{IJ} tensor.

Atom	*x*	*y*	*z*	U(eq)
Rh1	7714.5(2)	2513.9(2)	3715.0(2)	16.53(4)
P1	6723.5(4)	3641.5(3)	2283.7(3)	15.98(8)
Cl1	9590.3(5)	1328.1(3)	2960.9(3)	26.32(9)
C1	6278(2)	3293.1(15)	4352.3(12)	28.6(4)
O1	5349.0(16)	3768.4(13)	4766.6(10)	48.7(4)
C2	8742.6(16)	1588.4(12)	4942(1)	16.0(3)
N1	8482.2(15)	753.1(11)	5493.9(10)	18.9(3)
Fe1	9776.5(3)	2927.2(2)	5916.9(2)	20.80(6)
C3	9957.7(17)	1805.5(13)	5193.8(11)	18.7(3)
C4	10782.7(18)	1320.1(14)	6033.2(13)	24.8(4)
C5	11797.1(19)	1843.5(15)	5967.4(14)	30.3(4)
C6	11619.3(19)	2642.3(15)	5105.7(13)	28.8(4)
C9	8570(2)	3053.4(17)	7127.5(13)	33.8(4)
C8	7689(2)	3527.9(17)	6329.8(14)	33.8(4)
C7	10486.4(18)	2633.4(14)	4625.2(12)	22.6(3)
C10	9555(2)	3610.2(17)	7022.6(14)	34.5(4)
C11	9287(2)	4418.0(16)	6168.6(14)	36.2(5)
C12	8133(2)	4369.8(16)	5736.1(14)	34.8(4)
C13	7300.5(19)	408.5(15)	5401.2(14)	30.3(4)
C14	6144(3)	677(2)	6145(2)	61.7(7)
C15	6653(6)	516(4)	7159(4)	80(2)
C14A	6144(3)	677(2)	6145(2)	61.7(7)
C15A	5039(5)	122(5)	5919(5)	54.2(19)
C16	5092.0(16)	3473.7(13)	1989.0(11)	18.8(3)
C17	3832.2(17)	3810.3(14)	2661.9(12)	23.0(3)
C18	2542.6(18)	3605.4(14)	2403.5(13)	26.4(4)
C19	2890.1(19)	2427.8(15)	2408.3(14)	30.0(4)
C20	4137(2)	2083.0(16)	1735.4(15)	33.9(4)
C21	5438.7(19)	2284.4(14)	1974.7(14)	27.2(4)
C22	7918.9(17)	3395.9(13)	1248.3(11)	19.0(3)
C23	7272.1(18)	3800.5(16)	266.5(11)	26.8(4)
C24	8377(2)	3354.3(18)	-456.1(12)	34.0(4)
C25	9716(2)	3632.3(19)	-468.6(13)	37.7(5)

C26	10328.5(18)	3285.0(17)	510.1(12)	29.9(4)
C27	9215.4(17)	3741.3(14)	1223.9(11)	21.7(3)
C28	6174.7(17)	5080.6(13)	2296.7(12)	20.9(3)
C29	5675(2)	5907.2(14)	1361.6(14)	31.4(4)
C30	5084(2)	7055.4(16)	1500.3(18)	48.4(6)
C31	6164(3)	7302.0(18)	1964(2)	57.9(7)
C32	6639(2)	6487.6(17)	2888.0(18)	46.1(6)
C33	7264.9(19)	5350.1(15)	2741.6(14)	29.4(4)

Table 2: Anisotropic Displacement Parameters ($Å^2×10^3$). The Anisotropic displacement factor exponent takes the form: $-2\pi^2[h^2a^{*2}U_{11}+2hka^*b^*U_{12}+\ldots]$.

Atom	U_{11}	U_{22}	U_{33}	U_{23}	U_{13}	U_{12}
Rh1	16.74(6)	18.53(6)	11.87(6)	-2.91(4)	-1.11(4)	-3.37(5)
P1	14.76(19)	19.3(2)	13.22(18)	-2.43(15)	-1.34(15)	-5.78(16)
Cl1	30.8(2)	20.6(2)	16.84(19)	-1.55(15)	1.70(16)	1.28(17)
C1	28.6(10)	32.8(10)	16.6(8)	-4.2(7)	-7.1(7)	0.0(8)
O1	35.7(8)	63.2(10)	28.9(8)	-20.1(7)	-2.2(6)	12.1(7)
C2	16.9(7)	15.7(7)	12.9(7)	-5.9(6)	0.9(6)	-1.1(6)
N1	18.7(7)	18.1(7)	18.1(7)	-2.5(5)	-1.5(5)	-5.2(5)
Fe1	22.70(13)	23.95(13)	18.64(12)	-8.92(10)	2.85(9)	-9.63(10)
C3	19.7(8)	18.3(8)	18.2(8)	-7.2(6)	0.3(6)	-4.6(6)
C4	24.5(9)	22.5(8)	26.9(9)	-5.8(7)	-7.2(7)	-5.3(7)
C5	22.8(9)	34.4(10)	38.1(11)	-16.5(9)	-6.1(8)	-7.4(8)
C6	22.4(9)	35(1)	36.9(10)	-20.2(8)	9.7(8)	-13.9(8)
C9	36.8(11)	47.7(12)	22.8(9)	-16.1(9)	10.7(8)	-19.5(9)
C8	25.0(9)	50.5(12)	32.7(10)	-26.3(9)	9.8(8)	-12.1(9)
C7	24.4(9)	25.2(9)	21.0(8)	-10.8(7)	7.4(7)	-10.6(7)
C10	34.9(11)	50.6(12)	28.4(10)	-24.6(9)	5.8(8)	-17.8(10)
C11	44.2(12)	33.9(11)	39.1(11)	-24.1(9)	13.3(9)	-16.8(9)
C12	36.8(11)	30.9(10)	30.9(10)	-17.0(8)	3.5(8)	1.3(8)
C13	23.4(9)	23.0(9)	45.2(11)	-4.9(8)	-1.9(8)	-10.8(7)
C14	31.2(12)	65.3(17)	76.1(19)	-2.6(14)	16.5(12)	-17.7(12)
C15	104(4)	46(3)	82(4)	-28(3)	69(3)	-27(3)
C14A	31.2(12)	65.3(17)	76.1(19)	-2.6(14)	16.5(12)	-17.7(12)
C15A	18(3)	45(3)	85(5)	4(3)	-4(3)	-8(2)
C16	16.9(8)	23.5(8)	16.6(7)	-3.4(6)	-1.4(6)	-8.4(6)
C17	18.1(8)	26.5(9)	26.2(9)	-8.9(7)	3.5(7)	-9.3(7)
C18	17.2(8)	30.6(9)	32.9(10)	-8.2(8)	1.9(7)	-10.6(7)
C19	24.9(9)	31.7(10)	37.8(10)	-7.6(8)	0.4(8)	-15.9(8)

C20	29.2(10)	35.6(11)	47.9(12)	-21.2(9)	3.9(9)	-17.5(9)
C21	22.0(9)	27.5(9)	37(1)	-14.5(8)	3.4(8)	-10.7(7)
C22	17.5(8)	25.5(8)	13.3(7)	-3.3(6)	-1.0(6)	-7.3(7)
C23	20.4(8)	43.4(11)	15.3(8)	-4.0(7)	-2.2(7)	-11.0(8)
C24	29.3(10)	57.1(13)	16.8(8)	-11.2(9)	0.4(7)	-14.9(9)
C25	27.9(10)	66.0(14)	18.5(9)	-8.9(9)	6.6(8)	-18.3(10)
C26	16.1(8)	47.2(11)	25.0(9)	-9.9(8)	2.4(7)	-9.2(8)
C27	16.8(8)	30.1(9)	17.3(8)	-3.7(7)	0.2(6)	-8.8(7)
C28	17.5(8)	20.7(8)	24.9(8)	-5.3(7)	0.8(6)	-7.6(6)
C29	27.3(10)	24.1(9)	34.9(10)	4.1(8)	-4.3(8)	-6.5(8)
C30	37.3(12)	23.6(10)	68.3(16)	2.2(10)	7.0(11)	-3.5(9)
C31	44.9(14)	26.9(11)	105(2)	-23.1(13)	24.1(14)	-18.4(10)
C32	33.5(11)	41.6(12)	78.6(17)	-37.3(12)	15.8(11)	-20(1)
C33	23.7(9)	32.3(10)	39.0(11)	-16.2(8)	1.7(8)	-13.0(8)

Table 3: Bond Lengths

Atom	Atom	Length/Å	Atom	Atom	Length/Å
Rh1	C1	1.7985(19)	C9	C8	1.420(3)
Rh1	C2	2.0542(15)	C9	C10	1.421(3)
Rh1	P1	2.3388(4)	C8	C12	1.419(3)
Rh1	Cl1	2.3949(4)	C10	C11	1.412(3)
P1	C28	1.8501(17)	C11	C12	1.419(3)
P1	C16	1.8513(16)	C13	C14	1.517(3)
P1	C22	1.8546(16)	C14	C15	1.570(6)
C1	O1	1.148(2)	C16	C17	1.529(2)
C2	N1	1.301(2)	C16	C21	1.543(2)
C2	C3	1.465(2)	C17	C18	1.530(2)
N1	C13	1.457(2)	C18	C19	1.519(2)
Fe1	C4	2.0357(17)	C19	C20	1.522(3)
Fe1	C3	2.0382(16)	C20	C21	1.528(2)
Fe1	C10	2.0393(18)	C22	C27	1.530(2)
Fe1	C7	2.0434(16)	C22	C23	1.535(2)
Fe1	C5	2.0455(18)	C23	C24	1.527(2)
Fe1	C11	2.0458(19)	C24	C25	1.521(3)
Fe1	C9	2.0459(18)	C25	C26	1.522(2)
Fe1	C8	2.0512(19)	C26	C27	1.526(2)
Fe1	C12	2.0520(19)	C28	C29	1.532(2)
Fe1	C6	2.0575(18)	C28	C33	1.535(2)
C3	C4	1.438(2)	C29	C30	1.530(3)

C3	C7	1.439(2)	C30	C31	1.523(3)
C4	C5	1.421(2)	C31	C32	1.509(4)
C5	C6	1.415(3)	C32	C33	1.522(3)
C6	C7	1.417(2)			

Table 4: Bond Angles

Atom	Atom	Atom	Angle/˚	Atom	Atom	Atom	Angle/˚
C1	Rh1	C2	91.68(7)	C12	Fe1	C6	125.15(8)
C1	Rh1	P1	90.29(5)	C4	C3	C7	107.21(14)
C2	Rh1	P1	174.33(5)	C4	C3	C2	129.03(15)
C1	Rh1	Cl1	174.61(6)	C7	C3	C2	123.67(14)
C2	Rh1	Cl1	85.11(4)	C4	C3	Fe1	69.23(9)
P1	Rh1	Cl1	93.305(15)	C7	C3	Fe1	69.55(9)
C28	P1	C16	104.45(7)	C2	C3	Fe1	123.67(11)
C28	P1	C22	109.78(8)	C5	C4	C3	107.69(16)
C16	P1	C22	102.98(7)	C5	C4	Fe1	70.00(10)
C28	P1	Rh1	111.30(5)	C3	C4	Fe1	69.42(9)
C16	P1	Rh1	114.55(5)	C6	C5	C4	108.68(16)
C22	P1	Rh1	113.14(5)	C6	C5	Fe1	70.29(10)
O1	C1	Rh1	178.25(19)	C4	C5	Fe1	69.26(10)
N1	C2	C3	115.54(14)	C5	C6	C7	108.38(15)
N1	C2	Rh1	125.44(12)	C5	C6	Fe1	69.38(10)
C3	C2	Rh1	118.79(11)	C7	C6	Fe1	69.25(10)
C2	N1	C13	125.09(15)	C8	C9	C10	107.50(18)
C4	Fe1	C3	41.35(6)	C8	C9	Fe1	69.92(10)
C4	Fe1	C10	122.34(8)	C10	C9	Fe1	69.40(10)
C3	Fe1	C10	159.87(8)	C12	C8	C9	108.19(18)
C4	Fe1	C7	69.20(7)	C12	C8	Fe1	69.79(11)
C3	Fe1	C7	41.30(6)	C9	C8	Fe1	69.52(11)
C10	Fe1	C7	156.81(7)	C6	C7	C3	108.03(15)
C4	Fe1	C5	40.74(7)	C6	C7	Fe1	70.33(10)
C3	Fe1	C5	68.85(7)	C3	C7	Fe1	69.16(9)
C10	Fe1	C5	106.27(8)	C11	C10	C9	108.42(18)
C7	Fe1	C5	68.33(7)	C11	C10	Fe1	70.03(10)
C4	Fe1	C11	159.03(8)	C9	C10	Fe1	69.90(10)
C3	Fe1	C11	158.44(8)	C10	C11	C12	108.05(18)
C10	Fe1	C11	40.43(8)	C10	C11	Fe1	69.54(11)
C7	Fe1	C11	122.31(8)	C12	C11	Fe1	69.98(11)
C5	Fe1	C11	123.20(8)	C11	C12	C8	107.84(18)

C4	Fe1	C9	106.16(8)	C11	C12	Fe1	69.51(11)
C3	Fe1	C9	123.64(7)	C8	C12	Fe1	69.73(11)
C10	Fe1	C9	40.71(8)	N1	C13	C14	111.60(18)
C7	Fe1	C9	161.61(7)	C13	C14	C15	116.4(2)
C5	Fe1	C9	120.50(8)	C17	C16	C21	110.33(13)
C11	Fe1	C9	68.32(8)	C17	C16	P1	113.76(11)
C4	Fe1	C8	121.72(8)	C21	C16	P1	108.39(11)
C3	Fe1	C8	108.21(7)	C16	C17	C18	110.98(14)
C10	Fe1	C8	68.12(8)	C19	C18	C17	111.32(14)
C7	Fe1	C8	125.65(7)	C18	C19	C20	110.45(15)
C5	Fe1	C8	156.73(8)	C19	C20	C21	111.43(15)
C11	Fe1	C8	68.10(8)	C20	C21	C16	111.42(15)
C9	Fe1	C8	40.56(8)	C27	C22	C23	109.95(13)
C4	Fe1	C12	158.18(8)	C27	C22	P1	112.36(11)
C3	Fe1	C12	122.87(7)	C23	C22	P1	118.57(11)
C10	Fe1	C12	68.09(8)	C24	C23	C22	110.07(14)
C7	Fe1	C12	109.04(8)	C25	C24	C23	111.92(16)
C5	Fe1	C12	160.43(8)	C24	C25	C26	111.84(15)
C11	Fe1	C12	40.51(8)	C25	C26	C27	111.31(15)
C9	Fe1	C12	68.29(8)	C26	C27	C22	110.27(14)
C8	Fe1	C12	40.48(8)	C29	C28	C33	110.45(14)
C4	Fe1	C6	68.49(7)	C29	C28	P1	116.54(12)
C3	Fe1	C6	68.70(7)	C33	C28	P1	113.45(12)
C10	Fe1	C6	121.01(8)	C30	C29	C28	110.93(17)
C7	Fe1	C6	40.42(7)	C31	C30	C29	111.12(18)
C5	Fe1	C6	40.33(8)	C32	C31	C30	111.30(18)
C11	Fe1	C6	107.86(8)	C31	C32	C33	110.67(19)
C9	Fe1	C6	156.05(8)	C32	C33	C28	110.49(16)
C8	Fe1	C6	161.99(8)				

Table 5: Torsion Angles

A	B	C	D	Angle/°	A	B	C	D	Angle/°
C3	C2	N1	C13	177.57(15)	N1	C13	C14	C15	-39.2(3)
Rh1	C2	N1	C13	-8.1(2)	C28	P1	C16	C17	-56.09(13)
N1	C2	C3	C4	-9.6(2)	C22	P1	C16	C17	-170.81(12)
Rh1	C2	C3	C4	175.69(13)	Rh1	P1	C16	C17	65.92(12)
N1	C2	C3	C7	174.40(15)	C28	P1	C16	C21	-179.22(12)
Rh1	C2	C3	C7	-0.3(2)	C22	P1	C16	C21	66.07(13)
N1	C2	C3	Fe1	-99.08(15)	Rh1	P1	C16	C21	-57.20(12)

Rh1	C2	C3	Fe1	86.18(14)	C21	C16	C17	C18	-55.49(18)
C7	C3	C4	C5	-0.36(19)	P1	C16	C17	C18	-177.55(12)
C2	C3	C4	C5	-176.90(16)	C16	C17	C18	C19	57.3(2)
Fe1	C3	C4	C5	-59.78(12)	C17	C18	C19	C20	-57.1(2)
C7	C3	C4	Fe1	59.42(11)	C18	C19	C20	C21	56.2(2)
C2	C3	C4	Fe1	-117.12(17)	C19	C20	C21	C16	-55.5(2)
C3	C4	C5	C6	0.0(2)	C17	C16	C21	C20	54.82(19)
Fe1	C4	C5	C6	-59.42(13)	P1	C16	C21	C20	179.99(13)
C3	C4	C5	Fe1	59.41(12)	C28	P1	C22	C27	56.10(13)
C4	C5	C6	C7	0.4(2)	C16	P1	C22	C27	166.90(11)
Fe1	C5	C6	C7	-58.40(12)	Rh1	P1	C22	C27	-68.89(12)
C4	C5	C6	Fe1	58.79(13)	C28	P1	C22	C23	-74.00(15)
C10	C9	C8	C12	0.2(2)	C16	P1	C22	C23	36.80(15)
Fe1	C9	C8	C12	-59.28(13)	Rh1	P1	C22	C23	161.01(12)
C10	C9	C8	Fe1	59.46(13)	C27	C22	C23	C24	58.41(19)
C5	C6	C7	C3	-0.61(19)	P1	C22	C23	C24	-170.40(13)
Fe1	C6	C7	C3	-59.09(11)	C22	C23	C24	C25	-55.7(2)
C5	C6	C7	Fe1	58.48(12)	C23	C24	C25	C26	53.6(2)
C4	C3	C7	C6	0.59(18)	C24	C25	C26	C27	-53.8(2)
C2	C3	C7	C6	177.36(15)	C25	C26	C27	C22	56.8(2)
Fe1	C3	C7	C6	59.82(12)	C23	C22	C27	C26	-59.15(18)
C4	C3	C7	Fe1	-59.22(11)	P1	C22	C27	C26	166.47(12)
C2	C3	C7	Fe1	117.55(15)	C16	P1	C28	C29	-63.04(14)
C8	C9	C10	C11	-0.1(2)	C22	P1	C28	C29	46.79(14)
Fe1	C9	C10	C11	59.66(13)	Rh1	P1	C28	C29	172.83(11)
C8	C9	C10	Fe1	-59.80(13)	C16	P1	C28	C33	166.99(12)
C9	C10	C11	C12	0.0(2)	C22	P1	C28	C33	-83.18(14)
Fe1	C10	C11	C12	59.61(13)	Rh1	P1	C28	C33	42.87(14)
C9	C10	C11	Fe1	-59.57(13)	C33	C28	C29	C30	-55.6(2)
C10	C11	C12	C8	0.1(2)	P1	C28	C29	C30	173.03(13)
Fe1	C11	C12	C8	59.42(13)	C28	C29	C30	C31	54.9(2)
C10	C11	C12	Fe1	-59.33(13)	C29	C30	C31	C32	-55.9(3)
C9	C8	C12	C11	-0.2(2)	C30	C31	C32	C33	57.4(2)
Fe1	C8	C12	C11	-59.28(13)	C31	C32	C33	C28	-58.0(2)
C9	C8	C12	Fe1	59.11(13)	C29	C28	C33	C32	57.1(2)
C2	N1	C13	C14	-105.1(2)	P1	C28	C33	C32	-169.92(14)

Table 6: Hydrogen Atom Coordinates (Å×10^4) and Isotropic Displacement Parameters (Å^2×10^3)

Atom	*x*	*y*	*z*	U(eq)

H1	9030(20)	345(15)	5946(13)	23
H4	10665	721	6566	30
H5	12509	1682	6454	36
H6	12179	3143	4882	35
H9	8505	2442	7666	41
H8	6898	3303	6205	41
H7	10117	3119	4001	27
H10	10310	3455	7476	41
H11	9820	4933	5913	43
H12	7710	4843	5121	42
H13A	7653	-380	5462	36
H13B	6898	769	4767	36
H14A	5544	225	6195	74
H14B	5535	1439	5922	74
H15A	7272	-232	7388	121
H15B	5826	675	7587	121
H15C	7179	1006	7133	121
H14C	5689	1466	6061	74
H14D	6513	346	6791	74
H15D	4556	553	5329	81
H15E	4334	96	6436	81
H15F	5574	-613	5858	81
H16	4817	3931	1339	23
H17A	3583	4587	2633	28
H17B	4101	3397	3316	28
H18A	1753	3809	2861	32
H18B	2227	4064	1769	32
H19A	2049	2324	2215	36
H19B	3129	1972	3055	36
H20A	3860	2490	1081	41
H20B	4379	1306	1771	41
H21A	6208	2095	1501	33
H21B	5782	1814	2600	33
H22	8312	2593	1357	23
H23A	6443	3565	284	32
H23B	6940	4599	81	32
H24A	8627	2560	-305	41
H24B	7963	3654	-1091	41

H25A	9492	4421	-714	45
H25B	10435	3271	-900	45
H26A	11143	3539	483	36
H26B	10682	2487	718	36
H27A	8921	4539	1049	26
H27B	9629	3477	1858	26
H28	5322	5202	2731	25
H29A	6482	5849	900	38
H29B	4929	5749	1104	38
H30A	4835	7577	881	58
H30B	4208	7139	1900	58
H31A	6999	7295	1533	70
H31B	5736	8033	2077	70
H32A	5818	6533	3337	55
H32B	7360	6654	3163	55
H33A	7551	4826	3356	35
H33B	8123	5291	2325	35

Table 7: Atomic Occupancy

Atom	*Occupancy*	Atom	*Occupancy*	Atom	*Occupancy*
C14	0.585(5)	H14A	0.585(5)	H14B	0.585(5)
C15	0.585(5)	H15A	0.585(5)	H15B	0.585(5)
H15C	0.585(5)	C14A	0.415(5)	H14C	0.415(5)
H14D	0.415(5)	C15A	0.415(5)	H15D	0.415(5)
H15E	0.415(5)	H15F	0.415(5)		

Table 8: Solvent masks information

Number	X	Y	Z	Volume	Electron count	Content
1	-0.015	0.000	0.000	276	81	N9 O2.25